

POLYANILINE: SYNTHESIS, CHARACTERIZATION, SOLUTION PROPERTIES
AND COMPOSITES

A THESIS SUBMITTED TO
THE GRADUATE SCHOOL OF NATURAL AND APPLIED SCIENCES
OF
MIDDLE EAST TECHNICAL UNIVERSITY

BY

FARIS YILMAZ

IN PARTIAL FULFILLMENT OF THE REQUIREMENTS
FOR
THE DEGREE OF DOCTOR OF PHILOSOPHY
IN
POLYMER SCIENCE AND TECHNOLOGY

JULY 2007

Approval of the Graduate School of Natural and Applied Sciences.

Prof. Dr. Canan Özgen
Director

I certify that this thesis satisfies all the requirements as a thesis for the degree of Doctor of Philosophy.

Assoc. Prof. Göknur Bayram
Head of Department

This is to certify that we have read this thesis and that in our opinion it is fully adequate, in scope and quality, as a thesis for the degree of Doctor of Philosophy.

Prof. Dr. Zuhâl Küçükyavuz
Supervisor

Examining Committee Members

Prof. Dr. Duygu Kısakürek (METU, CHEM) _____

Prof. Dr. Serpil Aksoy (Gazi Univ, CHEM) _____

Prof. Dr. Ali Usanmaz (METU, CHEM) _____

Prof. Dr. Zuhâl Küçükyavuz (METU, CHEM) _____

Prof. Dr. Teoman Tinçer (METU, CHEM) _____

“I hereby declare that all information in this document has been obtained and presented in accordance with academic rules and ethical conduct. I also declare that, as required by these rules and conduct, I have fully cited and referenced all material and results that are not original to this work.”

Name, Last name : Faris YILMAZ

Signature :

ABSTRACT

POLYANILINE: SYNTHESIS, CHARACTERIZATION, SOLUTION PROPERTIES AND COMPOSITES

YILMAZ, Faris

Ph.D., Department of Polymer Science and Technology

Supervisor: Prof. Dr. Zuhal Küçükayavuz

July 2007, 148 pages.

Polyaniline was chemically synthesized at three different temperatures of 25, 0, and -25°C, by oxidative polymerization with ammonium peroxodisulfate at equimolar of aniline to oxidant ratio and 1M hydrochloric acid. The resulted polyaniline was in a powder form which was characterized by several techniques such as: electrical conductivity, elemental analysis, thermal analysis, wide-angle X-Ray diffraction, and scanning electron microscope . The solution properties of the reduced polymer were studied by viscometry, static and dynamic light scattering.

It was found that as the polymerization temperature decreases, the molecular weight, crystallinity, and thermal stability of polyaniline increased, while the electrical conductivity was independent of the polymerization temperature. Moreover, the morphology of the polymer was changed from granular to tubular with reducing polymerization temperature. Viscometry and static light scattering analysis showed that the polyaniline has a flexible random coil conformation when dissolved in N-methyl-2-pyrrolidinone which was proved to be a good solvent for this polymer. Dynamic light scattering indicated that the polymer solution is a polyelectrolyte with high hydrodynamic radius at low polymer concentrations.

All mechanical features except Young's modulus of polyaniline-filled low density polyethylene composites became poorer as polyaniline content increased. Moreover, a sudden increase in the electrical conductivity with increasing polyaniline contents was also observed.

The conductivity of the tubular composites of multi wall nanotubes (MWNTs)-filled polyaniline increased with increasing MWNTs loading, and became weakly temperature dependent. The morphological analysis indicated that the MWNTs were well dispersed and isolated, and the tubes became crowded proportionally to MWNTs weight percent used in the composites.

Keywords: Polyaniline, Emeraldine, Leucoemeraldine, Conductivity, Solution properties, Viscosity, Static and Dynamic light scattering, Composites, Mechanical properties.

ÖZ

POLIANİLİN: SENTEZİ, KARAKTERİZASYONU, ÇÖZELTİ ÖZELLİKLERİ, VE KOMPOZİTLERİ

YILMAZ, Faris

Doktora, Polimer Bilimi ve Teknolojisi

Tez Yöneticisi: Prof. Dr. Zuhal Küçükyavuz

Temmuz 2007, 148 sayfa.

Polianilin üç değişik sıcaklıkta: 25°C, 0 °C, -25°C de, anilinle eşit mol sayıda amonyum peroksidisulfat ve 1M HCl kullanılarak oksidatif polimerizasyon yöntemi ile sentezlendi. Elde edilen toz halindeki polianilin, elektriksel iletkenlik ölçme, element analizi, termal analiz, geniş açılı X-ışınları kırınımı ve taramalı electron mikroskopu gibi tekniklerle karakterize edildi.

Polimerizasyon sıcaklığı azaldıkça, polianilinin molekl ağırlığı, kristal yüzdesi ve termal dayanıklılığının arttığı buna karşın elektriksel iletkenliğin molekül ağırlığına bağlı olmadığı gözlemlendi. Ayrıca, polimerizasyon sıcaklığının azalması ile polimerin morfolojisi granüler formdan borumsu forma dönüştü. Viskometri ve statik ışık saçılması deney sonuçları, polianilinin iyi bir çözücü olan N-metil-2-pirrolidonda çözüldüğünde rastgele yumak konformasyonunu aldığını gösterdi. Dinamik ışık saçılması incelemelerinden polianilin N-metil-2-pirrolidon çözeltisinin polielektrolit çözeltisi gibi davrandığı ve düşük polimer derişiminde daha büyük hidrodinamik yarıçapa sahip olduğu sonucuna varıldı.

Polianilin-polietilen kompozitlerinde, polianilin yüzdesi arttıkça Young modülü dışında bütün mekanik özelliklerinde düşme olduğu sonucuna varıldı. Ancak, polianilin yüzdesi arttıkça elektriksel iletkenlikte birdenbire bir artma gözlemlendi.

Polianilin-çok-duvarlı karbon nanotüpleri (MWNT) kompozitlerinin elektriksel iletkenliklerinin, MWNT yüzdesi ile arttığı, ayrıca iletkenliğin sıcaklıkla daha az değiştiği bulundu. Morfolojik incelemeler nanotüplerin polimer içinde iyi dağıldığını ve MWNT yüzdesi arttıkça tüpsü yapıların oğaldığını gösterdi.

Anahtar Kelimeler: Polianilin, Emeraldin, Lükomeraldin, İletkenlik, Çözelti özellikleri, Viskometri, Statik ve Dinamik ışık saçılması, Molekül ağırlığı, Kompozitler, Mekanik özellikleri.

ACKNOWLEDGMENTS

The graduate school days of a student are the most important part of his or her academic life. These days are full of pleasure of finding and learning about the Nature, collaboration with teachers and colleagues, and finally the pain after each failure. I know and feel in the deepest parts of my heart that I would have never completed this long and adventurous journey without some special people. Here, I would like to record my thanks to these people whose help have brought me to the end of this invaluable journey.

I am particularly indebted to my supervisor Prof. Dr. Zuhail Küçükyavuz for her guidance, continuous encouragement and help throughout these years.

My sincere appreciation goes to my brother Dr. Emad Abu-Hasan for the financial supports, personal advices, and friendly attitude. Brother, I wish you from the deepest part of my heart: long, healthy, wealthy, glad and lovely life with your family and lovers.

I am grateful to Mr. Said Alfaleet for everything he has done for me. He was always available to assist me in every problem I had. Dear Said, thanks also for your unfailing interest, encouragement and support.

I owe a lot to my dear friend Mahmoud Kemal, with whom I spend my childhood and school days. He shared me all problems I had during my graduate days. He always encouraged and supported me. Dear Mahmoud, you deserve every goodness and happiness more than I can wish for you.

I had problems with \LaTeX in writing this thesis, Dr. Rezik Esteteh (Physics Department) helped me to overcome these problems. Then, I would like to thank him.

Special appreciation is due to my son Muaz and my daughter Zeynep for enduring so patiently the division of my attention during this research.

Finally, I am deeply indebted to my parents, sisters and brothers for their love, morale, encouragement and support throughout the years I lived far from them; and so I apologize for not taking care of them as much as I should have.

TO THE MEMORY OF MY
MOTHER
AND
FATHER.....

TABLE OF CONTENTS

ABSTRACT	iv
ÖZ	vi
ACKNOWLEDGMENTS	viii
DEDICATION	x
TABLE OF CONTENTS	x
LIST OF TABLES	xv
LIST OF FIGURES	xvi
1 INTRODUCTION	1
1.1 The Aim of this Study	3
2 GENERAL BACKGROUND	4
2.1 Types of Electroactive Materials	4
2.1.1 Conductivity	4
2.1.2 Qualitative Band Theory	6
2.1.3 Electronic Properties of Semiconductors	9
2.1.3.1 Intrinsic Semiconductors	9
2.1.3.2 Extrinsic Semiconductors	11
2.2 Conducting Polymer	14
2.2.1 The Concept of Doping	17
2.2.1.1 Redox Doping	18
2.2.1.2 Non-Redox Doping	20
2.2.2 Solitons, Polarons, Bipolarons and Band Structures of Intrinsically Conducting Polymers	20
2.2.3 Conductivity of Intrinsically Conducting Polymers	23

2.2.4	The Polyaniline	24
2.2.4.1	Methods of Synthesis	27
2.2.4.2	Polymerization Mechanism	28
2.2.4.3	Protonic Acid Doping of Polyaniline .	31
2.2.4.4	Properties of Polyaniline	33
2.3	Light Scattering Methods	33
2.3.1	Dynamic Light Scattering (DLS)	34
2.3.2	Static Light Scattering (SLS)	40
2.3.3	Advantages and Disadvantages of Light Scattering	43
2.4	Viscosity	43
2.5	Carbon Nanotubes and Conducting Polymers	45
2.6	Conducting Polymer and Thermoplastic Composites . . .	47
2.7	Mechanical Properties of Composites	49
3	MATERIALS AND INSTRUMENTATION	52
3.1	Materials	52
3.2	Instrumentation	53
3.2.1	DC-Conductivity Measurements	53
3.2.2	Elemental Analysis	55
3.2.3	Thermal Analysis	55
3.2.3.1	Thermogravimetric Analysis	55
3.2.3.2	Differential Scanning Calorimetry . .	56
3.2.4	Fourier Transform Infrared Spectroscopy	57
3.2.5	Solid-State ¹³ C-NMR	57
3.2.6	X-Ray Powder Diffraction Analysis	58
3.2.7	Light Scattering Methods	59
3.2.8	Intrinsic Viscosity Measurement	61
3.2.9	Scanning Electron Microscope	61
3.2.10	Tensile Strength	62

4	EXPERIMENTAL PROCEDURES	64
4.1	Synthesis of Polyaniline (Emeraldine Base) at 25°C	64
4.2	Synthesis of Polyaniline (Emeraldine Base) at 0°C	66
4.3	Synthesis of Polyaniline (Emeraldine Base) at -25°C	67
4.4	Preparation of Leucoemeraldine Base	67
4.5	Sample Preparation for Light Scattering Measurements	68
4.6	Preparation of Low Density Polyethylene-Polyaniline Composites	68
4.7	Preparation of Multi Wall Carbon Nanotubes-Polyaniline Composites	69
5	RESULTS AND DISCUSSION	71
5.1	Synthesis and Characterization of Polyaniline	71
5.1.1	Polyaniline Synthesis	71
5.1.2	Characterization of Polyaniline	74
5.1.2.1	Conductivity Measurement Analysis	74
5.1.2.2	Elemental Analysis	75
5.1.2.3	Thermal Analysis	76
5.1.2.4	Fourier Transform Infrared Spectroscopy Analysis	79
5.1.2.5	X-Ray Analysis	82
5.1.2.6	Solid-State ¹³ C-NMR Analysis	84
5.1.2.7	Morphological Analysis	87
5.2	Solution Properties of Polyaniline	89
5.2.1	Static Light Scattering (SLS)	89
5.2.2	Intrinsic Viscosity Measurement	96
5.2.3	Dynamic Light Scattering (DLS)	99
5.3	Low Density Polyethylene-Based Polyaniline Conducting Polymer Composites	105
5.3.1	Thermal Analysis	106
5.3.2	Mechanical Properties	108
5.3.3	Relation Between Conductivity and Elongation at Break	113
5.3.4	Morphological Analysis	115

5.4	Conducting Polymer Composite of Multi Wall Carbon Nanotubes Filled-Polyaniline	118
5.4.1	Composite Formation Mechanism	118
5.4.2	Fourier Transform Infrared Spectroscopy Analysis	120
5.4.3	X-Ray Analysis	123
5.4.4	Thermal Gravimetric Analysis	124
5.4.5	Morphological Analysis	125
5.4.6	Conductivity Measurement Analysis	128
6	SUMMARY AND CONCLUSIONS	131
6.1	Synthesis and Characterization of Polyaniline	131
6.2	Solution Properties of Polyaniline	133
6.3	Low Density Polyethylene-Based Polyaniline Conducting Polymer Composites	135
6.4	Conducting Polymer Composites of Multi Wall Nanotubes Filled-Polyaniline	136
	REFERENCES	138
	VITA	148

LIST OF TABLES

TABLE

3.1	Some properties of Low Density Polyethylene	53
3.2	Characteristics of Multi Wall Nanotubes (Nanocyl-7000)	53
5.1	Conductivity of doped polyaniline (Emeraldine salt) powder	74
5.2	Elemental composition of polyaniline base	75
5.3	IR vibrational modes of polyaniline base	81
5.4	Percentage crystallinity, X_c (%) of undoped polyaniline in powdered form, according to the temperature of synthesis.	84
5.5	^{13}C -CPMAS Chemical shifts of Emeraldine Base powder	86
5.6	Weight average molecular weight, \bar{M}_w , radius of gyration, R_g , and second virial coefficient, A_2 for polyaniline leucoemeraldine base synthesized at different temperatures.	90
5.7	Values of I_a , I_i , \bar{M}_w/\bar{M}_n , and \bar{M}_n	96
5.8	The intrinsic viscosity, $[\eta]$, Huggins coefficient, k_H and molecular weight (\bar{M}_w , found by static light scattering measurements, SLS) of EB/NMP/LiCl solutions.	98
5.9	D_o , k_D , and R_H data obtained from dynamic light scattering measurement for reduced polyaniline solutions at 25°C	102
5.10	The ratio of DLS $\langle R_H \rangle$ and SLS $\langle R_g \rangle$ data of polyaniline solutions. . .	104
5.11	The ratio $\langle R_g \rangle / \langle R_H \rangle$ for selected structures.	105
5.12	Melting temperatures, T_m and heat of fusions, ΔH_f , for pure LDPE and its composites.	107
5.13	Experimentally calculated data of tensile strength at maximum load (σ_{max}), tensile modulus (E), tensile strength at break (σ_b), and tensile strain at break (ε_b) with respect to polyaniline (PANI) contents in polyethylene matrix.	109
5.14	The relationship between conductivity and elongation at break at different content of PANI in PE matrix.	114

LIST OF FIGURES

FIGURE

2.1	Range of resistivities for various materials, including metals, semiconductors and insulators	5
2.2	Molecular orbitals in a diatomic molecule.	7
2.3	Bonds in molecules and bands in solids.	8
2.4	Schematic band structure diagram of an intrinsic semiconductor. . .	10
2.5	Band structure diagram of an extrinsic n-type semiconductor. . .	12
2.6	Band structure diagram of an extrinsic p-type semiconductor. . .	12
2.7	Extrinsic exhaustion and intrinsic stages in a semiconductor. . . .	13
2.8	Selected examples of intrinsically conducting polymers.	16
2.9	Schematic view of contributions of bulk conductivity of conducting polymers.	24
2.10	Polyaniline general formula.	25
2.11	Leucoemeraldine Base.	26
2.12	Pernigraniline Base.	26
2.13	Emeraldine Base.	26
2.14	The formation of the aniline radical cation and its different resonant structures.	28
2.15	Formation of the dimer and its corresponding radical cation. . . .	29
2.16	One possible way of PANI polymer formation.	30
2.17	Side reaction occurring during polyaniline synthesis.	31
2.18	Protonic Acid Doping of Polyanilines.	32
2.19	A stable polysemiquinone radical cation.	32
2.20	Schematic representation of experimental set up for DLS.	35

2.21	Schematic representation of a light scattering apparatus. Light scattering intensities are recorded according to sample concentration and angle (by means of a goniometer). The detector might rotate, as depicted, or be fixed and connected to an optical fiber supported by the rotating arm. In any case, the detection device and the laser source must be aligned toward the geometrical center of the sample cell. The measurement angle (θ) origin is the way of the transmitted laser beam.	41
2.22	A geometrical effect has to be considered when light scattering intensities are recorded according to angle. As the detection angle deviates from 90° , the probed volume increases, including particles that are not detected at right angle (open circles). This geometric effect is corrected by a sinus function.	42
2.23	A schematic diagram of the polymer molecules in solution (a) Dilute solution, (b) Semi-dilute solution, and (c) Concentrated solution.	44
3.1	Four point collinear probe method.	54
3.2	Tensile test specimen according to ASTM.	63
4.1	Oxidation of aniline hydrochloride with ammonium peroxydisulfate yields polyaniline (emeraldine) hydrochloride.	65
4.2	Polyaniline (emeraldine) salt is deprotonated in the alkaline medium to polyaniline (emeraldine) base.	66
5.1	TGA of Emeraldine Base (EB) synthesized at different temperatures	76
5.2	DSC of Emeraldine Base synthesized at different temperatures of 25°C , 0°C , and -25°C	77
5.3	DSC, second heating of Emeraldine Base synthesized at different temperatures	78
5.4	Thermal crosslinking reaction among EB-form polyaniline molecular chains.	79
5.5	FTIR of polyaniline (EB) powder.	80
5.6	WAXD of polyaniline (EB) powder synthesized at (a) 25°C , (b) 0°C and (c) -25°C	83
5.7	Solid-State ^{13}C -NMR spectra of polyaniline (EB) powder.	85
5.8	General form of polyaniline.	85
5.9	SEM micrographs of polyaniline (EB) powder synthesized at 25°C .	87
5.10	SEM micrographs of polyaniline (EB) powder synthesized at 0°C .	88
5.11	SEM micrographs of polyaniline (EB) powder synthesized at -25°C .	88

5.12	Berry plot of polyaniline leucoemeraldine base prepared at +25°C .	90
5.13	Berry plot of polyaniline leucoemeraldine base prepared at 0°C . .	91
5.14	Berry plot of polyaniline leucoemeraldine base prepared at -25°C .	91
5.15	Conformation plot of $\log R_g$ as a function of $\log \bar{M}_w$ for polyaniline prepared at deferent temperatures.	93
5.16	Plot of initial and asymptotic regions of the angular dependence of scattered light intensity for polyaniline leucoemeraldine base prepared at 25°C.	95
5.17	Reduced viscosity vs concentration for dilute EB/NMP/LiCl solutions at 28°C using three different EB molecular weights.	97
5.18	Intrinsic viscosity as a function of molecular weight for dilute solutions of EB/NMP/LiCl at 28°C.	99
5.19	The apparent diffusion coefficient (D_{app}) vs the square of the wave vector (q^2) for polyaniline prepared at +25°C.	100
5.20	The apparent diffusion coefficient (D_{app}) vs the square of the wave vector (q^2) for polyaniline prepared at 0°C.	100
5.21	The apparent diffusion coefficient (D_{app}) vs the square of the wave vector (q^2) for polyaniline prepared at -25°C.	101
5.22	R_H vs reduced PANI concentration for PANI in NMP.	103
5.23	DSC melting curves of LDPE and its PANI powder composites. .	106
5.24	TGA curves of LDPE and its PANI powder composites.	108
5.25	Tensile stress-strain curves of LDPE-PANI system.	110
5.26	The dependence of tensile stress on polyaniline content.	111
5.27	The dependence of elongation at break on polyaniline content. . .	112
5.28	The dependence of Young modulus on polyaniline content.	112
5.29	(●) Conductivity and (○) elongation at break of PEPANI composites as a function of the PANI content.	114
5.30	SEM micrographs of the surfaces of the stretched PEPANI composite: (a) pure LDPE, (b) 5 wt.%, (c) 10 wt.%, (d) 15 wt.%, (e) 20 wt.% and (f) 30 wt.% of PANI.	116
5.31	Schematic diagram of (a) the formation mechanism for tubular composites of MWNT and PANI, (b) in-situ polymerization and proposed composite interaction.	119
5.32	FTIR spectra of (a) PANI ES form and (b)15%wt CNT-PANI ES composite.	121

5.33	X-Ray diffractograms (Cu-K α) of (a)doped PANI emeraldine salt type, (b)composites containing 5wt%, (c)composites containing 10wt%, (d)composites containing 15wt%, (e)composites containing 30wt% of MWNTs and (f)MWNTs.	123
5.34	Thermogravimetric behavior (TGA) of pure Polyaniline (Emeraldine salt) and PANI/MWNTs composites.	124
5.35	SEM image of (a) pure MWNTs, (b) 5%wt, (c) 10%wt, (d) 15%wt, and (e,f) 30%wt of MWNT/PANI composites.	127
5.36	A semilogarithmic plot of the room-temperature conductivity of the composite vs the MWNT loading.	129
5.37	Temperature dependence on conductivity of the composites.	130

CHAPTER 1

INTRODUCTION

Those who recognize that our modern life style is dependent, to a large extent, on the use of organic polymers as thermal and electrical insulators, may be surprised to learn that specific plastics may also be used as conductors of electricity. In addition to demonstrating the versatility of polymers, this use as conductors will lead to developments which were not possible with other available materials of construction [1].

Just after World War II, a literal revolution took place in the area of solid state chemistry and physics. The solid-state century commenced from the humble beginnings of the transistor at Bell Laboratory [2]. Since then, the area of science and technology has been directed primarily towards the study of alloys, ceramics and inorganic semiconductors. After the invention of the integrated circuit, the size of electronic devices becomes smaller and smaller while the dimensionality of materials was also reduced. It is at this point that the advent of the discovery

of quasi one-dimensional conductors has opened up a whole new area of “non-classical” solid state chemistry and physics.

In the modern world, plastic and electrical devices are always tightly integrated together. However, it was in 1977 that an electrically conductive, quasi one-dimensional organic polymer, polyacetylene was discovered [3]. During the past 20 years, a variety of different conducting polymers have been developed [4]. Excitement about these polymeric materials is evidenced by the fact that the field of conducting polymers has attracted scientists from such diverse areas of interest as synthetic chemistry, electrochemistry, solid state physics, materials science, polymer science, electronics and electrical engineering.

Among the conducting polymers, polyaniline is emerging as the material of choice for many applications. The interest in this conducting polymer stems from the fact that many different ring- and nitrogen-substituted derivatives can be readily synthesized and that each of the derivatives can exist in several different oxidation states which can in principle be “doped” by a variety of different dopants either by non-redox processes or by partial chemical or electrochemical oxidation. These properties, combined with the fairly high conductivity after doping, their ease of synthesis and processing, satisfactory environmental stability and the relatively low cost of the starting materials strongly suggest their significant potential technological applicability.

1.1 The Aim of this Study

This research work is focused on preparation of polyaniline conducting polymeric particles by using so-called oxidative chemical polymerization method. The polyaniline was synthesized at three different temperatures of 25, 0, and -25°C . Then, the polyaniline that synthesized at 25 and 0°C were incorporated with Low Density Polyethylene (LDPE) and Multi Wall Carbon Nanotubes (MWNT) respectively, to study the following important points:

- (i) The effect of synthesis temperature on the molecular weight, crystallinity, conductivity, and morphology of the polymer in hand,
- (ii) The thermal and morphological properties of polyaniline in the form of emeraldine base synthesized at sub-zero temperature,
- (iii) The solution properties of polyaniline synthesized at different temperatures by viscometry, static and dynamic light scattering techniques, and
- (iv) Understanding the relative importance of the use of polyaniline in composites as a matrix and a filler respectively, and the effect of this incorporation on the DC conductivity of the resulting polymer composites.

CHAPTER 2

GENERAL BACKGROUND

2.1 Types of Electroactive Materials

2.1.1 Conductivity

Any material can, in principle, be classified as an insulator, semiconductor or metal, frequently based on its electrical resistivity. Insulators have high resistivities ($>10^{10}$ ohm.cm); metals have low resistivities ($<10^{-3}$ ohm.cm); semiconductors have intermediate resistivities. The range of resistivities from insulators to metals is enormous as shown in Figure 2.1. A good insulator such as quartz can have a resistivity as high as 10^{18} ohm.cm; a good metal such as copper can have a resistivity as low as 10^{-6} ohm.cm. It should be noted that, at a certain critical temperature, pressure and magnetic field, either insulators or semiconductors or metals can become superconductors with resistivities as low as 10^{-25} ohm.cm.

Electrical conduction occurs by the long range migration of either electrons

or ions. Migration of ions does not occur to any appreciable extent in most ionic and covalent solids such as oxides and halides [5]. Rather, the atoms tend to be essentially fixed on their lattice sites and can only move via crystal defects. Only at high temperatures, where the defects concentrations become quite large and the atoms have a lot of thermal energy, does the ionic conductivity become appreciable, e.g. the conductivity of NaCl at $\sim 800^\circ\text{C}$, just below its melting point, is $\sim 10^{-3}$ S/cm [5], whereas at room temperature, pure NaCl is an insulator. Usually, the ionic conductivity of electrolytes is in the range of 10^{-3} to 10 S/cm.

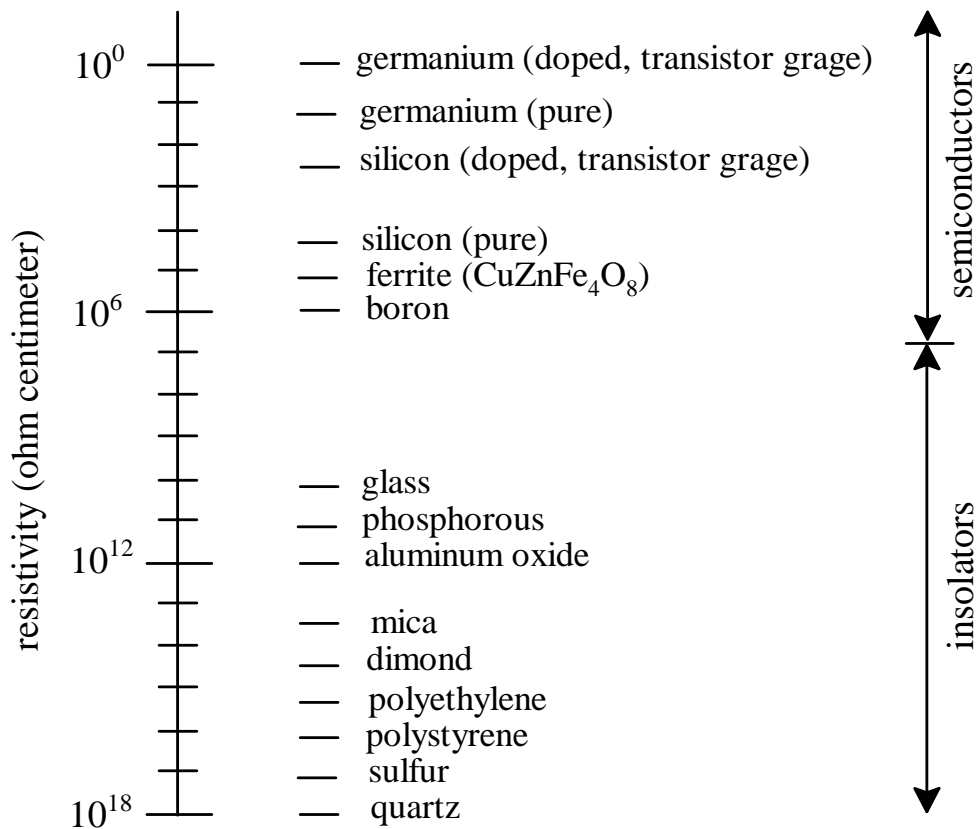


Figure 2.1: Range of resistivities for various materials, including metals, semi-conductors and insulators

The electronic conductivity is dependent on the migration of electrons or their counterpart holes. The conductivity (σ) is given by the equation:

$$\sigma = n.e.\mu \tag{2.1}$$

where n is the number of charge, e the charge and μ the mobility of the charge carriers. For metals, n is large and essentially unchanged with temperature. The only variable in σ is μ and since μ decreases slightly with increase of temperature due to collisions between the moving electrons and lattice atoms, σ also decreases with increase of temperature. For semiconductors and insulators, n usually increases exponentially with temperature. The effect of this dramatic increase in n more than outweighs the effect of the small decrease in μ . Hence, σ increases rapidly with temperature.

2.1.2 Qualitative Band Theory

The electronic structures of metals, semiconductors and many solids may be described in terms of band theory. The “chemical approach” to band theory is to take molecular orbital theory, as it is usually applied to small, finite-sized molecules and to extend the treatment to infinite, three-dimensional structures. In the molecular orbital theory of diatomic molecules, an atomic orbital from an atom 1 overlaps with an atomic orbital on atom 2, resulting in the formation of two molecular orbitals (either σ orbitals or π orbitals) that are delocalized over both atoms. One of the molecular orbitals is “bonding” and has lower energy than that of the atomic orbitals. The other is “antibonding” and is of higher

energy as shown in Figure 2.2.

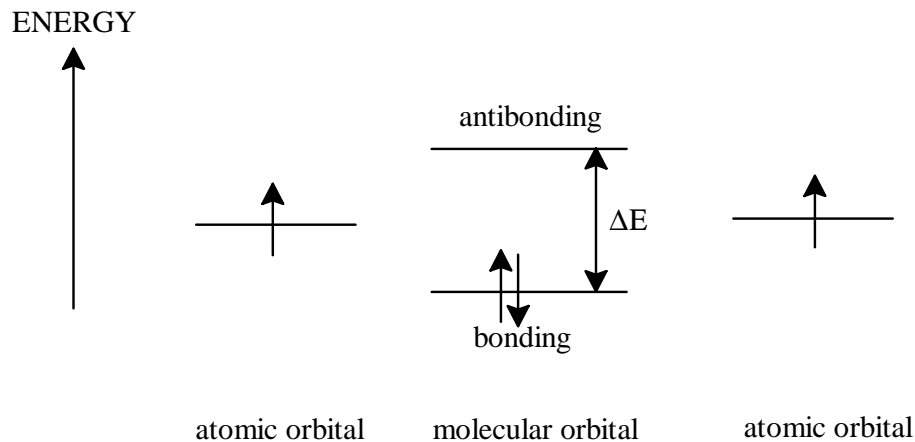


Figure 2.2: Molecular orbitals in a diatomic molecule.

Extension of this approach to large molecules leads to an increase in the number of molecular orbitals. For each atomic that is put into the system, one molecular orbital is created. As the number of molecular orbitals increases, the average energy gap between adjacent molecular orbitals must decrease as shown in Figure 2.3. The gap between bonding and antibonding orbitals also decreases until the situation is reached in which there is essentially a continuum of energy levels.

As shown in Figure 2.3, the energy band resulted from bonding orbitals of a molecule is called the valence band. The energy band resulted from antibonding orbitals of a molecule is called the conduction band. The width of individual bands across the range of energy levels is called band width. The gap between the highest filled energy level and lowest unfilled energy level is called band gap E_g . There is no band gap in metals, i.e., $E_g=0$ eV. In other words, there is a

finite density of states (electrons) at Fermi level (defined below) for metals and zero density of states at Fermi level for semiconductors and insulators.

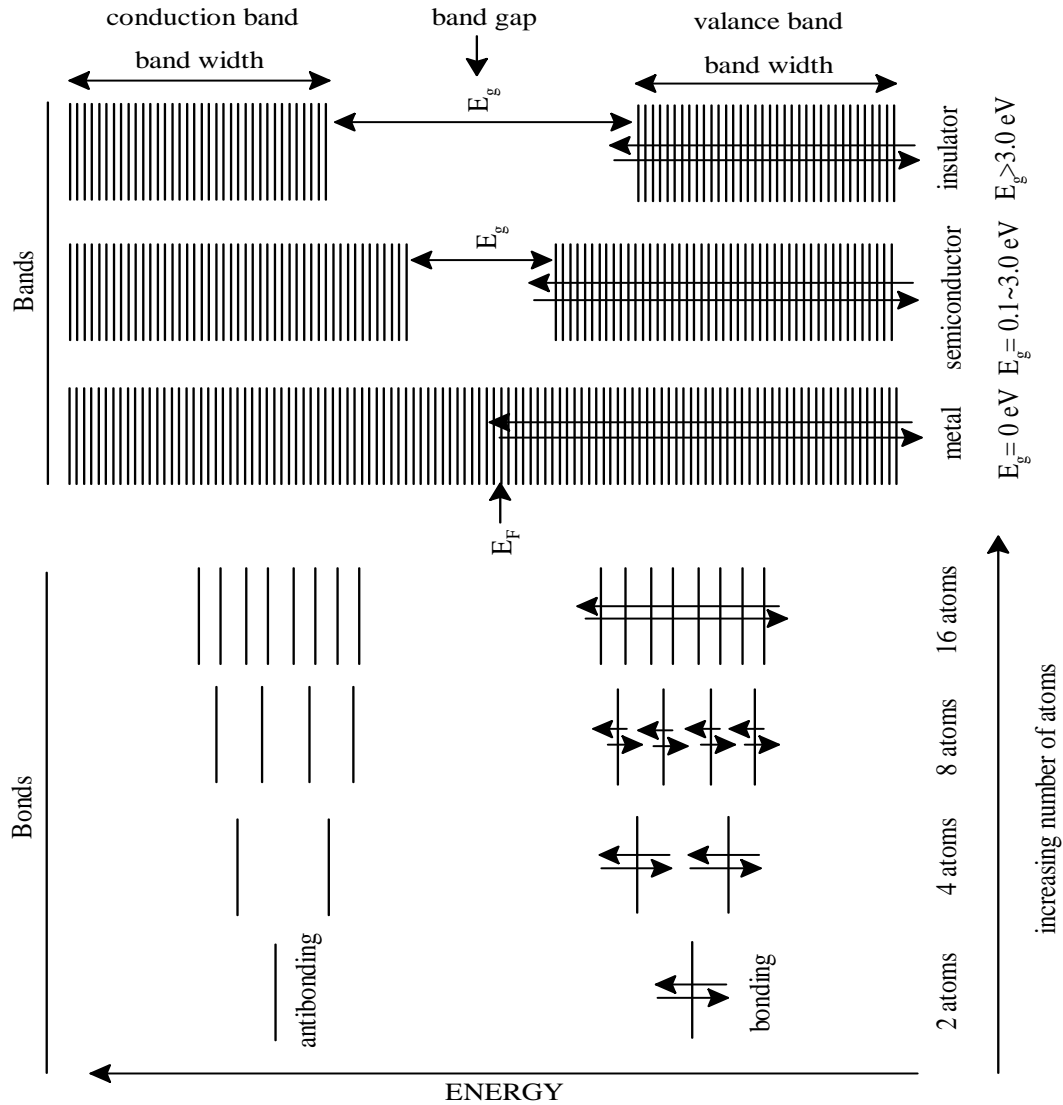


Figure 2.3: Bonds in molecules and bands in solids.

At absolute zero temperature (0K), when the electrons all occupy the lowest available energy state, the energy in the middle of the highest occupied state and the lowest unoccupied is the Fermi level [6]. This energy level separates the occupied from unoccupied electron levels. The corresponding energy is the

Fermi energy E_F . The location of the Fermi level in relation to the allowed energy state is crucial in determining the electrical properties of a solid. As can be seen from Figure 2.3, metals always have a partially filled free-electron band, so that the Fermi level corresponds to a level in the middle of the band and this makes the metals electrical conductors. Semiconductors and insulators always have completely empty electron bands at 0K. This means that the Fermi energy lies between the bands, and consequently they are poor electrical conductors at ambient temperatures [6].

2.1.3 Electronic Properties of Semiconductors

Most of the electronic properties of semiconductors can be described by reference to the simplified energy band diagrams shown below. There are no partially filled bands, just a filled valence band and an empty conduction band in a semiconductor at 0K. Therefore the Fermi level lies in the middle of the band gap. Semiconductors can be divided into two groups: intrinsic and extrinsic semiconductors.

2.1.3.1 Intrinsic Semiconductors

Intrinsic semiconductors are materials with relatively small band gaps. In these cases, a number of electrons can be thermally stimulated across the band gap at room temperature (300K) into the conduction band as shown in Figure 2.4. Once in the conduction band these electrons contribute to the electrical conductivity, as do the “holes” which are left behind in the valence band. Pure silicon is an

intrinsic semiconductor.

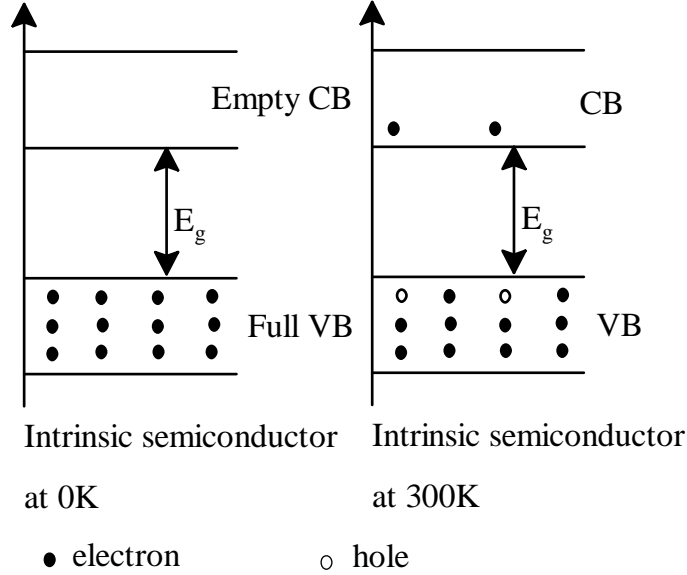


Figure 2.4: Schematic band structure diagram of an intrinsic semiconductor.

The number of electrons (holes) in the conduction band (valence band) determine the electrical properties of intrinsic semiconductors. The higher the temperature, the more electrons are found in the conduction band. Both electrons and holes can contribute to the electrical conductivity of the material. At room temperature an intrinsic semiconductor has about 10^{15} - 10^{20} conduction electrons per cubic meter caused by thermal stimulation alone. This contribution to the electrical conductivity is known as the “dark current” simply because it arises in the absence of incident light. The conductivity (σ) is given by the sum of contribution from electrons and holes:

$$\sigma = e \cdot N_e \cdot \mu_e + e \cdot N_h \cdot \mu_h \quad (2.2)$$

where e is the electronic charge, N_e and N_h are the number of electrons and holes

respectively. μ_e and μ_h are the mobilities of electrons and holes, respectively. The conductivity of an intrinsic semiconductor is also related to band gap E_g by the equation as follows:

$$\sigma = A \exp\left(-\frac{E_g}{2kT}\right) \quad (2.3)$$

which means that the intrinsic conductivity were the only mechanism taking place, we would expect, neglecting electron/phonon interaction, the conductivity σ to vary with temperature.

2.1.3.2 Extrinsic Semiconductors

Extrinsic semiconductors are materials whose conductivity is controlled by the presence of small amounts of impurity. The addition of small amounts of impurity is known as doping. The impurity added is called “dopant”. There are two types of dopants: donor and acceptor. Typical donor elements in extrinsic semiconductors are pentavalent elements such as phosphorus, arsenic and antimony. Typical acceptor elements in extrinsic semiconductors are trivalent elements such as boron, aluminum, gallium and indium.

When added in a few parts per million, donor elements contribute extra electrons. On the band description, these extra electrons occupy discrete levels (donor level) in the band gap that are found to lie -0.1 eV below the bottom of the conduction band as shown in Figure 2.5. These extra electrons are thermally stimulated from the donor level to the conduction band due to small energy gap between the donor level and the conduction band. The conduction mechanism in this type of semiconductor is via electrons which are the majority charge carriers. Materials

of this type are called “n-type” semiconductors. Since acceptor elements have one electron less than silicon, they demand more electrons from their neighboring atoms.

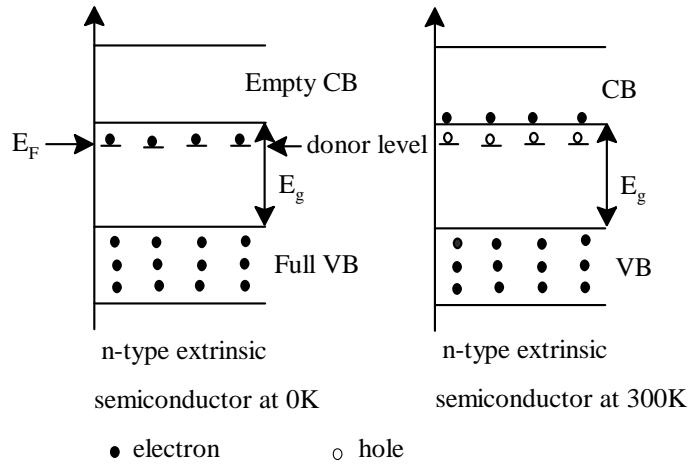


Figure 2.5: Band structure diagram of an extrinsic n-type semiconductor.

In view of the band structure, they form a discrete level (acceptor level) in the band gap just above the top of the valence band as shown in Figure 2.6.

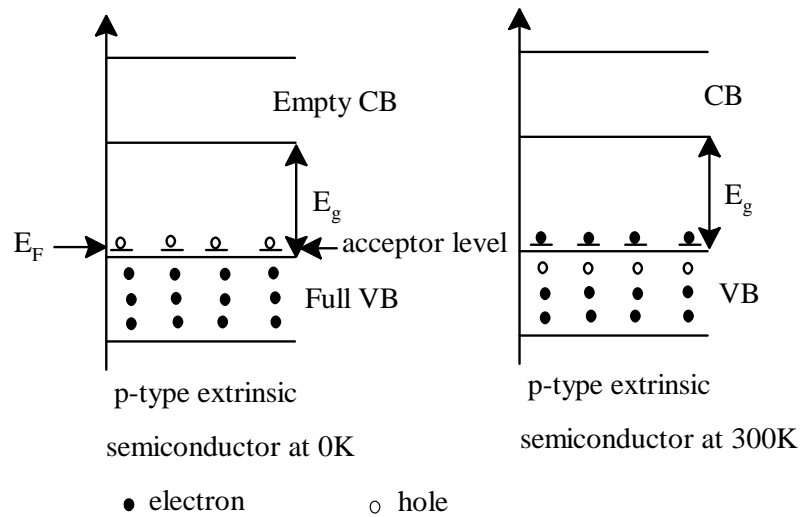


Figure 2.6: Band structure diagram of an extrinsic p-type semiconductor.

Consequently, electrons from the valence band are thermally promoted into this acceptor level. The acceptor level does not form a band because of the small amount of acceptor present. Therefore, it is not possible for electrons in the acceptor levels to contribute to conduction. The positive holes left behind in the valence band are able to move around. Since the majority of charge carriers are positive, this type of extrinsic semiconductor is known as “p-type” semiconductors. Since the population of electrons in the conduction band of an n-type semiconductor and the population of holes in the valence band of a p-type semiconductor are thermally promoted, the carrier concentration and conductivity of an extrinsic semiconductor is temperature dependent. At low temperatures, the small gap ~ 0.1 eV between acceptor (donor) level and valence (conduction) band is sufficiently large that only a limited number of electrons can make the transition. With increasing temperature, the number of thermally excited electrons increases so that the concentration of carriers and the conductivity of the material increase. This stage is called the “extrinsic” stage of a semiconductor as shown in Figure 2.7.

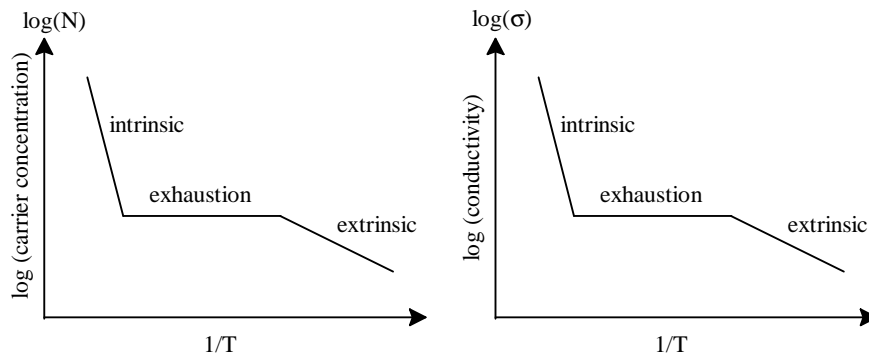


Figure 2.7: Extrinsic exhaustion and intrinsic stages in a semiconductor.

When the temperature increases to a certain level, all the electrons in the donor or acceptor levels have been thermally promoted to the conduction or valence band respectively. The concentration of extrinsic carriers attains its maximum value. At this stage the carrier concentration is independent of temperature and the conductivity may show a gradual decrease with a further rise in temperature due to the mobility effect. This stage is called the “saturation” or “exhaustion” stage as shown in Figure 2.7 (above). At still higher temperatures, the energy provided is sufficiently high so that the electrons in valence band are thermally excited to the conduction band, i.e., the intrinsic concentration of carriers exceeds the extrinsic concentration. Both the concentration of carrier and the conductivity increase sharply due to the exponential increase of charge carriers. This is the “intrinsic” stage (Figure 2.7) [7].

2.2 Conducting Polymer

In the past, it was believed that organic polymers are excellent insulators which provide significant advantaged for many application [8]. However, this concept was first challenged when reports of conducting or semiconducting polymeric materials such as polyacetylene and polyaniline began to appear in the literature [9]. It was only when the doping of polyacetylene had succeeded that new concepts of physics began to be realized and that a new class of organic polymers, conducting polymers, with the remarkable ability to conduct electrical current began to promote tremendous technological and scientific interest. In semiconductor physics undoped semiconductors are intrinsically conducting,

doped semiconductors extrinsically conducting. In contrast, doped polymers are often referred to as “intrinsically conducting polymers”. This to distinguish them from polymers which acquire conductivity by loading with conducting particles such carbon black, metal flakes, or fibers of stainless steel.

The intrinsically conducting polymers (ICPs), more commonly known as “synthetic metals”, refer to the large class of organic polymers which possess not only the mechanical properties and processibility of conventional polymers, but also unique electrical, electronic, magnetic, and optical properties of metals, which conventional polymers do not have [10]. The unifying characteristic property of this class of polymers is the intrinsic ability of the conjugated polymer backbone to support electrical conduction. Thus the fundamental property of conducting polymers is that electrical conductivity is achieved by charge carrier (electron or hole) through a π conjugated polymer backbone.

Since the initial discovery in 1977 [9] by Alan G. MacDiarmid and his co-workers, that polyacetylene, $(\text{CH})_x$, now commonly known as the prototype conducting polymer, could be either chemically or electrochemically, p- or n-doped, to become a conductor, the development of the conducting polymer field has continued to accelerate at an unexpectedly rapid rate. The rapid growth rate has been stimulated not only by the field’s fundamental synthetic novelty and importance to a cross-disciplinary section of investigators - chemists, electrochemists, experimental and theoretical physicists and electronic and electrical engineers - but to its actual and potential technological applications.

There are many different kinds of polymer systems which can undergo redox doping process other than *cis*- and *trans*- polyacetylene, $(\text{CH})_x$ [10]. It has been found that polymers such as polyparaphenylene [11], poly(phenylenevinylene) [11], polypyrrole [12], polythiophene [13], polyfuran [14], etc., and their ring- and N-substituted derivatives can also undergo redox p-doping and/or n-doping as listed in Figure 2.8. Moreover, the synthesis of new polymer systems such as poly(heterocycle)vinylenes, where $\text{Y}=\text{NH}$, NR , S and O , also attracted considerable attention because of their unique combination of physical properties, solution processibility and environmental stability in the doped form [10].

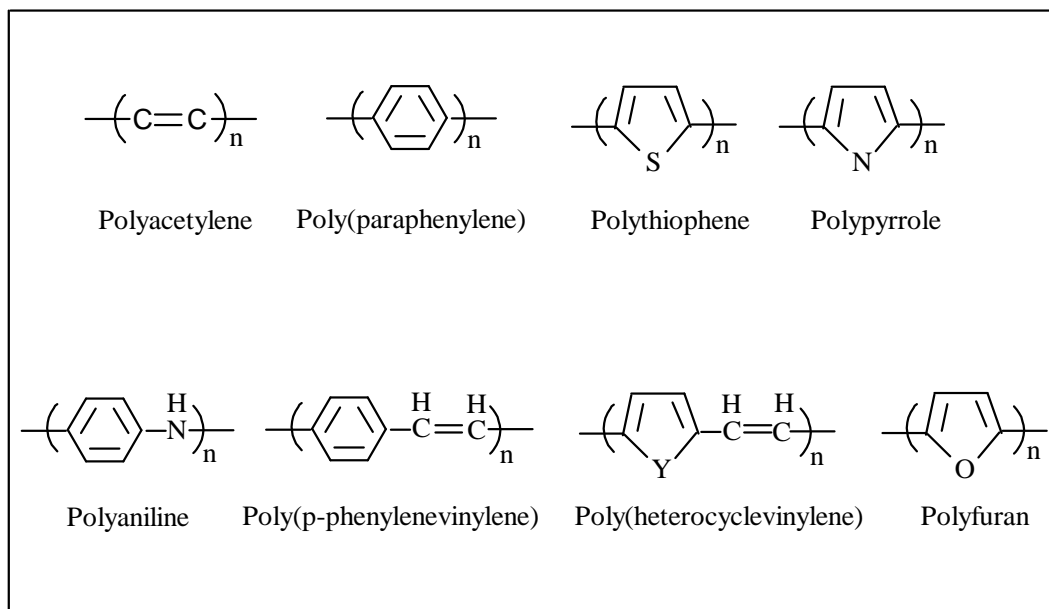


Figure 2.8: Selected examples of intrinsically conducting polymers.

2.2.1 The Concept of Doping

The concept of doping is the most important concept in conducting polymers which distinguishes “intrinsically conducting polymers” (ICPs) from all other types of polymers. Conducting polymers can exist in two different forms: non-conductive form (“non-doped” polymer) and conductive form (“doped” polymer). All conducting organic polymers are insulators or semiconductors in their neutral (“non-doped”) forms [15]. The process which converts the neutral polymer backbone to a charged π -conjugated system is known as “doping”.

By treatment of the neutral form of a polymer with small ($\leq \sim 10\%$), not necessarily stoichiometric quantities of chemical species, the electronic, electrical, magnetic, optical and structural properties of the polymer changes dramatically. The electrical conductivity of a “doped” material is typically 5~10 orders of magnitude higher than that of the “non-doped” material. It should be noted that doping and de-doping are generally reversible processes which do not change the chemical nature of the original polymer backbone. Both doping and undoping (or de-doping) processes can be carried out chemically or electrochemically. A conductivity anywhere between that of the undoped (insulating or semiconducting) and that of the fully doped (highly conducting) form of the polymer may be easily obtained, by controllably adjusting the doping level. Conducting blends of a (doped) conducting polymer with a conventional polymer (insulator) whose conductivity can be adjusted by varying the relative proportions of each polymer can be made. This permits the optimization of the best properties of each type

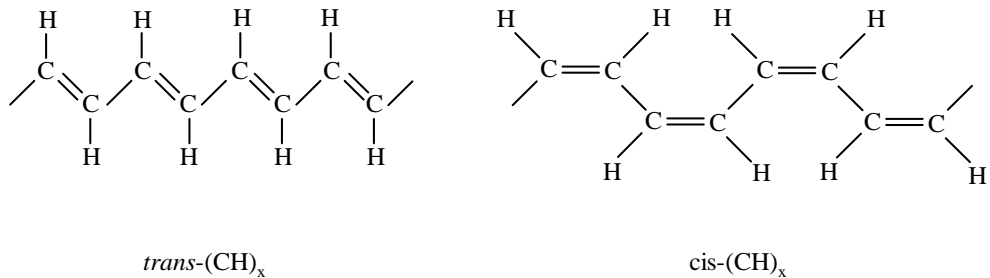
of material for various applications under different circumstances.

The “classical” method of “doping” involves redox doping, i.e., chemical or electrochemical partial oxidation (“p-doping”), or partial reduction (“n-doping”) of the conjugate polymer backbone [16]. During this process, the number of electrons associated with the polymer backbone changes. In the “doped” state, the backbone of a conducting polymer consists of a delocalized π system. In the “undoped” state, the polymer may have a conjugated backbone such as in *trans*-(CH)_x, which is retained in a modified form after doping, or it may have a non-conjugated backbone, as in polyaniline, (leucoemeraldine base form), which becomes conjugated only after p-doping.

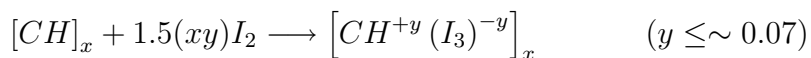
2.2.1.1 Redox Doping

Trans-(CH)_x, the most extensively investigated conducting polymer, is known as the prototype conducting polymer of all other conjugated polymers which are capable of redox doping processes [5]. It will be used to exemplify the basic concepts involved. These concepts can be applied with appropriate modifications as necessary to other conjugated polymers.

Free-standing films of *cis*-(CH)_x can be synthesized from gaseous acetylene at 78°C in the presence of an Al(C₂H₅)₃/Ti(OC₄H₉)₄ catalyst and can subsequently be isomerized at ~150°C to yield lustrous, silvery, films of the more thermodynamically stable *trans*-(CH)_x, as shown below.

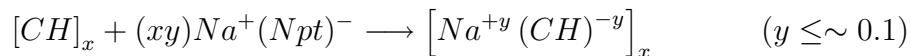


The bonding π system of the polymer can be readily partially oxidized, “p-doped”, by a variety of reagents such as iodine vapor or a solution of iodine in CCl_4 , e.g.,



with a concomitant increase in conductivity from $\sim 10^{-5}$ S/cm to $\sim 10^3$ S/cm. If the polymer is stretch-oriented 5 to 6 fold before doping, conductivity can be up to $\sim 10^5$ S/cm (parallel to the direction of stretching) can be obtained [6,17].

Analogously, the polymer backbone can be partially reduced, “n-doped” by, for example, a solution of sodium naphthalide [18], in THF, viz.,



with a very large increase in conductivity although values as large as those reported for iodine p-doping have not been obtained. The antibonding π^* system is partially populated by this process.

2.2.1.2 Non-Redox Doping

More recently, a non-redox doping process which neither involves adding nor removing electrons from the polymer backbone has been discovered [16]. For instance, a form of polyaniline (emeraldine base) can be doped by a non-redox process [19] which is accomplished by simply protonating the imine nitrogen atoms of the polymer to produce a polysemiquinone radical cation in which both charges and spin are delocalized along the polymer backbone. The conductivity of the polymer increases from 10^{-10} S/cm to $\sim 10^0$ S/cm. This protonic acid doping process has subsequently been extended to poly(heteroaromatic vinylenes) and its derivatives [20].

It should be noted that the non-redox doping of emeraldine base (EB) is not limited to protonic acid dopants. For example, alkylating agents such as $(\text{CH}_3)_2\text{SO}_4$, have been used as “pseudo protonic acid” doping of EB, in which, the CH_3^+ in $(\text{CH}_3)_2\text{SO}_4$ acts as if it were H^+ with respect to its addition to the imine nitrogen [16].

2.2.2 Solitons, Polarons, Bipolarons and Band Structures of Intrinsically Conducting Polymers

The band structure of *trans*-(CH) $_x$, assuming an idealized linear one dimensional molecules, can be regarded as being developed as shown diagrammatically in Figure 2.3, in which the bonding molecular orbitals are π orbitals and antibonding molecular orbitals are π^* orbitals. The formation of filled π band

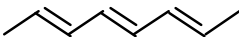
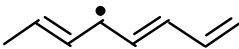
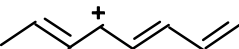
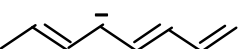
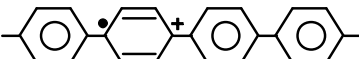
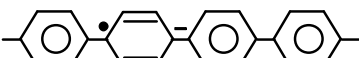
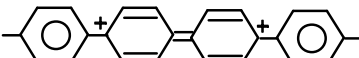
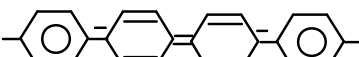
(valence band) can be regarded as by joining together of (CH) units containing an unpaired P_π electron.

Addition of electrons to the conduction band or removal of electrons from the valence band cause a change in the energy level of these bands which results in the formation of new bands. Since *trans*-(CH)_x has a doubly degenerate ground state, i.e., the energy of the molecule is the same regardless of the phasing of the double bonds, one new band is formed in the middle of band gap when the number of electrons in the π system of the molecule is changed. Removal of electron from valence band (oxidation of the π system, p-doping) results in the formation of an empty band, i.e., positive “soliton” band in the band gap. Addition of electron to the conduction band (reduction of the π system, n-doping) results in the formation of a filled band, i.e., negative “soliton” band in the band gap [21].

If a conjugated polymer such as poly(paraphenylene) does not have a degenerate ground state, two new bands will be formed in the band gap when the number of electron in the π system is changed. The upper band in the band gap lies under the bottom of conduction band while the lower band lies above the top of valence band. If the lower band is half filled (p-doping), it is called positive “polaron” band. If the upper band is half filled (n-doping), it is called negative “polaron” band. When both lower band and upper band are empty (p-doping), it is called positive “bipolaron” band. When both lower and upper bands are filled (n-doping), it is called negative “bipolaron” band. A given polymer may consist of polarons at one doping level and bipolarons at a different doping level or consist of significant amounts of polarons and bipolarons with each other under

certain conditions.

The Table below, presents both physical (solid state) and chemical terms of the defects mentioned above.

Physical terms	Chemical terms	
Non-doped state		Undisturbed conjugation
Neutral soliton		Free radical
Positive soliton		Carbocation
Negative soliton		Carbanion
Positive polaron		Radical cation
Negative polaron		Radical anion
Positive bipolaron		Carbocation
Negative bipolaron		Carbodianion

Besides the charged solitons, neutral solitons may be present in the π system of non-doped polyacetylene. The neutral soliton is formed at the point of structural alternation caused by rotation around the single C-C bond [22], i.e., in other words, the conjugation length of the π system of polyacetylene is disrupted by bending and twisting of the molecular chains. In general, a similar effect is also present in doped conducting polymers. This implies that the molecular conformation of conducting polymers is very important in defining the band structure

of a polymer. Since it is assumed that π system of the conducting polymers is completely conjugated in deriving the band structure as shown in Figure 2.3, the decrease of the π conjugation length will increase the band gap between valence band and conduction band which results in a decrease of wavelength of excitation absorption between valence band and conduction band.

2.2.3 Conductivity of Intrinsically Conducting Polymers

It should be held in mind that conducting polymers are not one dimensional conductors, they are quasi one dimensional. If they were truly only one dimensional, no matter how high the conductivity of an individual chain, the bulk conductivity would be zero since a single molecule does not stretch from one end of a bulk piece of a conducting polymer to the other. The electrons have to be transported from one polymer chain to the other. At lower doping levels, this transportation is called “hopping” or “phonon-assisted quantum mechanical tunneling” [23]. At higher doping levels (metallic state), band structure will develop - both along the polymer chains and between chains.

The bulk conductivity of conducting polymer consists of contributions from intramolecular, intermolecular and interdomain, i.e.,

$$\sigma = F(\sigma_{intra}); F(\sigma_{inter}); F(\sigma_{domain}) \quad (2.4)$$

As schematically shown in Figure 2.9 (below), electrons have to move along a polymer chain (intramolecular contribution), then “hopping” to another polymer chain (intermolecular contribution) and from one domain to another (interdomain

contribution) so that the polymer can be electrically conductive.

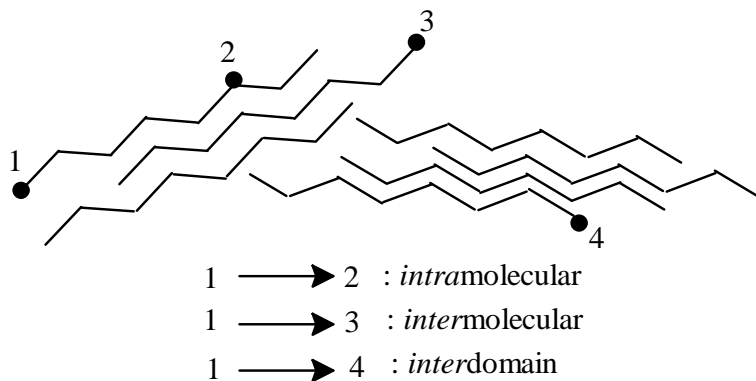


Figure 2.9: Schematic view of contributions of bulk conductivity of conducting polymers.

Interdomain may be from one crystalline region to another crystalline region where the crystallinity of the region is not aligned, or between crystalline region and amorphous regions. Even in highly doped (metallic) polymer, hopping will still occur between domains. Due to the “hopping” nature of charge transportation, the conductivity should increase with decrease the distance between polymer chains. Therefore it is expected that increase in crystallinity or alignment of polymer chains will increase the bulk conductivity of conducting polymers.

2.2.4 The Polyaniline

Polyaniline was first known in 1835 as “aniline black”, a term used for any product obtained by the oxidation of aniline. A few years later, Fritzche [24], carried out the tentative analysis of the products obtained by the chemical oxidation of this aromatic amine. Subsequent investigators [24,25] have verified these results, and similar observations have been made during the oxidation of aqueous

hydrochloride acid solutions of aniline.

The interest in polyaniline as an important conducting polymer has increased significantly over the past decade, resulting in a number of review articles published a few years ago [26-28]. At the same time, a number of groups looked at the reaction conditions necessary to produce optimum quality polyaniline [29-31], but none of these studied the reaction at low temperatures. More recently, reports of high molecular weight polyaniline synthesized at temperatures of between -30°C and -40°C appeared, which used lithium chloride as an inert solute to keep the reaction mixture mobile [32-35]. These used either a large molar deficit of ammonium persulfate oxidant to aniline, which gave a low yield of polymer, or electrochemical polymerization; but no attempts were made to assess the structural quality of the polyaniline.

The polyanilines, probably the earliest known synthetic polymer, [36-38], refer to a large class of conducting polymers which have the following general formula (Figure 2.10):

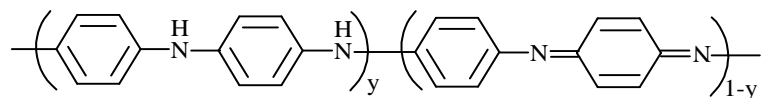


Figure 2.10: Polyaniline general formula.

A large variety of derivatives can be prepared through substitution in the ring or on the N atoms. One of the special properties of polyaniline is that it can be doped by protonic acids. Thus, the properties of the doped polymer can be turned by incorporating different dopant anions.

It has been found that polyaniline can exist in three different, isolable oxidation states at the molecular level [39]. They are the leucoemeraldine oxidation state, the emeraldine oxidation state, and the pernigraniline oxidation state. Other oxidation states are the result of physical mixture of these oxidation states.

(i) Leucoemeraldine base: the fully reduced form of non-doped polyaniline. It is composed solely of reduced units as shown below:

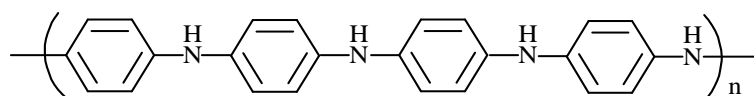


Figure 2.11: Leucoemeraldine Base.

(ii) Pernigraniline base: the fully oxidized form of non-doped polyaniline. It is composed solely of oxidized base units as shown below:

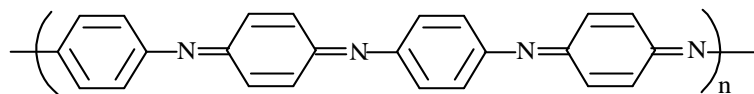


Figure 2.12: Pernigraniline Base.

(iii) Emeraldine base: the intermediate oxidation state of polyaniline. It is composed of equal amounts of alternating reduced base and oxidized base units as shown below:

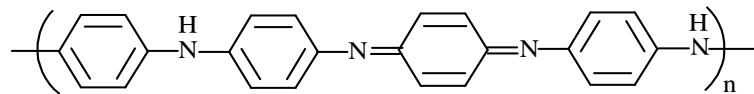


Figure 2.13: Emeraldine Base.

The oxidation state of polyaniline can be precisely determined by volumetric titration methods using TiCl_3 [40]. Several spectroscopic methods such as FTIR, Raman, and Uv/Vis can also provide qualitative information about the average oxidation state of the polymer [41].

2.2.4.1 Methods of Synthesis

Polyaniline can be chemically or electrochemically synthesized by the oxidative polymerization of aniline monomer in the presence of aqueous acid e.g., 1M HCl solution [42]. The formed polymer is called an emeraldine salt. For chemical synthesis, there are many different oxidizing agents, including: ammonium peroxydisulfate [42,43], hydrogen peroxide [44], ferric chloride [45] and ceric nitrate and sulfate [46,47]. Typically the ratio of oxidizing species to aniline has been reported to be oxidant/aniline ~ 1.25 (a stoichiometric equivalent of oxidant) [48,49]. Other chemical polymerization incorporate a stoichiometric deficiency of the oxidant with respect to aniline (oxidant/aniline ratio ~ 0.25) [42].

A typical chemical synthesis of polyaniline is carried out in aqueous 1M HCl at a pH of ~ 0 at temperatures between $\sim 0^\circ\text{C}$ and $\sim -4^\circ\text{C}$ [42]. It has also been shown that higher molecular weight polyaniline ($M_w > 100,000$) can be synthesized when the polymerization is carried out at temperatures below -20°C [50,51]. The neutral form of polyaniline, emeraldine base (EB), can be converted from the fully protonated emeraldine salt by deprotonation of the polymer with aqueous ammonium hydroxide. The ^{13}C [52] and ^{15}N NMR [53] spectra of emeraldine base are consistent with its being composed principally of alternating oxidized

and reduced repeat units.

Polyaniline can also be synthesized electrochemically by the oxidation of aniline on an inert metallic (e.g., Pt) [54-56] electrode or on a piece of conducting Indium Tin Oxide (ITO) glass [57]. Electrochemical polymerization of aniline can be carried out in acidic media by constant potential, constant current, and by repeatedly cycling the applied voltage between two pre-selected potentials. These polymerization methods offer the possibility of conveniently investigating various chemical and physical properties of polyaniline since spectroscopic techniques such as Uv/Vis, EPR, Raman and FTIR may be investigated *in situ*.

2.2.4.2 Polymerization Mechanism

No matter whether polyaniline (PANI) is synthesized electrochemically or chemically, it is generally assumed that there is a close similarity in their polymerization mechanism. In both case, the polymerization process proceeds via the following mechanism:

The first step is the formation of the radical cation by an electron transfer from the $2s$ energy level of the aniline nitrogen atom, as shown in Figure 2.14.

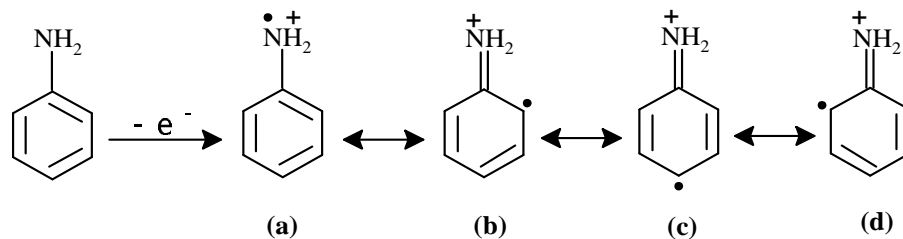


Figure 2.14: The formation of the aniline radical cation and its different resonant structures.

The formed aniline radical cation has several resonant forms, in which (c) is the more reactive one due to its important substituent inductive effect and its absence of steric hindrance.

The next step corresponds to the dimer formation by the so-called “head-to-tail” reaction between the radical cation and its resonant form (most probably form (c)) in acidic medium. Then the dimer is oxidized to form a new radical cation dimer, as shown in Figure 2.15.

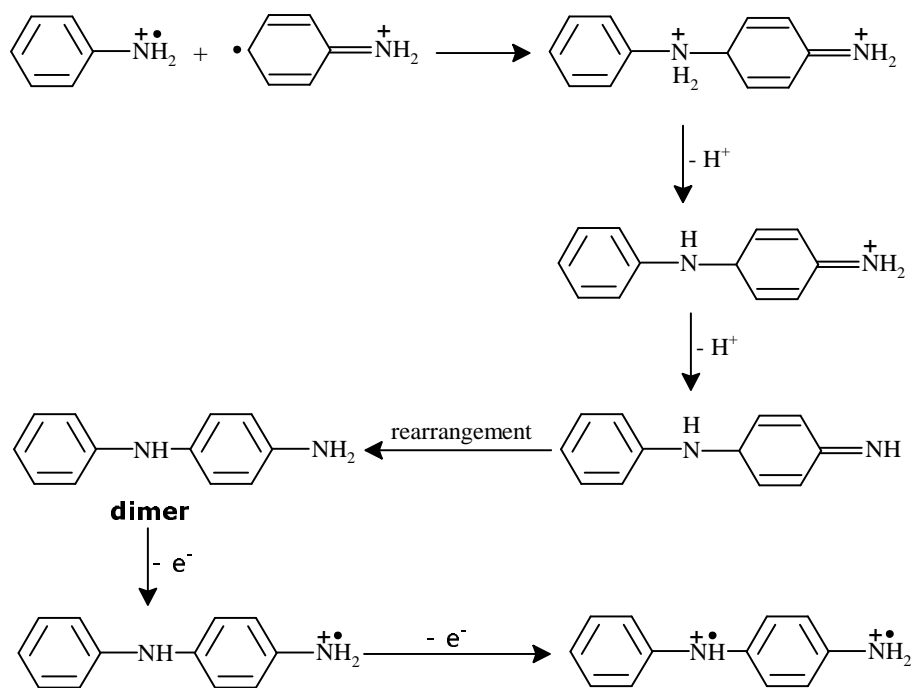


Figure 2.15: Formation of the dimer and its corresponding radical cation.

Next, the formed radical can react either with the radical cation monomer or with the radical cation dimer to form, respectively, a trimer or a tetramer. If this continues, similar to the above steps, the polyaniline (PANI) polymer is finally formed as shown in Figure 2.16.

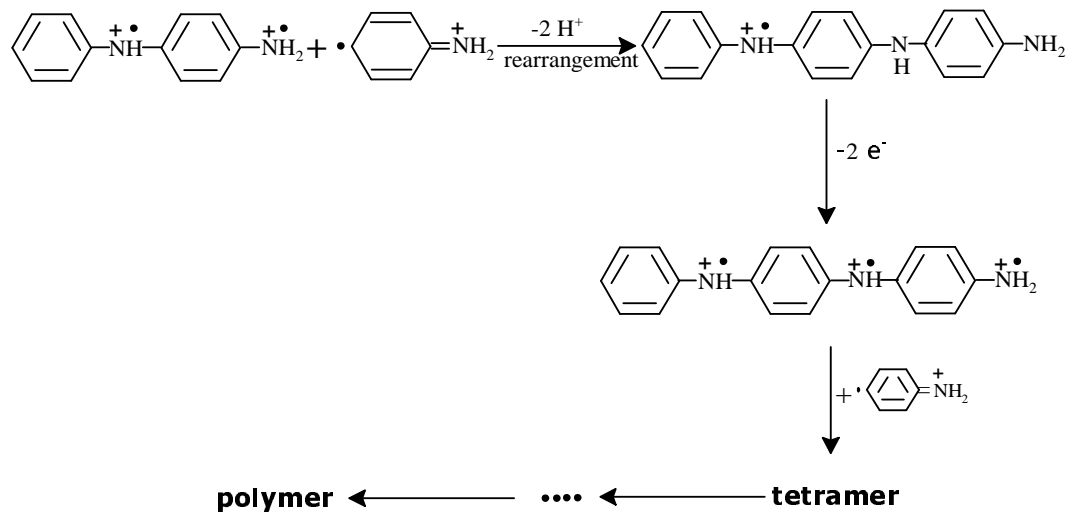


Figure 2.16: One possible way of PANI polymer formation.

At the end, it should be mentioned that beside idealized formation of p-coupled PANI chain in the reactions described above, some side reactions were also identified:

- coupling of aniline and its oligomers in “ortho” position;
- formation of benzidine groups (“tail to tail” coupling);
- chlorine substitution in aromatic ring (in systems with HCl and LiCl or NaCl);
- formation of N=N bonds (azo groups);
- formation of N-C_{Ar} grafting bridges between chains;
- polymer hydrolysis (=O and -OH groups).

All those reactions introduce undesirable elements to the structure of PANI and are considered as chain defects.

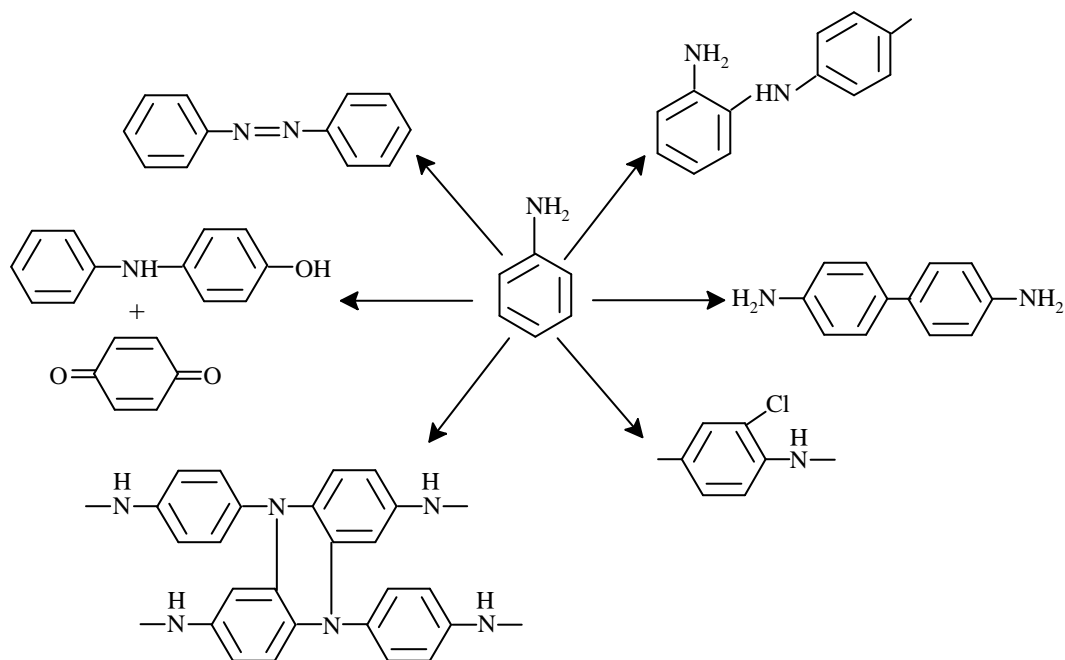


Figure 2.17: Side reaction occurring during polyaniline synthesis.

2.2.4.3 Protonic Acid Doping of Polyaniline

Among the three oxidation states, only the polymer in the emeraldine oxidation state can undergo non-redox doping process to convert it to a highly conductive form. The emeraldine base form of polyaniline was the first example [58] of the “doping” of an organic polymer to a highly conducting metallic regime by a charge transfer process in which the number of electrons associated with the polymer remained unchanged during the doping process. This was first accomplished by treating emeraldine base with aqueous protonic acids as shown below. The conductivity of the doped polymer (by HCl) is ~ 9 to 10 orders of magnitude greater than that of non-doped polymer ($\sim 1\text{-}5$ S/cm; 4 probe; compressed powder pellet). If the “fully doped” i.e., 100 percent protonated (of imine nitrogen

atoms) emeraldine base should have the above dictation i.e., bipolaron constitution as shown, it would be diamagnetic.

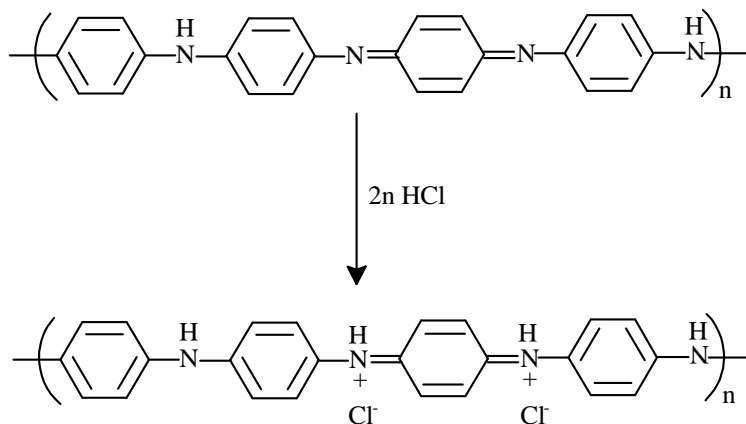


Figure 2.18: Protonic Acid Doping of Polyanilines.

However, extensive magnetic studies [59] have shown that it actually is strongly paramagnetic and that its Pauli (temperature independent) magnetic susceptibility increases linearly with the extent of protonation. These observations and other earlier studies [60] indicate that the doped polymer is a stable polysemiquinone radical cation, one resonance form consisting of two separated polarons as shown in Figure 2.19.

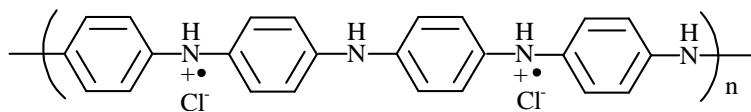


Figure 2.19: A stable polysemiquinone radical cation.

It can also be seen that there is an alternative resonance form where the charge and spin can be placed on the other two nitrogen atoms. This suggests that the

band structure of the doped polyaniline would be expected to have a half-filled lower polaron band.

2.2.4.4 Properties of Polyaniline

(i) Polyanilines electrical properties can be reversibly controlled by charge-transfer doping and protonation.

(ii) Polyaniline is environmentally stable and inert (noble) where stainless steel is corroded.

(iii) Polyaniline is applicable to electrical, electrochemical, and optical applications.

(iv) Polyaniline is currently used in cell phones and calculators, and other LCD technology etc.

2.3 Light Scattering Methods

There are many kind of light scattering [61]. If we limit ourselves just to the methods intended for solutions, there are two broad categories: dynamic light scattering (DLS) and static light scattering (SLS). Light scattering intensity is monitored either in the microsecond or in the second time range domain. This is the basic differences between DLS and SLS, respectively. Fluctuations in the intensity of light scattered by a small volume of a solution in the microsecond time range are directly related to the Brownian motion of the solute. Averaging the intensity over the second time range interval will cause a loss of the solute dynamic properties information; that is why light scattering is named either static

or dynamic. In general, the differences between SLS and DLS are shown as the following:

1. Dynamic light scattering (DLS)

- Alias: quasielastic light scattering, photon correlation spectroscopy, Brillouin scattering (a special variant).
- Relies on rapid fluctuations in the scattered signal.
- Can measure a transport property, the mutual diffusion coefficient, absolutely.
- This size is easily converted to a hydrodynamic radius, R_h .
- The size range is very wide: <1 nm to >500 nm.

2. Static light scattering (SLS)

- Alias: total intensity light scattering.
- Relies on the intensity of scattered light and its variation with concentration of polymer and/or scattering angle.
- Can produce thermodynamic data: molecular weight and virial coefficient.
- Can produce size (for sizes $>$ about 10 nm).
- The size returned is so-called “radius of gyration”, R_g .

2.3.1 Dynamic Light Scattering (DLS)

Dynamic light scattering [62-65] is one of the most popular methods used to determine the size of particles. Shining a monochromatic light beam, such as a laser, onto a solution with spherical particles in Brownian motion causes a Doppler Shift when the light hits the moving particle, changing the wavelength of the incoming light (see in Figure 2.20). This change is related to the size

of the particle. It is possible to compute the sphere size distribution and give a description of the particle's motion in the medium, measuring the diffusion coefficient of the particle and using the autocorrelation function.

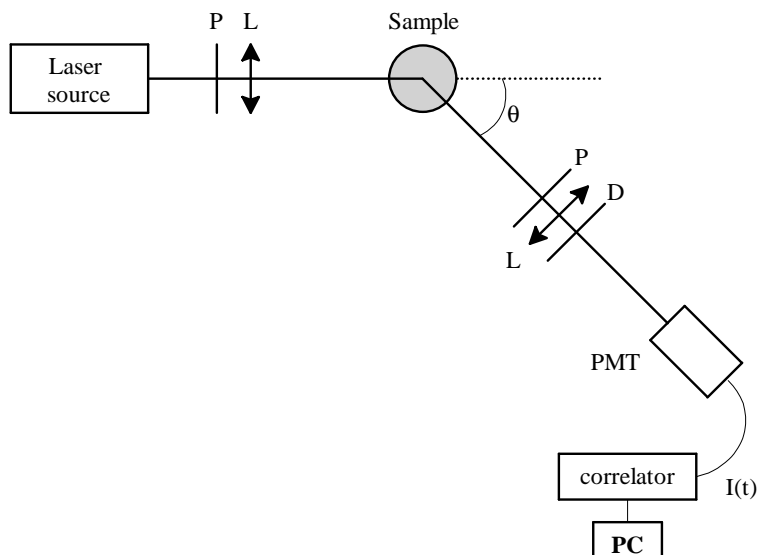


Figure 2.20: Schematic representation of experimental set up for DLS.

In Dynamic Light Scattering, light is scattered by the interaction of the electrons with the incident radiation (only the electric component will be considered here). The oscillating electric field causes a vibration on the electrons turning them into oscillating dipoles. These dipoles reemit radiation. As the electrons are moving sources (due to the Brownian motion) of radiation, the frequency of the radiation is shifted to higher or lower frequencies depending on its velocity and direction relative to the detector (Doppler effect). Molecules in solution move in all directions with equal probability and have a continuous speed distribution, thus a continuous broadening of the spectrum, relative to the incident frequency line (ν_o) is observed. The scattering of light is not exactly elastic, but

quasi-elastic instead. This is why DLS is also named quasi-elastic light scattering (QELS). Because in SLS we are only concerned with the total intensity of the scattered light, ignoring the spectral distribution, SLS is also named intensity light scattering (ILS).

The power spectrum broadening is related to the Brownian motion of the particles in solution and hence to their diffusion coefficient, D , which in turn is related to the size and shape. However, the motion of large molecules is so slow that the broadening in the power spectrum is too small to be studied by interferometry. Therefore, instead of working in the frequency domain, we will work in the time domain (Fourier transform of the power spectrum). And the attention will be focused on how to obtain the time domain function to obtain the characteristic decay time of this function.

Light scattering intensity fluctuations detected in a small volume and in the microsecond time range are related to the Brownian motion of the particles due to density fluctuations, caused by incidental agglomeration of molecules and vibration in the number of molecules in the scattering volume. The diffusion coefficient of the solute can be measured by means of an autocorrelation function ($g_2(t)$). Consider $I_{t'}$, the number of photons arriving at the detector at the time interval t' . The correlation function is built multiplying the number of photons from two successive time intervals and storing the result in the first instrumental channel. This calculation is repeated hundreds of thousands of times, averaged and stored in channel 1. In the successive channels the average products of $I_{t'}I_{t'+t}$, are stored

where t is the delay time:

$$g_2(t) = \langle I_t \bullet I_{i+t} \rangle \quad (2.5)$$

$$\lim_{t \rightarrow 0} g_2(t) = \langle I_t^2 \rangle \quad (2.6)$$

$$\lim_{t \rightarrow \infty} g_2(t) = \langle I_t \rangle^2 \quad (2.7)$$

because correlation is maximal for close instants (most molecules have not collided, yet) and does not exist for very distant instants. For small monodispersed particles and homogeneous spheres of any size the normalized scattered electric field autocorrelation function ($g_1(t)$) is:

$$g_1(t) = e^{-\Gamma t} \quad (2.8)$$

which is related to the intensity correlation function (eqn 2.5) by the Siegert relation (eqn 2.9); the quadratic dependence comes from the relation between the amplitude of the electric wave and the intensity, i.e., the rate of flow of radiation through unit area.

$$g_2(t) = \langle I_t^2 \rangle . b . g_1^2(t) + \langle I_i \rangle^2 \quad (2.9)$$

where b is an instrumental constant that reflects the deviations from ideal correlation (ideally $b=1$) and

$$\Gamma = \frac{D}{q^2} \quad (2.10)$$

$$q = \frac{4n_o\pi}{\lambda} \sin\left(\frac{\theta}{2}\right) \quad (2.11)$$

where D is the diffusion coefficient, and Γ is the reciprocal of the characteristic decay time ($\tau = 1/\Gamma$).

$$g_1(t) = \int_0^\infty G(\Gamma) e^{-\Gamma t} d\Gamma \quad (2.12)$$

$G(\Gamma)$ is the Γ distribution function and can be evaluated by inverse Laplace transform techniques, as $g_1(t)$ is the Laplace transform of $G(\Gamma)$. The most common routine used to perform the inverse Laplace transform (ILT) is CONTIN. CONTIN is a numerical method that starts from a preliminary unsmoothed solution in a frame of equally spaced $\log \Gamma$. After that, a regularization process is used according to statistical criteria. In the end, a “chosen solution” is selected. Such a chosen solution might be misleading; and very high signal-to-noise ratio data are required so that a unique solution can be admitted as the chosen solution. Anyone using CONTIN or related methods should be aware of its limitations and artifacts that might be generated by this routine, including spurious peaks. These artifacts are related to integration processes (e.g., oversmooth and undersmooth), baseline definition (e.g., spurious peaks in skewed distributions), and edge effects (e.g., ripples in the distribution).

If other variables related to Γ are used instead of Γ , a transformation of equation 2.11 has to be considered. The measured D value changes according to angle and concentration:

$$D = D_o \left(1 + k'_D R_E^2 q\right) \cdot (1 + k_D c) \quad (2.13)$$

where k'_D and k_D are constants and $D_o = \lim_{q \rightarrow 0, c \rightarrow 0} D$. D_o is related to the hydrodynamic radius (R_h) by the Stokes-Einstein relationship:

$$D_o = \frac{kT}{6\pi\eta R_h} \quad (2.14)$$

where k is the Boltzmann constant, and η is the solvent viscosity. For broad distributions and even for narrow distributions (i.e., quasi-monodispersed) the

reference D value, commonly named effective diffusion coefficient (D_{eff}) used for calculation is:

$$D_{eff} = \frac{\langle \Gamma \rangle}{q^2} \quad (2.15)$$

The ratio: where $\langle \Gamma \rangle$ is the average value of Γ in a peak. D_{eff} , is the so-called z-average diffusion coefficient (D_z).

$$D_{eff} = \langle D \rangle = \frac{\sum_i w_i M_i D_i}{\sum_i w_i M_i} = D_z \quad (2.16)$$

(D_i is averaged by the scattered intensities since in Rayleigh scattering $I_i \propto n_i V_i^2 \propto w_i M_i$, where V_i is the volume of the particle i and n_i is the number of particles i in solution, per unit volume). Multimodal are usually described by several $\langle \Gamma \rangle$, one for each peak of the distribution. If peaks are overlapped, it is impossible in practical terms to evaluate $\langle \Gamma \rangle$. In this situation it is a common procedure to consider the Γ value where the maximal value of peak occurs (Γ_{max}) instead. If the peaks are symmetrical, this approximation is always valid.

It should be stressed that some methods of data treatment lead to information on average diffusion coefficients over all the distribution function. This is the case, for instance, for the method proposed by Koppel (1972) (CUMULANTS) which results from the application of the statistical cumulants generating function. (The cumulants generating function of $G_x(t)$ is simply defined as $G_x(t) = \ln(G_x(t))$). If the constant baseline has already been subtracted from $g_2(t)$ the plot of $\ln(g_2(t))$ versus t should be strictly linear for a monodispersed system. Any deviation from the linear dependence is indicative of polydispersity.

2.3.2 Static Light Scattering (SLS)

Static light scattering [66-68] intensity integrated over a period of time of seconds or more varies with the measurement angle and concentration according to (Zimm, 1948):

$$\frac{K.c}{R_\theta} = \frac{1}{MP_\theta} + 2A_2c \quad (2.17)$$

$$K = \frac{4\pi^2 n_o^2}{N_A \lambda^4} \left(\frac{dn}{dc} \right)^2 \quad (2.18)$$

$$R_\theta = \frac{d^2}{\sin^2 \theta_z} \frac{I_s}{I_o} \quad (2.19)$$

where;

c : represents concentration,

I_o : is the intensity of the incident light (vertical polarization),

I_s : is the scattered light intensity,

θ_z : is the measurement angle relative to the vertical axis,

d : is the sample-detector distance,

n_o : is the refractive index of the solvent,

n : is the refractive index of the solution,

A_2 : is the second virial coefficient (which accounts for interparticle interaction),

M : is the molecular weight, and,

$$P_\theta = \frac{I_{s,\theta}}{I_{s,\theta=0}} \quad (2.20)$$

is the intra-particle structure factor, which accounts for the interference of light scattered from different points in the same molecule or molecular assembly. P_θ

can be evaluated by (e.g., Oster, 1972):

$$P_\theta \approx 1 - \frac{16\pi^2 n_o^2 R_g^2}{3\lambda^2} \sin^2\left(\frac{\theta}{2}\right) \quad (2.21)$$

where R_g is the radius of gyration.

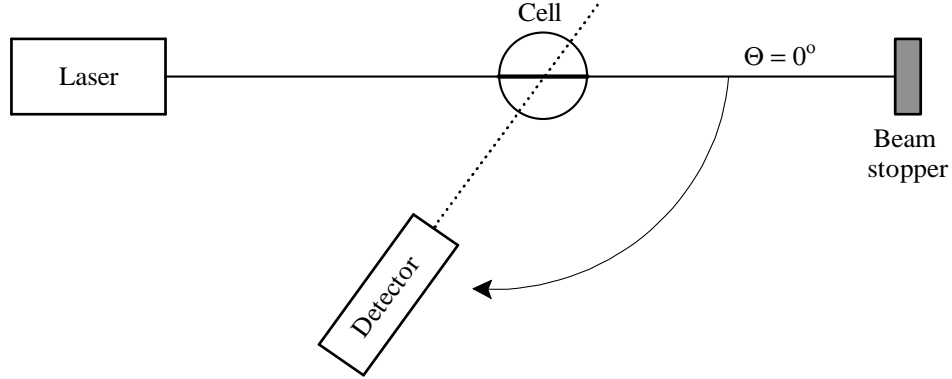


Figure 2.21: Schematic representation of a light scattering apparatus. Light scattering intensities are recorded according to sample concentration and angle (by means of a goniometer). The detector might rotate, as depicted, or be fixed and connected to an optical fiber supported by the rotating arm. In any case, the detection device and the laser source must be aligned toward the geometrical center of the sample cell. The measurement angle (θ) origin is the way of the transmitted laser beam.

If the samples are polydisperse, then the values of M , R_g , and A_2 obtained by means of equation 2.17 are averaged. Textbooks and scientific papers often mention the averaged M ($\langle M \rangle$) as the weight average molecular weight (M_w), but a demonstration is hard to find. Moreover, what kind of average is obtained for R_g , and A_2 is usually overlooked. It is demonstrated that:

$$\langle M \rangle = \frac{\sum_i w_i M_i}{\sum_i w_i} = M_w \quad (2.22)$$

$$\langle R_g^2 \rangle^{1/2} = \left(\frac{\sum_i w_i R_{g,i}^2}{\sum_i w_i} \right)^{1/2} \quad (2.23)$$

$$\langle A_2 \rangle = \frac{\sum_i w_i^2 M_i A_{2,i}}{\sum_i w_i \sum_i w_i M_i} \quad (2.24)$$

where w_i , M_i , $R_{g,i}$, and $A_{2,i}$ represent the total mass, molecular weight, radius of gyration, and second virial coefficient, respectively, of kind i particles, in a polydisperse sample. The parameters between angle brackets represent the average value.

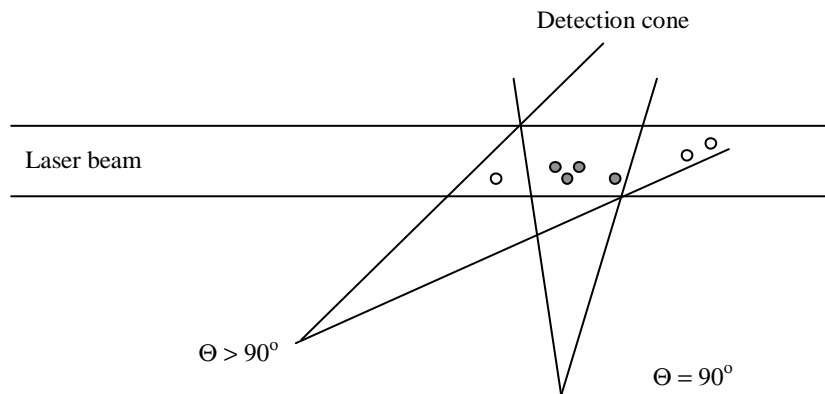


Figure 2.22: A geometrical effect has to be considered when light scattering intensities are recorded according to angle. As the detection angle deviates from 90° , the probed volume increases, including particles that are not detected at right angle (open circles). This geometric effect is corrected by a sinus function.

The comparison of R_h with the radius of the gyration R_g which can be determined from static light scattering measurements was as parameter ρ (BURCHARD, 1979):

$$\rho = \frac{R_g}{R_h} \quad (2.25)$$

For polydisperse coil $\rho=1,73$; for spheres $\rho= 0,775$.

2.3.3 Advantages and Disadvantages of Light Scattering

I. Advantages

1. Capable of absolute measurements of several parameters of interest (molecular weight, mean square radius of gyration, translational diffusion coefficient, second virial coefficient).
2. Useful over a very wide range of molecular weight and provides well-defined average properties of heterodisperse polymers.
3. May be utilized as an on-line detector in chromatographic separations, such as for size exclusion chromatography.
4. May be able to elucidate intermolecular association in solution.

II. Disadvantages

1. Requires a solvent with a different refractive index than the solute (or dispersed particle), scrupulous removal of extraneous scattering moieties (“dust”), and may require dialysis of solutes in a mixed solvent (e.g., an aqueous salt solution).
2. Analysis may be difficult with copolymers, and may not be suitable for very low molecular weight solute or with strongly absorbing system.
3. Results may be biased by a small fraction of an aggregated species.

2.4 Viscosity

Polymer molecules [69-72] in a dilute solution exist as ball like with the diameter determined by the radius of gyration. The radius of gyration depends

on the interaction of the polymer molecule with the solvent. When the concentration of the polymer increases, the number of balls increases until they start interacting each other. This structure is seen in a semidilute concentration. In a concentrated solution, the polymer molecules no longer exist as separate balls but interact each other. In a sense a polymer chain is a solvent of another chain. As a polymer chain is a good solvent of itself, the polymer chains are much more stretched and sometimes the chains form molecular entanglement if the molecular weight is above a certain value. This special molecular weight is called the *entanglement molecular weight*. For atactic polystyrene, the entanglement molecular weight is around 37,000. A schematic diagram of the molecules in solution is shown in Figure 2.23.

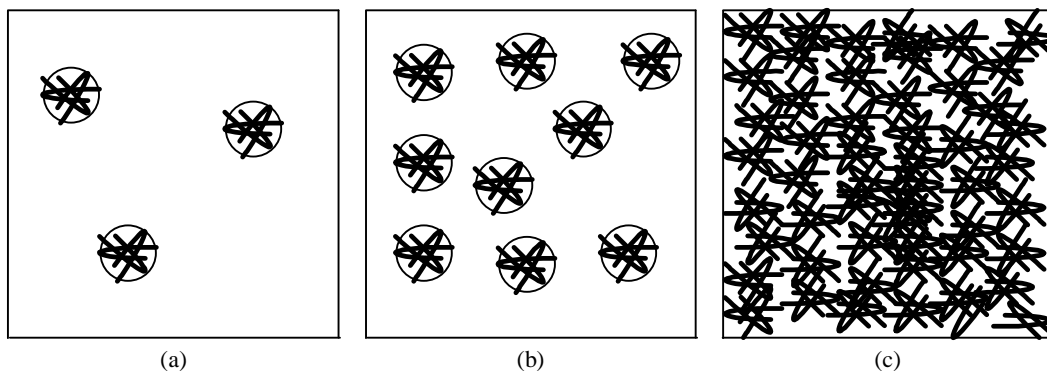


Figure 2.23: A schematic diagram of the polymer molecules in solution (a) Dilute solution, (b) Semi-dilute solution, and (c) Concentrated solution.

When solvent molecules move through these polymer balls, the solvent receives resistance. The difficulty to flow is expressed by a quantity called *viscosity*, η . The higher the viscosity, the more difficult to move around. Since the viscosity of a polymer solution is a function of the polymer in the solution, the solution

viscosity, η , can be expressed in terms of the viscosity of the solvent, η_o , and the concentration of the polymer molecules, C .

$$\eta = \eta_o \left(1 + aC + bC^2 + \dots \right) \quad (2.26)$$

The coefficient a relates to the properties of the individual polymer chain and the coefficient b relates to the polymer-solvent interaction. In order to obtain the quantity a , the above equation is extrapolated to $C=0$. Thus, the higher terms can be ignored.

$$\lim_{C \rightarrow 0} \frac{\eta - \eta_o}{\eta_o C} = a \quad (2.27)$$

Thus quantity a is called intrinsic viscosity, $[\eta]$. The ratio between the solution and the solvent viscosities is called *relative viscosity*, $\eta_r = \eta/\eta_o$. According to Einstein, the viscosity of a very dilute solution with spheres can be expressed as follows.

$$\eta = \eta_o \left(1 + \frac{5}{2} \phi \right) \quad (2.28)$$

where ϕ is the *packing fraction*. In general, the intrinsic viscosity of a polymer is expressed by the following equation.

$$[\eta] = KM^a \quad (2.29)$$

where $0.5 \leq a \leq 0.8$. This equation is called *Mark-Howwink-Sakurada equation*.

2.5 Carbon Nanotubes and Conducting Polymers

Carbon nanotubes can be broadly classified into two types, one is called single-walled carbon nanotubes (SWNT) and the other is called multi-walled carbon

nanotube (MWNT). SWNT is simply a rolled-up graphene tube with a half fullerene molecule at both ends, while MWNT are concentric graphene sheets rolled-up together with a large annular space in the center.

Carbon nanotubes (CNTs) were first discovered in 1991 by Iijima [73] with their novel carbon structure consisting of multi-layer concentric hollow fibres with nanometer scale diameters. Since then, carbon nanotubes have been proven to possess extraordinary properties, such as high tensile strength (100 GPa), high Young's modulus (0.6 TPa) [74], and exceptional electrical conductivity (5000 S/cm) [75]. These properties have led to the use of carbon nanotubes as sensors [76], super capacitors [77], actuators [78], and conductive yarns [79]. The remarkable properties of carbon nanotubes not only make them a new class of functional materials, but also make them potentially useful as reinforcement fillers within a host polymer matrix. The formation of carbon nanotubes/polymer composites is considered as an approach for fabricating promising polymer based devices [80-84].

The first composite was prepared by Ajayan et al. [85] through mechanically mixing the multi-walled carbon nanotubes (MWNTs) and epoxy resin. Cran et al. [83] reported that carbon nanotube powder was mixed with poly(m-phenylenevinylene-co-2,5-dioctoxy-p-phenylenevinylene)(PmPV) to get CNT/PmPV composite. It has been reported that the incorporation of carbon nanotubes into a polymer matrix improves the electrical conductivity as well as the mechanical properties of the original polymer [86-90].

As described earlier, among the wide range of conducting polymers, polyaniline (PANI) is a unique and promising material due to its good processability, environmental stability and switching properties by both charge-transfer doping and protonation. Consequently CNT/PANI composites have drawn more attention and have been reported on by several groups of researchers [91-93]. CNT/PANI composites can be formed by both in-situ chemical [92,94-96] or electrochemical polymerization [97,98] of aniline in presence of carbon nanotubes and ex-situ dispersion of carbon nanotubes into the polyaniline solution [99-103]. In this thesis, only in-situ polymerization of CNT/PANI composites were used.

2.6 Conducting Polymer and Thermoplastic Composites

Electrically conductive composites with a thermoplastic matrix are considered to be an important group of relatively inexpensive materials for special applications. Conductivity in a highly insulating matrix is achieved by the admixtures of conductive additives, for example, fine metal powder or conductive polymers [104-107]. Conducting polymers such as polyaniline and polypyrrole exhibit excellent electrical conductivities and outstanding thermal stability, while their chemical solubility and mechanical properties are poor leading to a reduced processability [108-111]. To overcome these difficulties most research efforts were focused on the chemical functionalization of such conducting polymers and on composites of conducting polymers with elastomers [107-112].

A straightforward application of these materials is the fabrication of conductive plastics which would combine electrical conductivity with good mechanical

properties and, if possible, high transparency. This is not an easy task for two principal reasons: (i) mechanical properties of the neat conductive polymers are poor, and (ii) conductive polymers exhibit very high extinction coefficients for visible light which make them opaque even for relatively thin films. A solution to this problem is the preparation of low percolation threshold conductive polymer blends with commercially available industrial polymers [113]

A proper balance among the electrical conductivity, mechanical properties, and processing characteristics is an important requirement for the design of electroconductive thermoplastic composites. It is well known that, at low loading of the conductive filler, a modest conductivity increase is observed with an increasing filler content. A sudden conductivity increase occurs in a relatively narrow concentration range around the so-called percolation threshold. At this concentration, a conductive network is formed within the insulating phase and a dramatic increase in conductivity by several orders of magnitude is observed. This phenomenon was broadly studied and well described in numerous articles and several reviews [114-116].

The presence of a filler in a thermoplastic matrix [117] has a significant effect on the behavior of the material, especially regarding mechanical properties and processing characteristics. The presence of a filler leads usually to higher stiffness of the material, demonstrated by an increase in the Young's modulus and a decrease in deformability and toughness. The extent of these changes depends on the concentration and on the parameters of the filler, especially on the filler surface area, which is decisive for the filler-reinforcing ability. An addition of the

filler results always in a more difficult processing because of the increase of the melt viscosity.

In this thesis, the electrical, mechanical, thermal, and morphological properties of low density polyethylene (LDPE)- which has excellent flexibility, extensibility, and widely used to blow film, to produce vessels and to extrude pipe, etc., but it has drawbacks such as poor rigidity and low softening point and hence limits its application scope to some extent- and polyaniline (PANI) (LDPE/PANI) composites were investigated.

2.7 Mechanical Properties of Composites

The mechanical behavior of a material reflects the relationship between its response or deformation to an applied load or force. Important mechanical properties are strength, hardness, ductility, and stiffness.

One of the most common mechanical stress-strain tests is performed in tension. The tension test can be used to ascertain several mechanical properties of materials that are important in design. The output of such a tensile test is recorded on a strip chart as load or force versus elongation. These load-deformation characteristics are dependent on the specimen size. For example, it will require twice the load to produce the same elongation if the cross-sectional area of the specimen is doubled. To minimize these geometrical factors, load and elongation are normalized to the respective parameters of engineering stress and engineering strain.

Engineering stress σ is defined by the relationship:

$$\sigma = \frac{F}{A_o} \quad (2.30)$$

in which F is the instantaneous load applied perpendicular to the specimen cross section, in units of pounds force (lb_f) or Newtons (N), and A_o is the original cross-sectional area before any load is applied (in^2 or m^2). The units of engineering stress are pounds force per square inch, psi, or megapascals MPa. Engineering strain ε is defined according to:

$$\varepsilon = \frac{l_i - l_o}{l_o} = \frac{\Delta l}{l_o} \quad (2.31)$$

in which l_o is the original length before any load is applied, and l_i is the instantaneous length. Sometimes the quantity $l_i - l_o$ is denoted as Δl , and is the deformation elongation or change in length at some instant, as referenced to the original length. Engineering strain is unitless, but inches per inches or meters per meters are often used; the value of strain is obviously independent of the unit system. Sometimes strain is also expressed as a percentage, in which the strain value is multiplied by 100.

Deformation in which stress and strain are proportional is called elastic deformation; a plot of stress (ordinate) versus strain (abscissa) results in a linear relationship. The slope of this linear segment corresponding to the modulus of elasticity. This modulus may be thought of as stiffness, or a material's resistance to elastic deformation. The greater the modulus, the stiffer the material, or the smaller the elastic strain that results from the application of a given stress.

The modulus is important design parameter used for computing elastic deflections. Elastic deformation is nonpermanent, which means that when the applied load is released, the piece returns to its original shape. Plastic deformation, from an atomic perspective, corresponds to the breaking of bonds with original atoms neighbors and then reforming bonds with new neighbors as large numbers of atoms or molecules relative to one another; upon removal of the stress they do not return to their original positions. The mechanism of this deformation is different for crystalline and amorphous materials. For crystalline solids, deformation is accomplished by means of a process called slip. Plastic deformation in noncrystalline solids as well as liquids occurs by a viscous mechanism.

Most structures are designed to ensure that elastic deformation will result when a stress is applied. It is therefore desirable to know the stress level at which plastic deformation begins, or where the phenomenon of yielding occurs. After yielding, the necessary to continue plastic deformation increases to a maximum and then decreases to the eventual fracture. The tensile strength TS (psi or MPa) is the stress at the maximum on the engineering stress-strain curve. This corresponds to the maximum stress that can be sustained by a structure in tension; if this stress is applied and maintained, fracture will result. All deformation up to this point is uniform throughout the narrow region of the tensile specimen. However, at this maximum stress, a small constriction or neck begins to form at some point, and all subsequent of deformation is confined at this neck. This phenomenon is termed “necking”, and fracture ultimately occurs at the neck. The fracture or rupture strength corresponds to the stress at fracture [118,119].

CHAPTER 3

MATERIALS AND INSTRUMENTATION

3.1 Materials

Acids and bases used in this thesis, including hydrochloric acid (HCl, 37%), and ammonium hydroxide (NH_4OH , 24%) were used as purchased from Aldrich Chemicals Co. In all cases where solution of an acid or base in a specific concentration was needed, the solution was made using deionized water.

Ammonium peroxydisulfate (used as oxidant) [$(\text{NH}_4)_2\text{S}_2\text{O}_8$, 98%] and phenyl hydrazine (used as reductant) ($\text{C}_6\text{H}_5\text{NHNH}_2$, 97%) were used as received from Aldrich Chemicals Co.

N-methyl-2-pyrrolidinone (NMP, 99%, water content less than 0.01%, density of 1.032 g/cm^3 , viscosity of 0.002 Pas, melting point range of -24°C , and boiling point of $78\text{-}79^\circ\text{C}$), toluene ($\text{C}_6\text{H}_5\text{CH}_3$, 99.5%, water content less than 0.0075%) from Aldrich Chemicals Co., and acetone (99.9%) from Merck, were used as received. Finally, aniline monomer from Merck was distilled and stored under

0°C before use. Low density polyethylene (LDPE, obtained from Petkim), Multi-Wall carbon nanotubes (from Nanocyl S.A), lithium chloride (LiCl), a mobile phase, obtained from Aldrich Chemicals Co., were used as received.

Table 3.1: Some properties of Low Density Polyethylene

Property	Unit	Value	Method of Measurement
Melt Flow Index (2.16 kg, 190°C)	g/10 min.	2.0-3.5	ASTM D-1238, TS-1675
Density (23°C)	g/cm ³	0.918-0.822	ASTM D-1505, TS-1818
Film Quality	-	A	Alkathene 36
Ash	% wt	0.20	ALKT-509
Permeability	%	4.9	ASTM D-1003
Brilliance	-	76	ASTM D-2457

Table 3.2: Characteristics of Multi Wall Nanotubes (Nanocyl-7000)

Property	Unit	Value	Method of Measurement
Average diameter	nanometers	10	TEM
Length	microns	0.1-10	TEM
Carbon Purity	%	90	TGA
Metal Oxide (impurity)	%	10	TGA
Surface area	m ² /g	250-300	BET

3.2 Instrumentation

3.2.1 DC-Conductivity Measurements

For measuring the conductivity of a sample with resistance in the range of kilohms to megaohms, a simple two-probe technique is sufficient. For materials

having high conductivity, the resistance of the electrical contacts between the probe and the sample may be relatively large compared to the resistance of the sample itself. Because of this, a simple two-probe technique is usually inadequate. The problem is eliminated by using the four-probe technique [120].

For measurement of conductivity of compressed pellet and composite's films, a four point colinear method [120] was employed as shown in Figure 3.1. The four point contacts (labeled 1-4) are made on the surface of the sample in a linear array. A current (I) is passed through the outer contacts (1 and 4) and the voltage drop (V) across probes 2 and 3 is measured.

The conductivity (σ) of the compressed pellet is given by:

$$\sigma = \left(\frac{\ln 2}{\pi t} \right) \left(\frac{I}{V} \right) \quad (3.1)$$

Where ; σ is the conductivity of the film (in S/cm), I is the current applied between probes 1 and 4 (in mA), V is the voltage drop across probes 2 and 3 (in mV), and t is the thickness of the pellet.

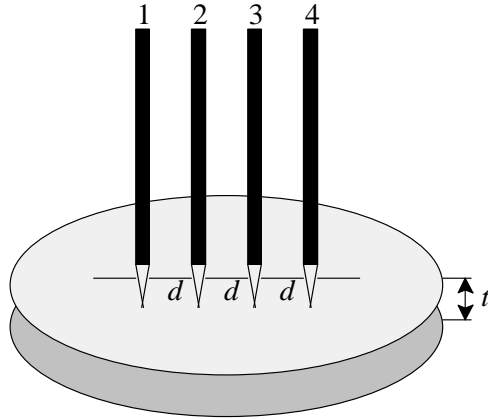


Figure 3.1: Four point collinear probe method.

3.2.2 Elemental Analysis

Elemental analysis were carried out by using a Perkin-Elmer model 240 CHN analyzer. Acetanilide was used as primary standard for calibration of the instrument. It usually took two runs for analysis of polyaniline emeraldine base powder. The first run was taken on the polyaniline powder itself so that accurate hydrogen content was obtained. The second run was performed on the same batch of polyaniline powder which was mixed with 2~3 drops of 1M HCl after weighing of the polyaniline powder so that accurate carbon and nitrogen contents were obtained. The final reported results of polyaniline emeraldine base powder were a combination of these two runs, i.e., hydrogen value from the first run and carbon and nitrogen from the second run.

3.2.3 Thermal Analysis

Thermal analysis can be used to detect the physical or chemical changes in a material related to thermal properties. This technique includes thermogravimetric analysis (TGA), differential scanning calorimetry (DSC), and differential thermal analysis(DTA).

3.2.3.1 Thermogravimetric Analysis

Thermogravimetric analysis (TGA) is a technique that permits the continuous weighing of a sample as a function of temperature and/or as a function of time at a desired temperature [121].

In TGA, the sample is heated at a rate between 5°C and 10°C/min, from

room temperature up to 1700°C. The experiments involve several combinations of programmed and isothermal steps. TGA experiments can be conducted in various atmospheres, e.g., vacuum or static flowing inert gases. Modern instruments coupled with mass spectrometry (TGA/MS) offer the possibility for identifying the nature of the weight changes revealed by TGA.

In this thesis, TGA was used to determine the weight change of polyaniline powder, polyaniline-multi wall carbon nanotubes composites and polyethylene-polyaniline composites with respect to applied temperature. The instruments used were either a Perkin Elmer Pyris1 Thermal Gravimetric Analyzer system equipped with a computer or a DuPont 2100 thermal analyzer system. All experiments were performed in a inert static flowing gas such as argon or nitrogen gases. The temperature was increased at a rate of 10°C/min from room temperature to 1000°C.

3.2.3.2 Differential Scanning Calorimetry

Many of the physical (e.g., evaporation) or chemical (e.g., decomposition) transformation are associated with heat absorption (endothermic) or heat liberation (exothermic) [121]. Differential Scanning Calorimetry (DSC) measures the differential heat between an inert reference and the sample upon heating or cooling at a particular rate or under isothermal conditions. Only in the case of a thermal event characteristic of a particular material, will a differential heat flow exist and DSC will register a signal.

DSC has found applications in almost every class of materials. Examples include evaluation of phase transformation (glass transition, melting, solidification, etc.), decomposition, polymerization, gelation, and curing; evaluation of processing, thermal, and mechanical histories and process modeling.

In this thesis, DSC was carried out on a DuPont 2100 thermal analyzer system equipped with appropriate modules and interface.

3.2.4 Fourier Transform Infrared Spectroscopy

Fourier Transform Infrared Spectroscopy (FTIR) method allows one to characterize vibrations in molecules by measuring the absorption of light of certain energies that correspond to the vibrational excitation of the molecules from lower to higher states. For the purpose of this thesis, Bruker IFS 66/S FTIR spectrometer was used to characterize all the samples.

3.2.5 Solid-State ^{13}C -NMR

Nuclear magnetic resonance (NMR) is one of the most important techniques for determination of chemical structure, yielding detailed conformational and configurational information as well as information about the molecular dynamics and interactions of molecules in solution. In this thesis solid-state ^{13}C -NMR spectra were obtained either on a Bruker AC-250 spectrometer or on a Bruker AMX-11 500 spectrometer. Unfortunately, we could not carry out the solution-state ^{13}C -NMR due to the solvent used to dissolve the polyaniline (emeraldine base). This solvent (N-methyl-2-pyrrolidinone, anhydrous) was not used by NMR

instruments in both Chemistry Department and Central Laboratory.

3.2.6 X-Ray Powder Diffraction Analysis

Wide Angle X-Ray powder diffraction is used to obtain information about the structure, composition, and state of polyaniline materials. Some typical applications are: identification of an unknown based on the crystalline peaks, variable temperature studies, precise measurements of lattice constant and residual strains, and refinement of atomic coordinates [122].

In common with other types of electromagnetic radiations, interaction between the electric vector of X-Radiation and the electrons of the matter through which it passes results in scattering. When X-Ray are scattered by the ordered environment in a crystal, interference (both constructive and destructive) takes place among the scattered rays because the distances between the scattered centers are of the same order of magnitude as the wavelength of the radiation. Diffraction is the result. The requirements for X-Ray diffraction are : (1) the spacing between layers of atoms must be roughly the same as the wavelength of the radiation and (2) the scattering center must be spatially distributed in a higher regular way. The X-Ray, however, appear to be reflected from a crystal only if the angle of incidence satisfies the Bragg equation:

$$n\lambda = 2d \sin \theta \quad (3.2)$$

Where θ is the angle at which the constructive interference of the X-Ray beam occurs, n is an integer, λ is the wavelength of X-Ray used, and d is the interplanar

distance of the crystal.

The X-Ray diffraction method is the most powerful technique available for the examination of polymers in the solid state. The following types of information can be obtained: (1) estimate of the degree of crystallinity; (2) determination of the extent of orientation of crystalline; (3) analysis of the “macrostructure”-the way in which the crystallites or bundles of chains are packed together; and (4) determination of the molecular structure, including the chain conformation and the position of individual atoms. The wide-angle X-Ray diffraction (WAXD) experiments in this thesis were performed on a Rigaku Miniflex X-Ray diffractometer. Cu-K α anode radiation, generated at a generator tension of 30 kV and a generator current of 15 mA was used as the X-Ray source. The diffraction patterns were collected at a diffraction angle 2θ from 5° to 60° at a scanning rate and step size of $1^\circ/\text{min}$ and 0.05° , respectively. The diffraction instrument is interfaced with a computer, which controls and analyzes the X-Ray diffraction data. All X-Ray measurements were performed at room temperature.

3.2.7 Light Scattering Methods

One important method for the characterization of particles in the solution phase involves scattering visible light in the solution. The theory behind light scattering in gases was first proposed by Rayleigh in the late 1800's, and Smoluchowski and Einstein extended light scattering theory to liquids in 1908 and 1910 respectively. These two scientists proposed that the patterns of light scattered from a pure liquid are caused by irregularities in the medium due to random

thermal motion. In a solvent/solute system, light scattering is also caused by small variations in the solute concentration [123].

Static and dynamic light scattering are two different experimental methods for measuring the patterns of light scattered from a solvent/solute system. Static light scattering measures light intensity as a function of scattering angle and solute concentration. This allows the determination of average molecular weight, radius of gyration, and shape information for the solute. Dynamic light scattering (DLS) is an experimental method which uses the intensity and polarization of light scattered from a solution to characterize the size, shape, and interactions of the particles in a solution. Photon correlation is the most common way to analyze dynamic light scattering data [124].

Static and dynamic light scattering give complementary pieces of information, and for this reason they are commonly used in tandem for characterization of polymer solutions [124]. In this thesis, static and dynamic light scattering were used to characterize the polydispersity, effective diameter and average molecular weight of reduced form of polyaniline (Leucoemeraldine base). For this purpose, two different instruments were used. The instruments used in this thesis were ALV/CGS-3 Compact Goniometer System with ALV/LSE-5003 Correlator, and DAWN-B Laser photometer produced Wyatt-Technology Corporation for dynamic and static light scattering, respectively.

3.2.8 Intrinsic Viscosity Measurement

One of the most precise measurements in polymer science is also the simplest and cheapest. Intrinsic viscosity, which is measured from the flow time of a solution through a simple glass capillary, has considerable historical importance for establishing the very existence of polymer molecules. It also provides considerable physical insight.

The most useful kind of viscometer for determining intrinsic viscosity is the “suspended level” or Ubbelohde viscometer. The viscometer is called “suspended level” because the liquid initially drawn into the small upper bulb is not connected to the reservoir as it flows down the capillary during measurement. The capillary is suspended above the reservoir. In conjunction with the pressure-equalization tube, this ensures that the only pressure difference between the top of the bulb and the bottom of the capillary is that due to the hydrostatic pressure-i.e., the weight of the liquid. Other designs, e.g., the Cannon-Fenske viscometer, do not provide for this, and will give erroneous results in an intrinsic viscosity determination. Such viscometers are useful in other experiments-e.g., checking the stability of some polymer solution, where one is only interested in measuring a change in the flow time.

3.2.9 Scanning Electron Microscope

Scanning electron microscope (SEM) is widely used for the study of the morphology and microstructure of conducting polymers. It involves scanning of an

electron beam across a sample surface and secondary electrons are ejected from the surface. Upon interacting with a solid, secondary electron images are generated by synchronizing the optical output of the detector system with the raster of the electron probe across the solid surface. SEM images are used to examine the surface morphology and microstructure or to investigate the inner microstructure from fracture cross-sections.

The instrument used in this thesis was JEOL JSM-6400 low voltage (20 kV) scanning electron microscope.

3.2.10 Tensile Strength

Tensile testes were performed by Lloyd Universal Testing Machine for all specimens. Tests were done according to ASTM D638 (Standard Test Method for Tensile Properties of Plastics). The dimensions of the specimens were specified according to Type-IV in this standard. The shape and the dimensions of the specimens used in this thesis are illustrated in Figure 3.2, below. The extension rate was 5 mm/min.

The stress-strain values were calculated from the load (F)-elongation (ΔL) values during the test by the following relations:

$$\sigma = \frac{F}{A_o} \quad (3.3)$$

Where σ (MPa), is the tensile stress, F , is the axial load (N) applied, and A_o (mm^2) is the initial cross sectional area of the specimen. Strain, ε , is defined as:

$$\varepsilon = \frac{\Delta L}{L_o} \quad (3.4)$$

Where L_o (mm), is the original gauge length of the test specimen, and ΔL (mm), is the elongation. The elastic modulus, E (MPa), which is the slope of the linear part of the stress-strain curve, can also be calculated from the relation:

$$E = \frac{\Delta\sigma}{\Delta\varepsilon} \quad (3.5)$$

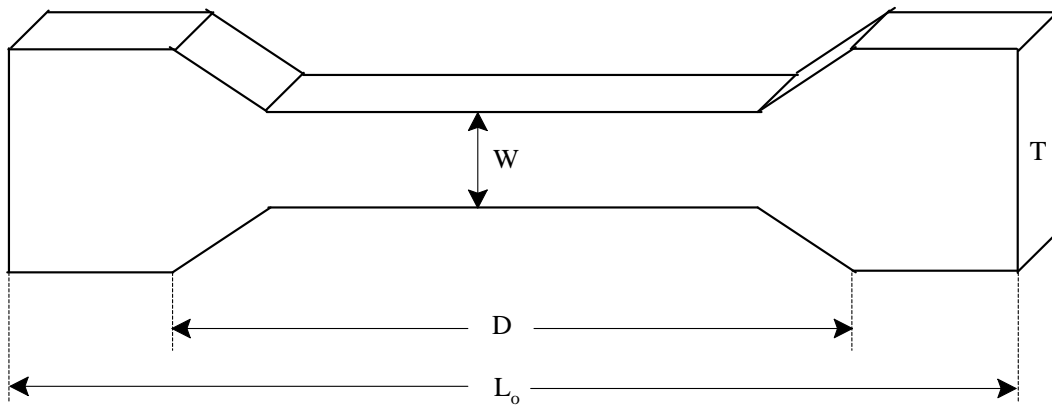


Figure 3.2: Tensile test specimen according to ASTM.

W , width of narrow section : 4.4 mm

D , distance between grips : 50 mm

L_o , total length of specimen : 110 mm

T , thickness of specimen : 2.05 mm

CHAPTER 4

EXPERIMENTAL PROCEDURES

4.1 Synthesis of Polyaniline (Emeraldine Base) at 25°C

Ammonium peroxydisulfate, $(\text{NH}_4)_2\text{S}_2\text{O}_8$ (12.3 g, ~ 0.054 mol), was dissolved in 70 ml of 1M HCl in a 500 ml beaker and kept at 25°C. Aniline (5 g, 0.054 mol), was dissolved in 75 ml of 1M HCl in another 500 ml beaker and also kept at 25°C. Then, ammonium peroxodisulfate solution was added slowly to the aniline solution over a period of ~ 1 minute. The flask was left for 30 minutes, during which the temperature remained constant at 25°C. The reaction is shown in Figure 4.1.

The solution started to take on a blue-green tint after one to three minutes, then became intense blue green with a coppery glint. After 30 minutes, the precipitate was collected on a Büchner funnel and flask using a water aspirator. The precipitate cake was washed portionwise (80 ml/portion) with deionized water until the filtrate became colorless. The liquid level in the filter should be constantly adjusted to be above the top of the precipitate. This prevented cracking

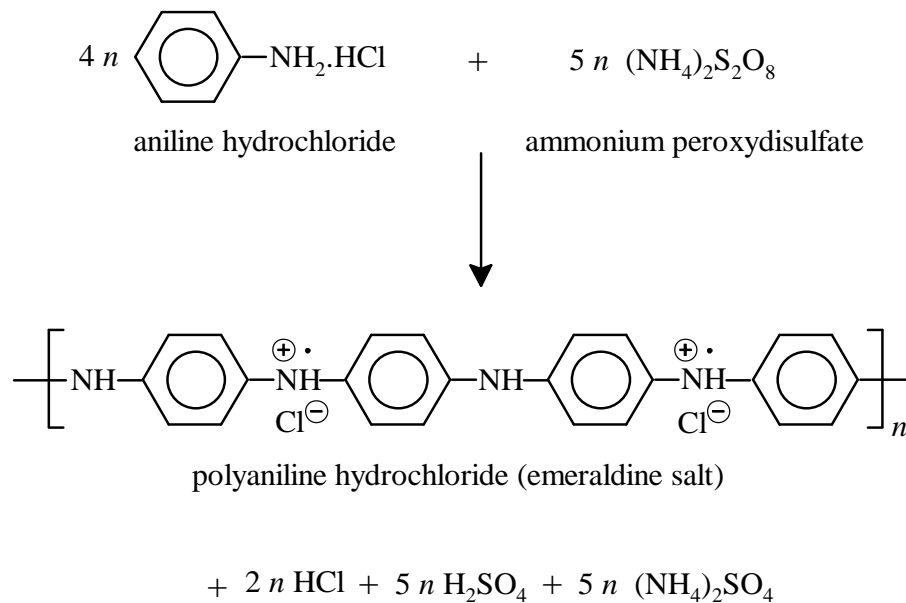


Figure 4.1: Oxidation of aniline hydrochloride with ammonium peroxydisulfate yields polyaniline (emeraldine) hydrochloride.

of the precipitate cake, and hence avoid inefficient washing of the precipitate. A minimum of 800 ml of deionized water was used. After washing, the precipitate remained under section for ~ 10 minutes until significant cracking of the moist filter cake occurred. Afterwards, the partially dried precipitate cake was suspended with constant stirring in 100 ml of NH_4OH (24%) solution in order to convert the polyaniline hydrochloride (emeraldine salt) to polyaniline (emeraldine) base as shown in Figure 4.2 below.

The suspended solution was stirred for one hour. The powder was collected on a Büchner funnel and flask using a water aspirator and partially dried under suction for ~ 10 minutes. The precipitate cake was then washed with 1 liter (100 ml per portion) deionized water. The black cake was partially dried on the funnel under suction for ~ 30 minutes on completion of the last washing, following by

drying under vacuum at 60°C for 48 hours to give 4.32 g of purple powder, which corresponds to ~86.4% yield based on the aniline starting material.

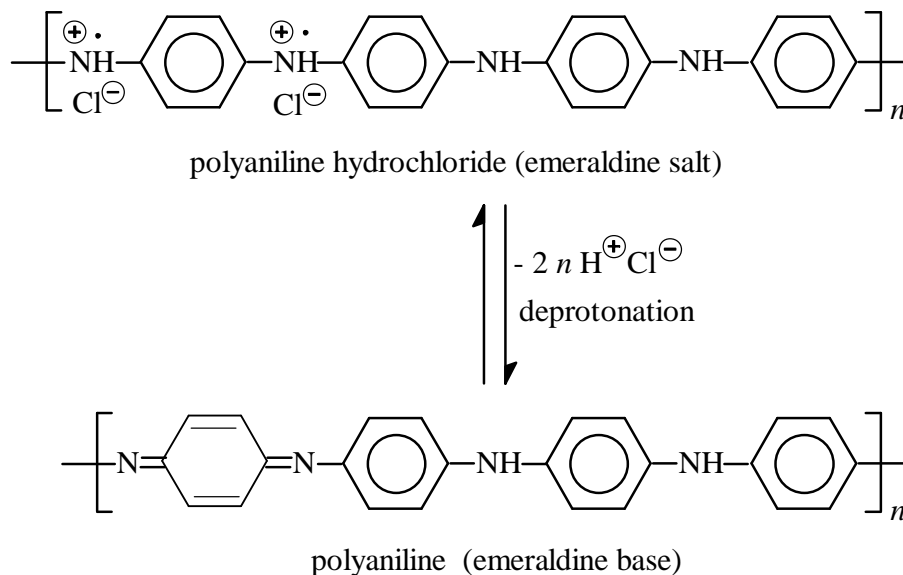


Figure 4.2: Polyaniline (emeraldine) salt is deprotonated in the alkaline medium to polyaniline (emeraldine) base.

4.2 Synthesis of Polyaniline (Emeraldine Base) at 0°C

Lithium Chloride (3.0 g, 0.071 mol), was dissolved in hydrochloric acid (143 g, 1M). Aniline (5.0 g, 0.054 mol) was dissolved in 75 ml of this solution and cooled to 0°C. Ammonium persulfate oxidant (12.3 g, 0.054 mol) was dissolved in the remaining HCl/LiCl solution and cooled to 0°C. The two solutions were mixed together and left to stand at 0°C for 2 hours. The reaction mixture was then filtered using a Büchner funnel and flask, and the filter cake washed with 10x80 ml of deionized water. The filter cake was stirred in ammonium hydroxide solution (100 ml, 24%) for 1 hour before refiltering and rewashing with 10x100

ml of deionized water, followed by drying under dynamic vacuum at 60°C for 48 hours to give 4.45 g of purple powder, which corresponds to ~89% yield based on the aniline starting material.

4.3 Synthesis of Polyaniline (Emeraldine Base) at -25°C

Lithium Chloride (20.76 g, 0.490 mol), was dissolved in hydrochloric acid (125 g, 1M). Aniline (5 g, 0.054 mol) was dissolved in 75 ml of this solution and cooled to -25°C. Ammonium persulfate (12.3 g, 0.054 mol) was dissolved in the remaining HCl/LiCl solution and also cooled to -25°C. The two solutions were mixed together and left to stand at -25°C for 36 hours in a chiller unit. The reaction mixture was then filtered, washed, deprotonated, rewash and dried as above to give 4.52 g of brown powder, which corresponds to 90.4% yield based on the aniline starting material.

It should be noted that for very low temperatures, the best salt to use is lithium chloride, (LiCl), due to its low molecular mass and high depression of the freezing point of water. Further, salt addition will also increase the dielectric constant of the medium, so an aqueous solution of lithium chloride would appear to be the best reaction medium for aniline polymerization at sub-zero temperatures.

4.4 Preparation of Leucoemeraldine Base

Emeraldine base (1 g) was dissolved in anhydrous N-methyl-2-pyrrolidinone (NMP) (20 g) and phenylhydrazine (1.5 g) added to this with stirring. The solution was allowed to stand for 24 hours before placing in a glove box under

nitrogen atmosphere. Anhydrous toluene (500 ml) was placed in a tall 1 liter beaker equipped with a magnetic stir bar used to agitate the solution. The reduced polyaniline solutions were then added slowly to the toluene. The grey precipitate of leucoemeraldine base was filtered using a Büchner funnel and flask. The filtered cake was washed with four portions of toluene (500 ml). The resulting grey powder was dried under dynamic vacuum for 24 hours at 25°C and was used for the light scattering measurements.

4.5 Sample Preparation for Light Scattering Measurements

A stock solution of 1 g/dl of leucoemeraldine base (synthesized in the previous section) in NMP was prepared in dry box under nitrogen, then diluted to 0.2 g/dl. Approximately 0.07 ml of hydrazine was added to 1 ml of this solution to ensure that the leucoemeraldine base was fully reduced. The solution, a pale yellow in color, was then used to make a series of solutions having a minimum concentration of 0.05 g/dl which were found to be suitable for light scattering measurements. Dilutions were made with NMP containing 0.07 ml of hydrazine per ml of NMP to keep the concentration of hydrazine relatively constant in each solution. Solutions were filtered into a sample tube through a 0.45 micron filter.

4.6 Preparation of Low Density Polyethylene-Polyaniline Composites

Grains of low-density polyethylene (LDPE) with a degree of crystallinity of about 60% and a melting temperature of about 110°C have been mixed with the submicron powder of polyaniline at 60 rpm for 20 minutes using Brabender

Plasti-Corder. The Polyaniline used in this composite was obtained chemically at 25°C with a conductivity of about 0.2 S m⁻¹. Composites were compressed in a mould for 5 minutes at 210°C and then the moulds were quenched. Composites of polyethylene/polyaniline (PE/PANI), containing 0, 5, 10, 15, 20, and 30% polyaniline (in weight) have been obtained. Before mixing, the components were dried at 70°C, under vacuum, for 24 hours. The specimens for mechanical characterization were prepared by injection molding using a laboratory scale injection molding machine (Microinjector, Daga Instruments). During molding; barrel temperature (210°C), mold temperature (0°C), injection pressure (16 bars) and cycle time (3 min) were identical for the preparation of each sample.

The resulting PE/PANI composites were homogenous, presenting a good stability of electrical and mechanical properties. Sets of 5 samples, prepared in identical conditions, were subjected to mechanical, electrical, thermal, and morphological studies. The experimental results presented in the next sections represent the average over all 5 identical samples.

4.7 Preparation of Multi Wall Carbon Nanotubes-Polyaniline Composites

A solution (150 ml) of 1M HCl, containing multi wall carbon nanotubes (MWNTs) was sonicated at room temperature to disperse the carbon nanotubes. The aniline monomer (5 g, 0.054 mol) was dissolved in 100 ml 1M HCl and then added to the MWNTs suspension. A solution of HCl 1M (50 ml) containing the oxidant (NH₄)₂S₂O₈ (12.3 g, 0.054 mol) was slowly added with a constant

sonication at a temperature of about 3°C to the mixture of aniline/MWNTs. After a few minutes, the dark suspension became green indicating good polymerization of aniline, and then was sonicated for 3 hours at 3°C. The composite is obtained by filtering and rinsing the suspension with HCl 1M followed by drying of the remaining powder under vacuum at room temperature for 24 hours. In this process, the polyaniline exists in its primary doped form called the “emeraldine salt”. Different composites were synthesized by this process, using 0, 5, 10, 15, and 30wt% of MWNTs (in weight of monomer).

CHAPTER 5

RESULTS AND DISCUSSION

5.1 Synthesis and Characterization of Polyaniline

Polyaniline was synthesized at three different temperatures of +25, 0, and -25°C. The resulted polymer was in a powder form which was characterized by several techniques. These techniques were DC-Conductivity Measurement Analysis, Elemental Analysis, Thermal Analysis, (TGA, DSC), FTIR Analysis, Wide-Angle X-Ray Analysis, Solid-State ¹³C-NMR Analysis, and, Morphological (SEM) Analysis. The results of these analysis are discussed in detail in this Chapter.

5.1.1 Polyaniline Synthesis

Chemically synthesized polyaniline is a precipitated product from an aqueous solution containing typical reagents; like ammonium peroxodisulfate (or persulfate), acids like hydrochloric, sulphuric, nitric or perchloric, and aniline. This

direct route represents the classical approach to polyaniline synthesis in which, the monomer is converted directly to conjugated polymer by a condensation process. One of the disadvantages of this direct approach stems from the experimental observation that an excess of the oxidant leads to materials that are essentially intractable [125].

During oxidative condensation of aniline, the solution progressively becomes colored and yields a black precipitate. The coloration of the solvent is probably due to the soluble oligomers. The intensity of coloration depends on the nature of the medium and the concentration of the oxidant.

There are four major parameters that affect the course of the reaction, and the nature of the final product. These are: (1) nature of medium, (2) concentration of the oxidant, (3) duration of the reaction and, (4) temperature of the medium.

While choosing a medium for the synthesis of chemically synthesized polyaniline, some factors such as low ionic strength, volatility, and non-corrosive nature of the medium have to be kept in mind to obtain desirable results. Unfortunately, no medium satisfies all of the above requirements. In this thesis, hydrochloric acid was used as a medium of synthesis. Hydrochloric acid (HCl) is a corrosive medium with high volatility [126,127].

The oxidant used in this study was ammonium persulfate $(\text{NH}_4)_2\text{S}_2\text{O}_8$, which is most extensively used as the oxidant for polymerization of aniline in acidic media, with an initial monomer/oxidant mole ratio (r) of one ($r=1$). It should be noted that, the yield, elemental composition, conductivity and degree of oxidation of the resulting polymer are essentially independent of the value of the initial

aniline/oxidant mole ratio (r) when $r \leq 1.5$. However, an $r > 1.15$ results in over-oxidation of the polyaniline with a relative decrease in the conductivity and yield of the polymer. Also, a marked change in morphology was observed [128].

The effect of temperature on aniline polymerization process in this study was fully understood. This study showed that the values for the molecular weight and yield increased at reaction temperatures below 0°C . Lowering the reaction temperature (and therefore increasing the amount of lithium chloride present, to prevent the reaction mixture from freezing), increased the molecular weight of polyaniline. The molecular weight of polyaniline synthesized at -25°C using ammonium persulfate as an oxidant and lithium chloride as an inert salt was five times higher than that of the same polymer synthesized at 25°C with no inert salts.

Many published works [129,130] showed that a reaction carried out at -3°C with ammonium sulphate as an inert salt had a molecular weight three times higher than an identical reaction carried out at $+1^\circ\text{C}$, with no inert salt. Therefore, both inert salts and lower temperatures are thought to give higher molecular weights.

The samples synthesized here were obtained in high yield (86.4%, 89%, 90.4% based on the amount of aniline starting material), due to the acceptable amount of oxidant ($r=1$) and lithium chloride present.

5.1.2 Characterization of Polyaniline

5.1.2.1 Conductivity Measurement Analysis

The conductivity of doped polyaniline powder synthesized at different temperatures is shown in Table 5.1.

Table 5.1: Conductivity of doped polyaniline (Emeraldine salt) powder

Synthesis Temperature ($^{\circ}\text{C}$)	25	0	-25
Conductivity (S/cm)	1.96×10^{-3}	1.40×10^{-2}	5.64×10^{-3}

The reduction of polymerization temperature from 25°C to -25°C had no regular effect on the conductivity. The conductivity of polyaniline synthesized at 25°C was measured as $1.96 \times 10^{-3} \text{ S cm}^{-1}$ and increased up to $1.40 \times 10^{-2} \text{ S cm}^{-1}$ when the polymerization temperature was reduced to 0°C . However, the conductivity was decreased to 5.64×10^{-3} when the same polymer prepared at -25°C . Such behavior was theoretically predicted [131] for the cases when charges hopping from one polymer chain to another are much faster in comparison with the lifetime of the charge on the chain, i.e., when the interchain transport occurs more readily than the intrachain one. In this sense, polyaniline resembles low molecular weight charge transfer salts (intermolecular conductors) rather than conjugated polymers (intramolecular one-dimensional conductors). The independence of the electrical conductivity on molecular weight is in agreement with the theoretically

predicted weak dependence of electronic properties on chain length of polyaniline.

5.1.2.2 Elemental Analysis

The elemental composition of polyaniline emeraldine base form prepared under standard conditions in an acidic media of 1 M HCl is shown in Table 5.2.

Table 5.2: Elemental composition of polyaniline base

Reaction conditions	%C	%H	%N	%S	%(Total)
Calculated	79.53	5.01	14.46	-	100
Exp-1 (25°C)	71.00	4.79	13.87	0.41	90.07
Exp-2 (0°C)	66.90	4.86	13.94	-	85.70
Exp-3 (-25°C)	68.23	4.58	13.83	-	86.64

The results of elemental analysis clearly indicate the presence of oxygen in polyaniline. This may be due to bound water molecules or, more likely, to partial oxidation of polyaniline chains. Hydrochloric acid is removed from the aniline hydrochloride after deprotonation with ammonium hydroxide. The relative participation of carbon and nitrogen in polyaniline emeraldine base form (PANI) is thus increased, at the expense of the lower content of chlorine. However, some amount of chlorine is expected to remain in PANI base even after deprotonation, indicating a partial benzene-ring substitution with chlorine. The content of covalently bound chlorine will be higher if the oxidation of aniline hydrochloride

takes place in excess HCl. Partial sulfonation of benzene rings is responsible for the presence of sulfur in the PANI base (Table 5.2).

5.1.2.3 Thermal Analysis

The thermal behavior of polyaniline synthesized in the medium of hydrochloric acid was studied using TGA and DSC methods in an attempt to find the best processing conditions. Figure 5.1 shows the TGA results of pure polyaniline (Emeraldine base) powder prepared at 25°C, 0°C, and -25°C.

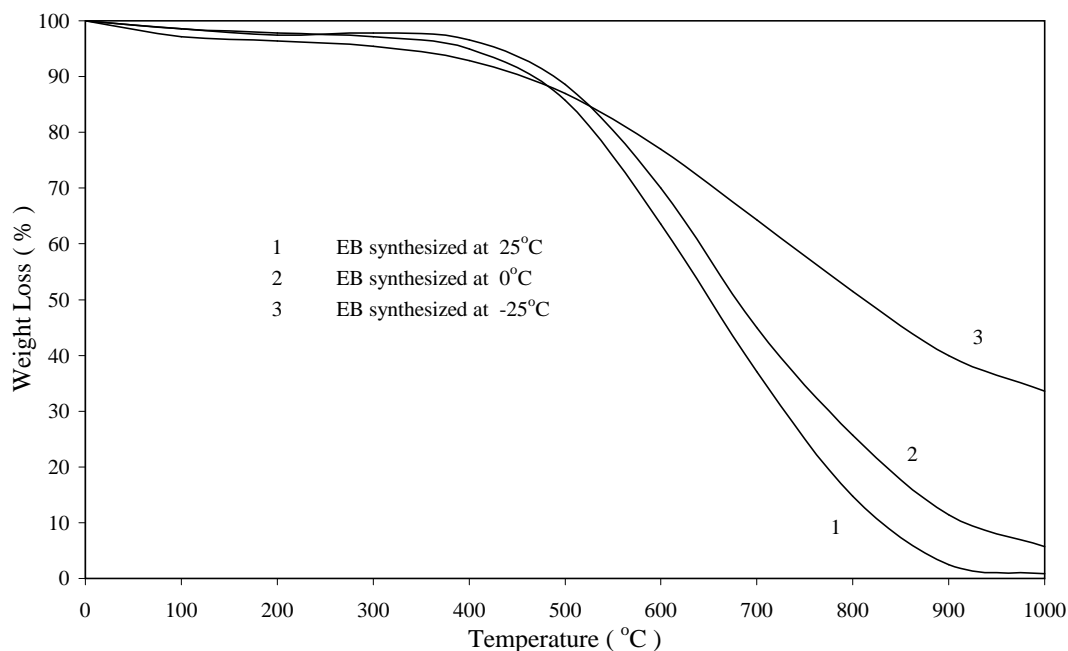


Figure 5.1: TGA of Emeraldine Base (EB) synthesized at different temperatures

All experiments approximately show the same thermal stability. They show a typical three step weight loss behavior. In the first step, 2-3% weight loss at temperatures up to 100°C is seen. This can be attributed to loss of water molecules from the polymer matrix. The second weight loss starting at around 200°C. This

may be attributed to possibly co-evolution of water or evolution of acid. The third step, starting at 250°C onwards, represents oxidative degradation of the polymer, and this also indicates that the chemical structure decomposition of the backbone of polyaniline. It illustrated the degradation temperature of polyaniline was around 420-450°C. In the present case, the sample undergoes complete weight loss. Furthermore, Figure 5.1 indicates that the polymer stability increases with increasing molecular weight.

Figure 5.2 shows the DSC results of pure polyaniline (Emeraldine base) powder prepared at three different temperatures.

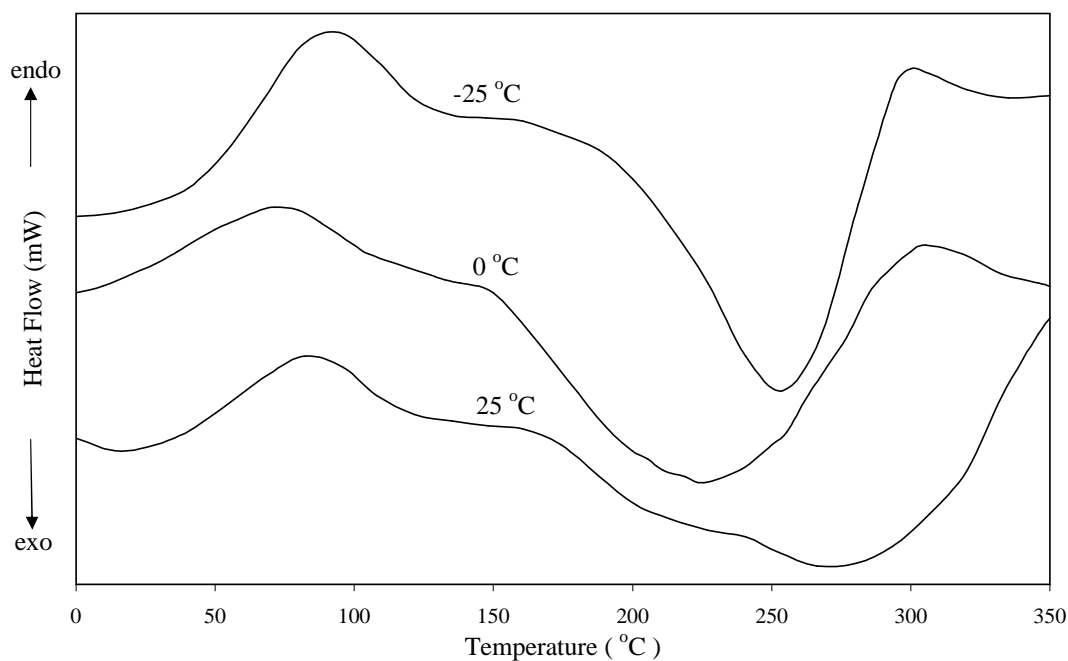


Figure 5.2: DSC of Emeraldine Base synthesized at different temperatures of 25°C, 0°C, and -25°C.

In this figure, there are two peaks, namely, an endothermic peak at 40-140°C, and an exothermic peak at 150-310°C in polyaniline results prepared at 0°C and

-25°. However, the exothermic peak for polyaniline prepared at 25°C, lies between 150 and 350°. According to studies reported previously [132-134], the polyaniline (EB) powder had a discernible moisture content. Therefore, the endothermic peak was most likely due to the vaporization of water. This was in agreement with the TGA results. The chemical process related to the exothermic peak was due to crosslinking reaction. This crosslinking reaction resulted from a coupling of two neighboring -N=Q=N- groups (where Q represents the quinoid ring), to give two -NH-B-NH- groups (where B represents the benzenoid ring) through a link of the N with its neighboring quinoid ring, as suggested by Scherr et al [135]. The DSC thermogram of EB-form polyaniline powder for the second run indicates no significant endothermic or exothermic peaks as shown in Figure 5.3, because no apparent moisture existed in the sample.

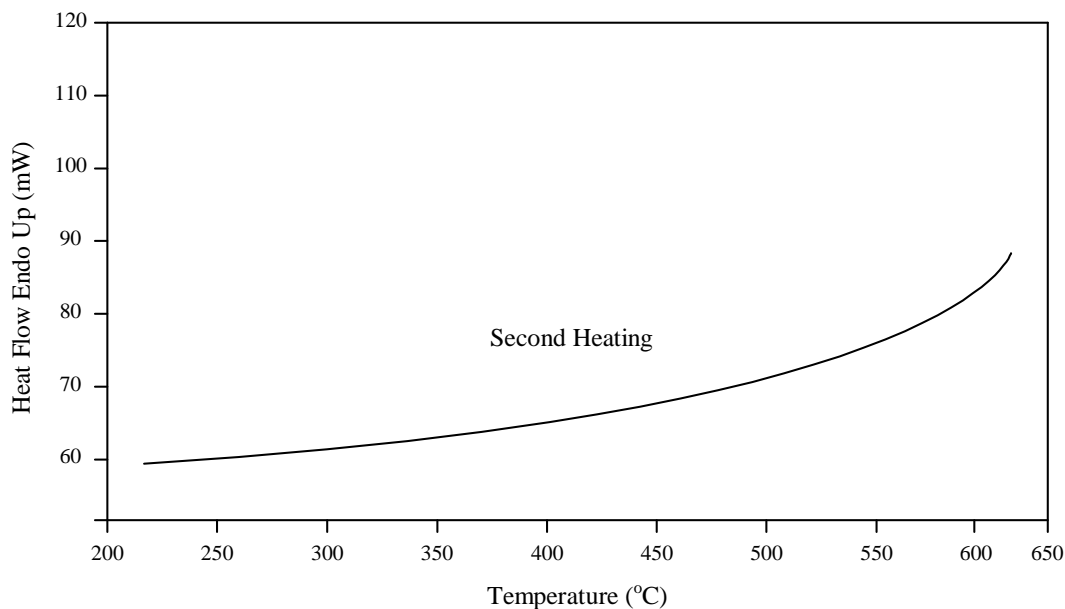


Figure 5.3: DSC, second heating of Emeraldine Base synthesized at different temperatures

Moreover a crosslinking reaction during the first run DSC thermal treatment that resulted in three-dimensional (3-D) chemical structure of EB-form polyaniline is shown in Figure 5.4. Therefore, no apparent exothermic peak was observed.

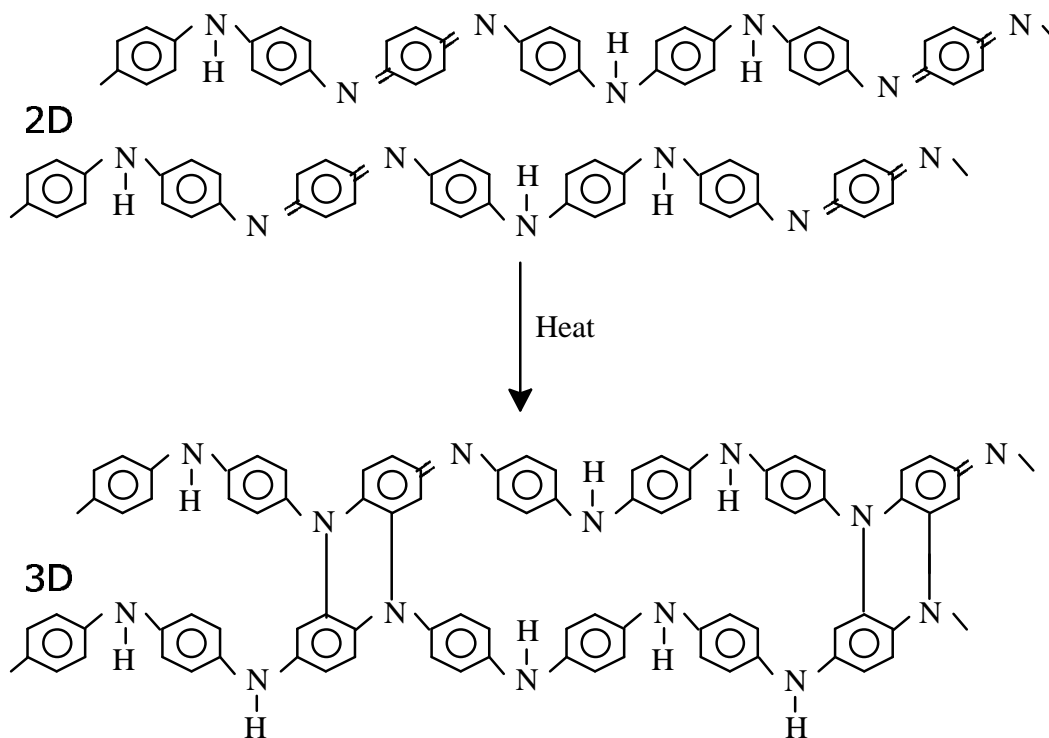


Figure 5.4: Thermal crosslinking reaction among EB-form polyaniline molecular chains.

5.1.2.4 Fourier Transform Infrared Spectroscopy Analysis

Figure 5.5, represents the FTIR spectra of polyaniline (EB) powder synthesized at different temperatures of 25, 0, and -25°C. The common bands and their characteristics observed in three polymers are discussed here. FTIR spectrum of EB powder shows the following five major vibrational bands, 1597, 1500, 1145,

and, 820 cm^{-1} . These are in excellent agreement with previously published values [136-138]. In addition, it is important to note that there are two bands associated with N-H stretching vibrations- a major broad band located at $\sim 3385\text{ cm}^{-1}$ and a minor sharp band located at $\sim 3394\text{ cm}^{-1}$.

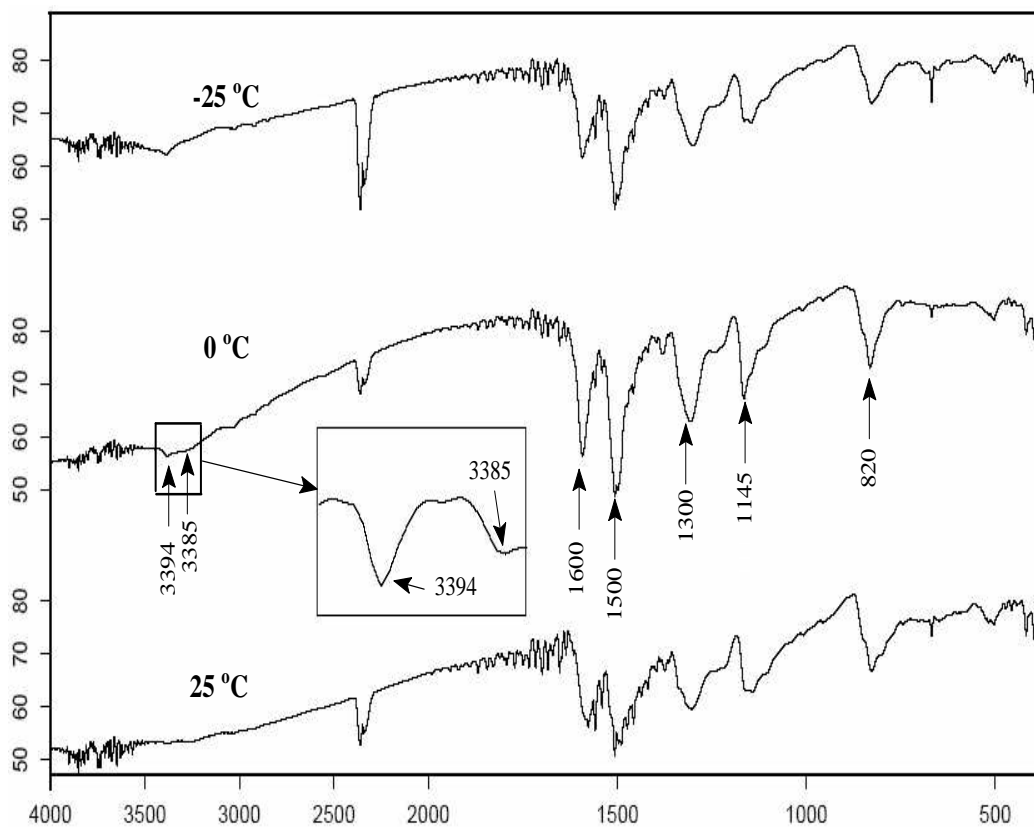


Figure 5.5: FTIR of polyaniline (EB) powder.

It is believed that the H-bonding in EB occurs between amine and imine sites. Theoretical calculations reported by Rossi et al [139], indicate that H-bonding between amine/imine sites is energetically favorable whereas, H-bonding between amine/amine sites is significantly less favorable. The N-H stretching bands mentioned above represent the characteristic of a free or non-bonded band

Table 5.3: IR vibrational modes of polyaniline base

Wave no. (cm^{-1})	Attribution
~ 3500	N-H stretch
~ 3400	O-H bond stretching
~ 3000	C-H stretch
1583	C=C stretch in a quinoid ring
1492	C-C stretch in a benzenoid ring + C-H mixed vib.
1378	C-C stretch in a quinoid ring + C-H bending in a benzenoid ring
1306	C-H bending
1214	C-N stretch + C-H bending
1161	C-H bending
1107	Deformation of aromatic ring + C-H bending
826, 506	Deformation C-H (out of plane) of 1-4 disubstituted aromatic ring

at 3394 cm^{-1} and a H-bonded N-H band at 3385 cm^{-1} . It is important to note that the intensity of the hydrogen-bonded N-H stretching band is significantly higher than that of the free N-H band in EB powder. This indicates that the as-synthesized EB is significantly self-associated via hydrogen bonding. These specific results do not distinguish between interchain hydrogen bonding between different polyaniline molecules and intrachain hydrogen bonding between different “folded back” segments of the same polyaniline molecule. It should also be noted that a quantitative determination of the degree of hydrogen bonding cannot be made from the present infrared data alone [140].

The bands close to 820 cm^{-1} are characteristic of the p-substituted chains and are seen in all spectra with a small displacement according to the synthesis temperature. The band close to 1145 cm^{-1} is described as being characteristic of the conducting polymer due to the delocalization of electrical charges caused

by deprotonation and it can be attributed to bands characteristics of B-NH-Q or B-NH-B, where B refers to the benzenic-type rings and Q to the quinonic-type rings [141]. In the region close to 1300 cm^{-1} , the peaks are attributed to the presence of aromatic amines present in all types of polyaniline discussed here.

The bands around $1500\text{-}1600\text{ cm}^{-1}$ are related to the stretching of the C-N bonds of the benzenics and quinonics rings, respectively. The intensity of these bands gives an idea of the oxidation state of polyaniline when they present similar intensities, the polyaniline is in the emeraldine form.

The appearance of wider band instead of a peak is due to the presence of a high concentration of these groups in the sample.

There is evidence of a peak of low intensity in the area associated with O-H bond stretching around 3400 cm^{-1} due to the presence of moisture in the sample.

5.1.2.5 X-Ray Analysis

Because of amorphous nature of polyaniline, information obtained from X-Ray and neutron diffraction is quite limited, while its limited solubility restricts the use of standard characterization techniques for classical polymers. Only in the past decade was polyaniline, in the form of its emeraldine salt, recovered in crystalline form from a solution in sulphuric acid, by precipitation with water or methanol [142]. It was also stated that, the polymerization at reduced temperature was found to increase the molecular weight of the products and to reduce the polydispersity expressed by the weight-to-number average molecular weight ratio [143], and hence increases crystallinity.

Wide angle X-Ray diffraction (WAXD) spectra of polyaniline (EB) powder synthesized at 25, 0, and -25°C, are shown in Figure 5.6.

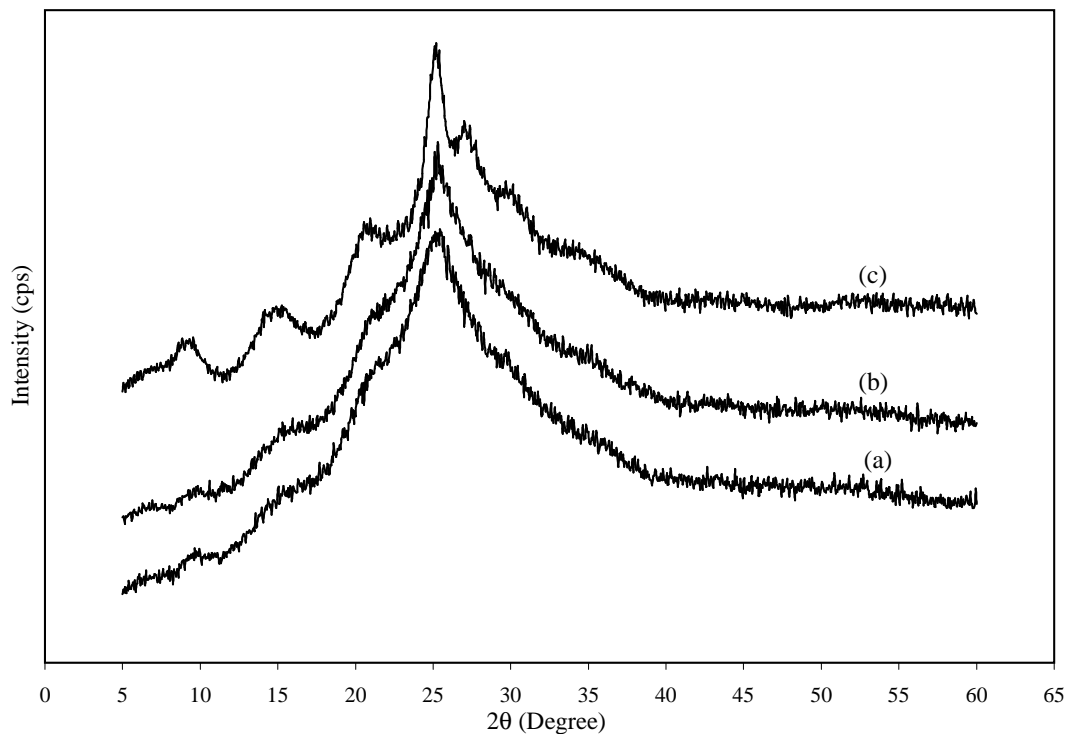


Figure 5.6: WAXD of polyaniline (EB) powder synthesized at (a) 25°C, (b) 0°C and (c) -25°C.

Polyaniline crystallizes in the monoclinic space group $P2_1$. The diffractograms show a well-developed crystallinity in the sample prepared at -25°C (Figure 5.6 (c)), while the sample prepared at +25°C is nearly amorphous (Figure 5.6 (a)). According to the method suggested by Kelkar et al. [144] for any polymer, the resolution of the peak R is given by:

$$R = \frac{m_1 + 2m_2 + \dots + m_{n-1}}{h_1 + h_2 + \dots + h_n} \quad (5.1)$$

where m_1, m_2, \dots are the heights of minima between two peaks, and h_1, h_2, \dots are the heights of the peaks from the base line. Then $(1 - R)$ gives the lateral order

or the index of crystallinity. Figure 5.6 (b, and c), indicate that the peaks are quiet sharp and well resolved; hence the percentage crystallinity was calculated from equation 5.1 and tabulated in table 5.4.

Table 5.4: Percentage crystallinity, X_c (%) of undoped polyaniline in powdered form, according to the temperature of synthesis.

Synthesis Temperature ($^{\circ}\text{C}$)	Percentage Crystallinity, X_c (%)
+25	1.17
0	7.6
-25	16.3

While the molecular weight reflects the macromolecular structure of polyaniline, the degree of crystallinity is associated with the supramolecular organization of polyaniline chains. For polyaniline samples, the fraction of crystalline phase increased as the molecular weight grew. The increase was more pronounced for the sample prepared at low temperature. This may indicate that chains pronounced under lower temperature conditions have less structural defects.

5.1.2.6 Solid-State ^{13}C -NMR Analysis

The ^{13}C cross-polarization magic angle spinning (CP-MAS) NMR spectra of EB powder synthesized at different temperatures shown in Figure 5.7, are nearly the same. To assign the chemical shifts of EB powder, let us consider first the general formula of polyaniline as shown in Figure 5.8 below.

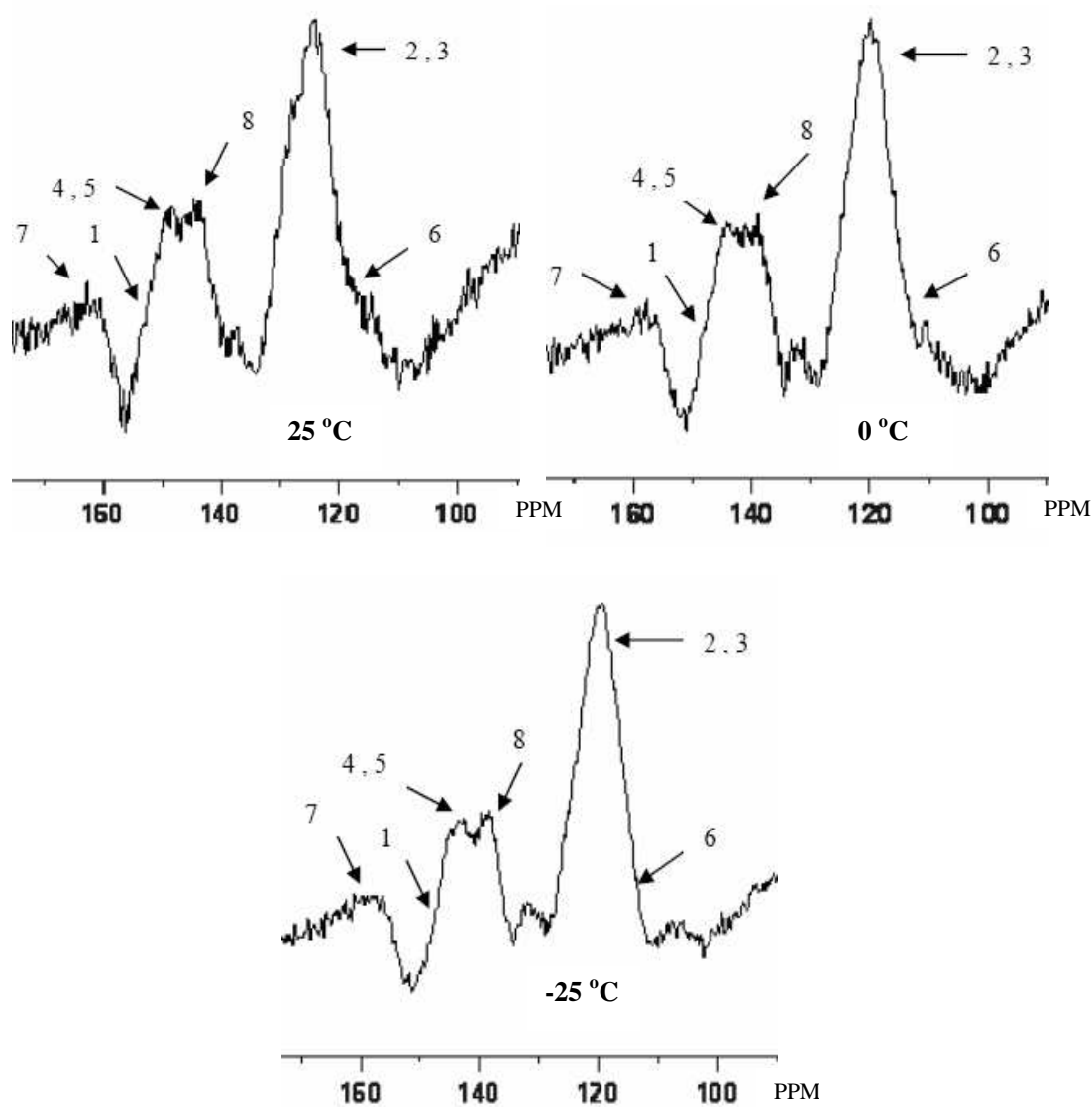


Figure 5.7: Solid-State ^{13}C -NMR spectra of polyaniline (EB) powder.

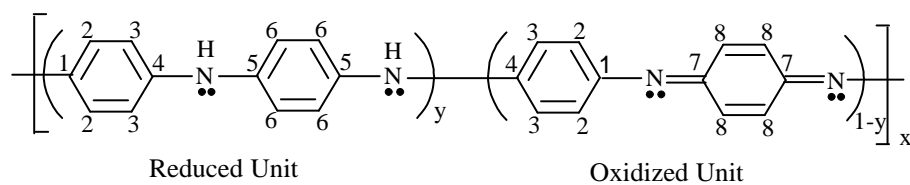


Figure 5.8: General form of polyaniline.

The spectrum from EB polyaniline has peaks nearly close to each other (within experimental error) as shown from the chemical shifts in Table 5.5.

Table 5.5: ^{13}C -CPMAS Chemical shifts of Emeraldine Base powder

Carbon Number	Exp-1 (+25°C)	Exp-2 (0°C)	Exp-3 (-25°C)
1	152	144	144
2,3	123	122.5	118.5
4,5	147	143.8	143
6	118	114.5	117.5
7	161	157.3	157.5
8	142.5	136	138.3

The quinoid peaks, C-7 and C-8, are readily identified from their chemical shifts and intensities as the most deshielded peaks. The strong resonance peak is assigned to protonated carbons of the benzenoid ring directly attached to the quinoid ring (C-2, C-3). C-6 is identified as a protonated carbons of the benzenoid rings that are one ring away from quinoid rings. Other nonprotonated carbons corresponding to both benzenoid and quinoid rings (C-4, C-5) appear below ~ 150 ppm. Therefore, it can be concluded that Emeraldine base is primarily an alternating head-to-tail copolymer to reduced $[-(\text{C}_6\text{H}_4)\text{N}(\text{H})(\text{C}_6\text{H}_4)\text{N}(\text{H})-]$ and oxidized $[-(\text{C}_6\text{H}_4)\text{N}=(\text{C}_6\text{H}_4)=\text{N}-]$ repeat units.

5.1.2.7 Morphological Analysis

Studies on morphology of chemically synthesized polyaniline are important for investigating the intrinsic characteristics of the polymer [141]. Many of the studies [145-148] are rudimentary and exploratory in nature. The dependence of morphology upon variables such as different anions employed in the synthesis and difference in chemical procedures need to be investigated in detail.

Figure 5.9 shows the morphology of polyaniline Emeraldine base form powder synthesized at 25°C.

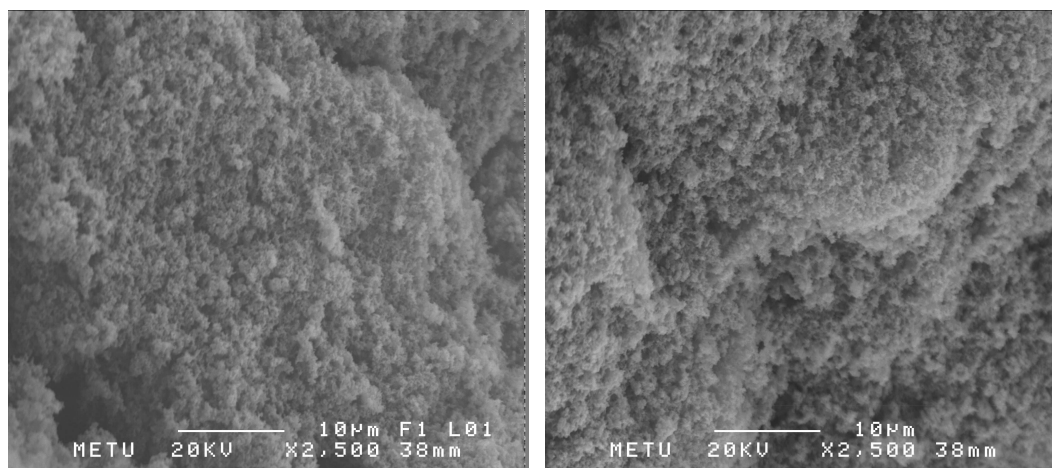


Figure 5.9: SEM micrographs of polyaniline (EB) powder synthesized at 25°C.

The SEM photographs show typical features of the polymer. Both photographs are mainly composed of irregularly arranged granular and flakes with sharp edges. Moreover, the structure looks more porous. Besides the SEM pictures shown in Figure 5.10 illustrate the morphology of polyaniline (EB) powder synthesized at 0°C. It can be seen that the polyaniline particles have microtubules

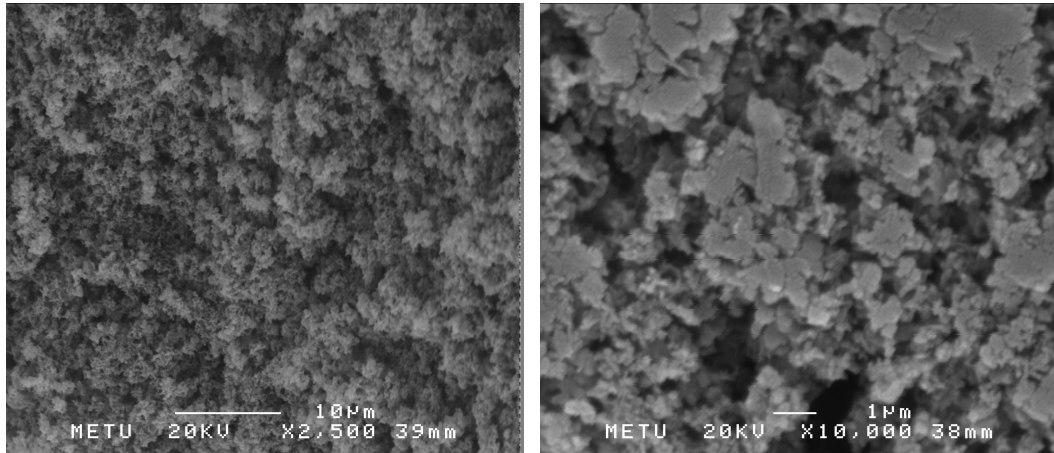


Figure 5.10: SEM micrographs of polyaniline (EB) powder synthesized at 0°C.

type morphology which differ from the morphology of polyaniline particles synthesized at 25°C. This indicates that reduction in synthesis temperature gives longer chains and hence larger molecular weight as proved before by many researchers.

Figure 5.11 shows the scanning electron micrograph of polyaniline particles prepared at -25°C.

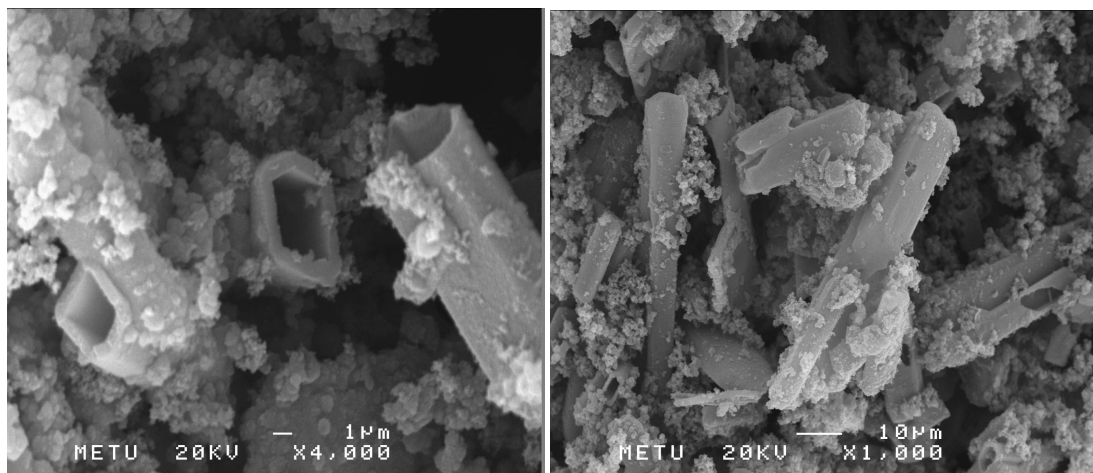


Figure 5.11: SEM micrographs of polyaniline (EB) powder synthesized at -25°C.

It can be observed that polyaniline particles have a hollow microtubules morphology with average size of about $50\mu\text{m}$ and the shape of the polyaniline dispersions is somewhat similar to sample shown in Figure 5.10 (tubular type morphology) but certainly the size has been increased and regulated tubular morphology became dominant as compared to sample shown in Figure 5.10. These results also suggest that the chains length of the polymer increase with decreasing the synthesis temperature.

5.2 Solution Properties of Polyaniline

The solution properties of polyaniline synthesized previously in sections 4.1, 4.2, and 4.3 at three different temperatures of $+25^{\circ}\text{C}$, 0°C , and -25°C are studied by static light scattering, dynamic light scattering, and intrinsic viscosity measurement. The result of each are discussed here.

5.2.1 Static Light Scattering (SLS)

Static light scattering measures light intensity as a function of scattering angle and solute concentration. This allows the determination of average molecular weight, radius of gyration, and shape information for the solute.

The specific refractive index increment (dn/dc), where n is the refractive index and c is the concentration in g/ml of the solutions, is necessary for the determination of molecular weight. This value defines the change of refractive index of a solution as a function of solution concentration. The refractive index increment was tried to be measured by KMX-16 laser differential refractometer. The value

was inaccessible due to the dye effect, and was taken from literature as $0.25 \text{ cm}^3/\text{g}$ [149,150].

The Berry plots for polyaniline leucoemeraldine base prepared at $+25^\circ\text{C}$, 0°C , and -25°C are shown in Figures 5.12-5.14 respectively.

Table 5.6: Weight average molecular weight, \bar{M}_w , radius of gyration, R_g , and second virial coefficient, A_2 for polyaniline leucoemeraldine base synthesized at different temperatures.

Synthesis Temperature ($^\circ\text{C}$)	\bar{M}_w (g/mol)	R_g (nm)	A_2 (mol ml/g ²)
+25	29200	20.1	1.54×10^{-2}
0	78700	31.7	1.53×10^{-3}
-25	157000	39.8	1.02×10^{-3}

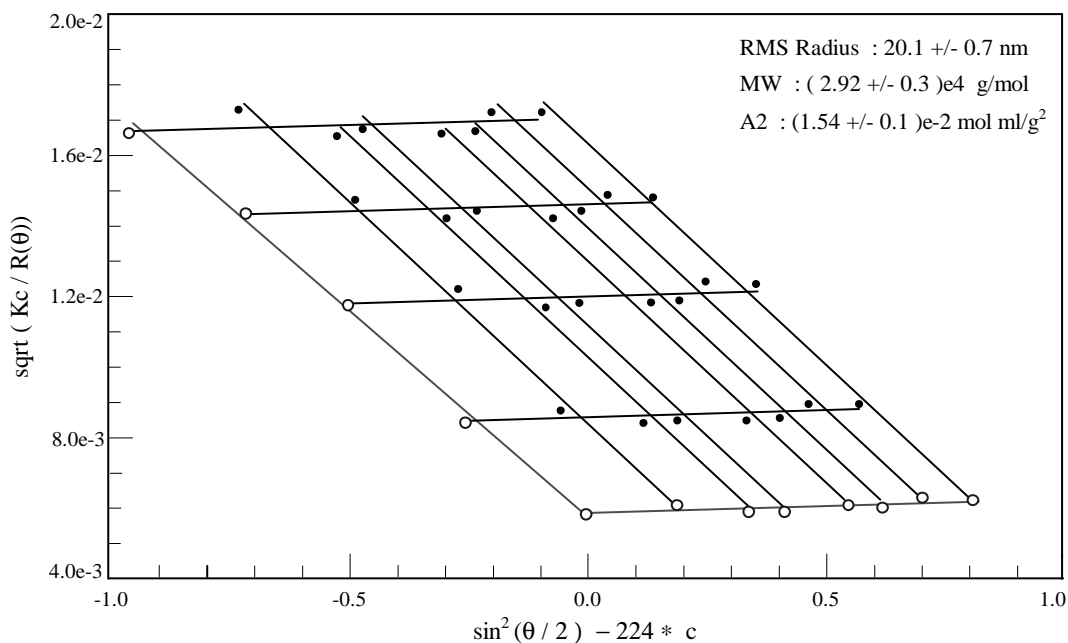


Figure 5.12: Berry plot of polyaniline leucoemeraldine base prepared at $+25^\circ\text{C}$.

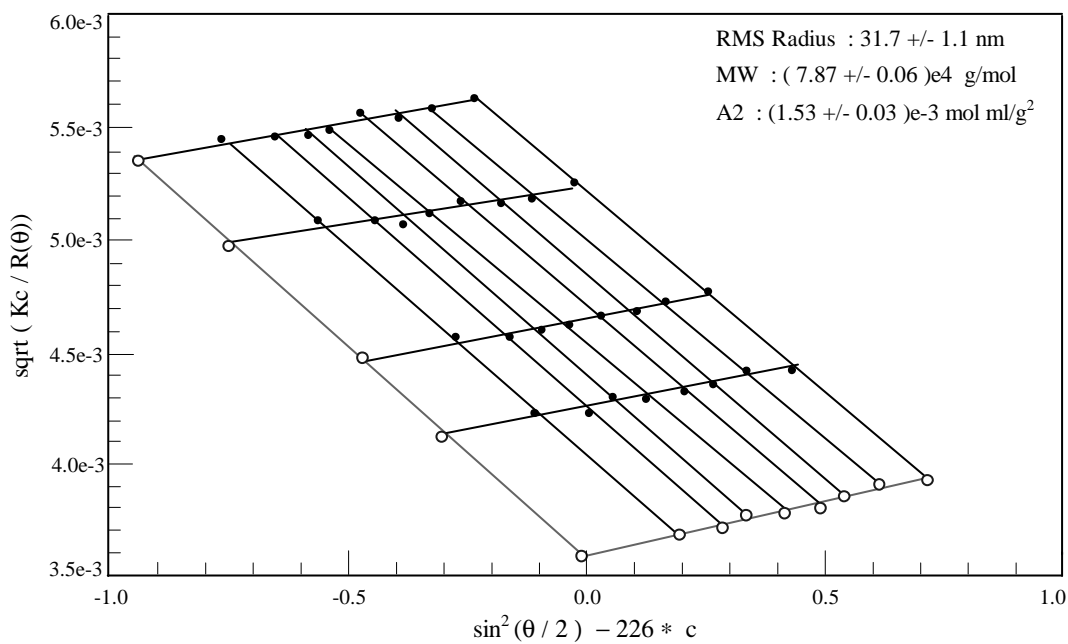


Figure 5.13: Berry plot of polyaniline leucoemeraldine base prepared at 0°C .

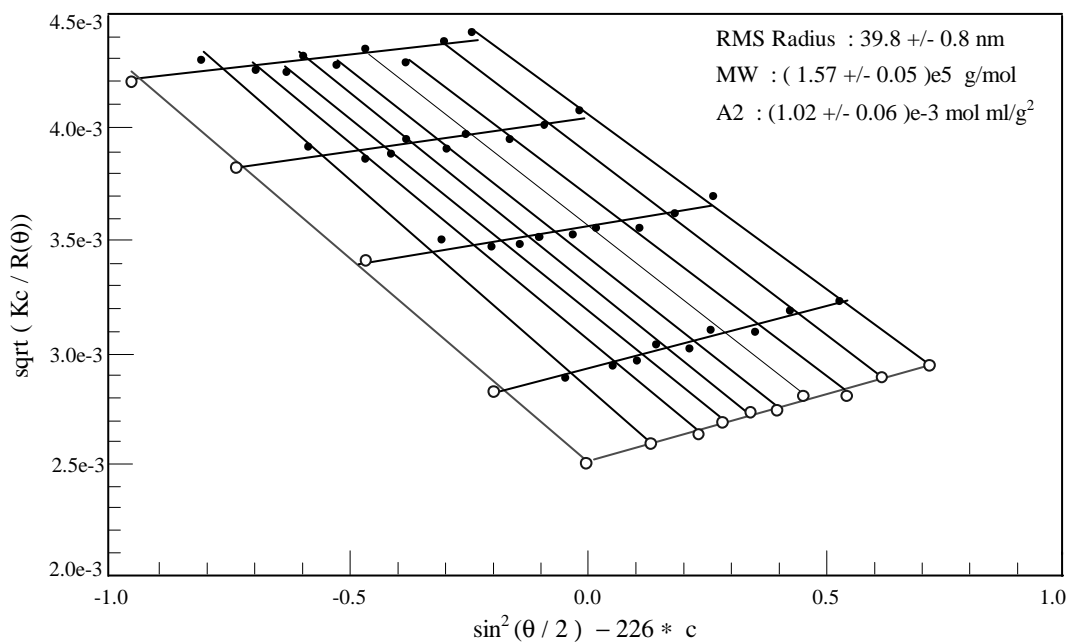


Figure 5.14: Berry plot of polyaniline leucoemeraldine base prepared at -25°C .

Weight average molecular weights, \bar{M}_w , calculated from the limiting intercepts; $c \rightarrow 0$ and $\theta \rightarrow 0$, R_g and A_2 which were deduced from the slope with $\sin^2(\theta/2)$ at $c = 0$ and from the slope with c at $\theta = 0$, respectively, were given in each plot and tabulated in Table 5.6.

The molecular weight of polyaniline increases as the the reaction temperatures is lowered (Table 5.6). Polyaniline polymerization is an exothermic reaction, so at low temperature, side reactions get depressed and the molecular weight can be increased. Moreover, cationic chain polymerizations are usually carried out at low temperatures, which favor propagation over competing side reactions, and use solvents with a high dielectric constant, which favors both initiation and propagation leading to high molecular weight polymers.

One of the ways of controlling macromolecular properties of polyaniline (PANI), namely, its molecular weight, is the selection of the reaction temperature. In this study, it was found that the molecular weight of polyaniline leucoemeraldine base increased rapidly with decreasing polymerization temperature. As shown in Table 5.6, the molecular weight of polyaniline leucoemeraldine base synthesized at -25°C is two times higher than the molecular weight of the same polymer synthesized at 0°C and five times higher than the polymer synthesized at $+25^\circ\text{C}$. MacDiarmid and Epstein [151] reported that the molecular weight of PANI can be increased by decreasing the polymerization temperature. Ohtani et al. [152] observed that weight average molecular weight of PANI, \bar{M}_w , increased from 120000 to 160000 when polymerization was carried out above 20 and below -3°C , respectively. Oh et al. [153] polymerized aniline at 0 and -30°C ; \bar{M}_w was 6.8 times higher at lower

temperature. Mattoso et al. [154] similarly found that \bar{M}_w increased 7.3 times when polymerization proceeded at -40 instead at 0°C. Adams et al. [155-157] showed that the molecular weight of PANI prepared by oxidation of aniline with ammonium peroxodisulfate was $\bar{M}_w=29700$ at 18°C and 122000 at 0°C while it increased to 166000 at -35°C.

The conformational plot shown in Figure 5.15 representing the dependence of $\log R_g$ on $\log \bar{M}_w$.

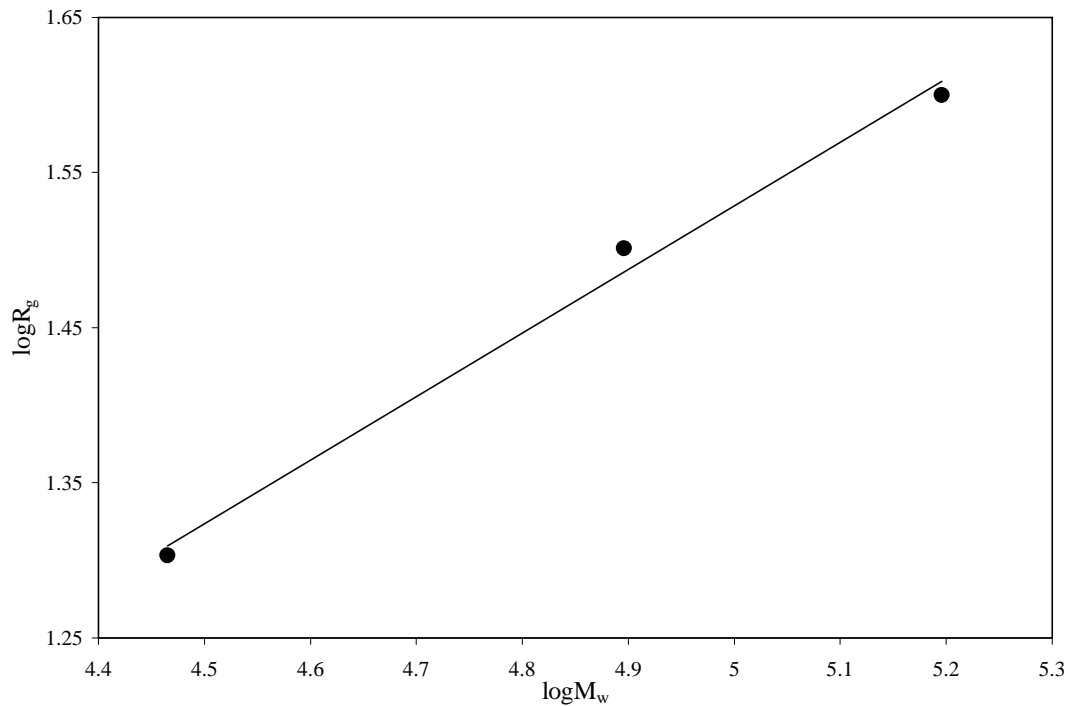


Figure 5.15: Conformation plot of $\log R_g$ as a function of $\log \bar{M}_w$ for polyaniline prepared at different temperatures.

This figure is plotted according to the relation:

$$R_g = k\bar{M}_w^\alpha \quad (5.2)$$

where $k = 19.055$ (calculated from the intercept in Figure 5.15) is a constant

depends on the polymer solvent system and $\alpha = 0.4098$ (slope of the line in Figure 5.15). Since the exponent values of 0.5-0.6 are expected for random coil, whereas a value of 1 is expected for rods [158], our result reveal that the polyaniline samples investigated have random coil conformation in NMP (the slope of the line around 0.5 in Figure 5.15).

From the data given in Table 5.6 and Berry plots mentioned above, the second virial coefficient, A_2 , is decreasing as the molecular weight, \bar{M}_w , increased. This means that the conformation of polyaniline synthesized at lower temperature coils is more compact than that of polyaniline synthesized at higher temperature coils. These result can be explained as the side reactions are depressed at lower temperatures and leading to greater number of intramolecular interactions in the polymer chains. Therefore, polyaniline synthesized at -25°C has the lowest A_2 value (Table 5.6) and the most compact sphere conformation. Moreover, the positive value of the second virial coefficient, ($A_2 > 0$), indicates that the polymer molecules prefer contacts with solvent molecules to contact with other polymer molecules. The solvation reduces the free volume available for concentration fluctuations to take place and, thereby, the probability of fluctuations. A solvent in which polymer-solvent contacts are energetically favored is a good solvent for the polymer.

Figures 5.16, a plot of $Kc/R(\theta)$ versus $\sin^2(\theta/2)$, of polyaniline leucoemeraldine base synthesized at $+25^\circ\text{C}$, shows the initial and asymptotic regions of the angular dependence of scattered light intensity for 0.001 g/ml concentration.

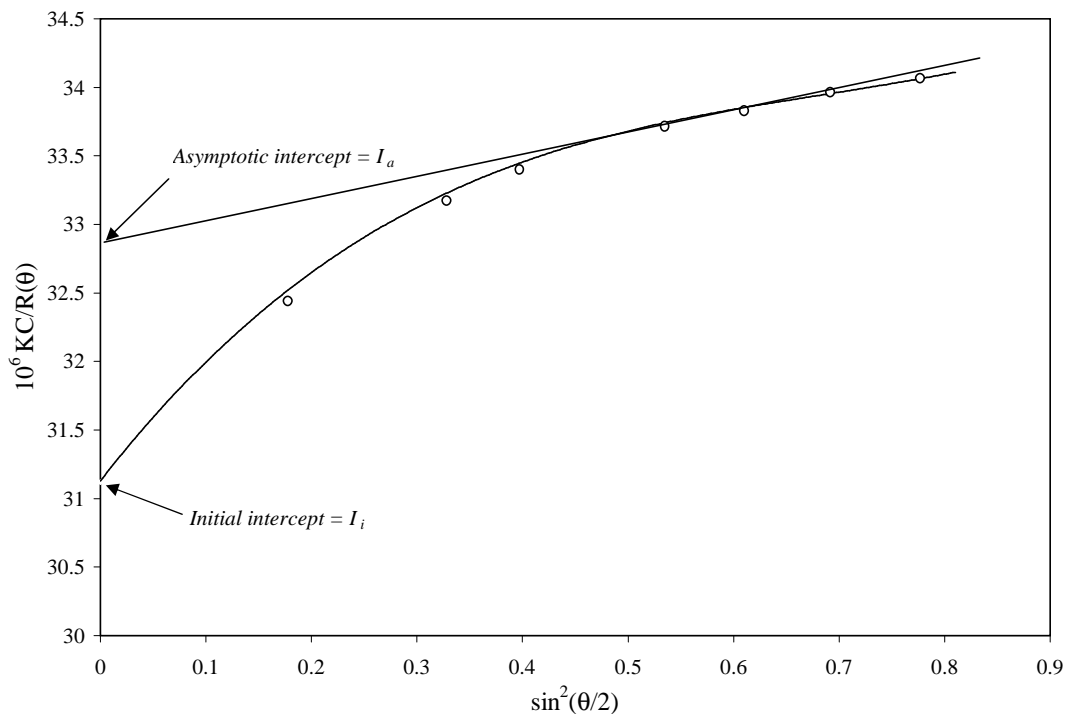


Figure 5.16: Plot of initial and asymptotic regions of the angular dependence of scattered light intensity for polyaniline leucoemeraldine base prepared at 25°C.

Using the intercept of the asymptotic portion of the curve (I_a) and the intercept of the initial curve (I_i), the \bar{M}_w/\bar{M}_n value can be determined using the relation:

$$\frac{\bar{M}_w}{\bar{M}_n} = \frac{2I_a}{I_i} \quad (5.3)$$

A detailed explanation of this method can be found in ref. [159]. Inserting the values for I_a and I_i , \bar{M}_n can be calculated. Moreover, polyaniline leucoemeraldine base prepared at both 0, and -25°C were also treated in the same way and the results of all were calculated and tabulated in Table 5.7.

Table 5.7: Values of I_a , I_i , \bar{M}_w/\bar{M}_n , and \bar{M}_n .

Polyaniline Type	I_a	I_i	\bar{M}_w/\bar{M}_n	\bar{M}_n (g/mol)
Reduced PANI at 25°C	32.93x10 ⁻⁶	31.12x10 ⁻⁶	2.12	13774
Reduced PANI at 0°C	11.83x10 ⁻⁶	11.03x10 ⁻⁶	2.16	36435
Reduced PANI at -25°C	6.16x10 ⁻⁶	5.53x10 ⁻⁶	2.23	70404

5.2.2 Intrinsic Viscosity Measurement

For dilute solutions, the Huggins equation was used in determining the intrinsic viscosity and the Huggins constant. These parameters are qualitative measures of the hydrodynamic volume of the polymer chain and the interaction between different polymer chains and/or between the polymer chains and the solvent molecules, respectively [160]. The Huggins equation 5.4, describes the relationship between intrinsic viscosity and the concentration of the dilute polymer solutions as:

$$\frac{\eta_{sp}}{c} = [\eta] + k_H [\eta]^2 c \quad (5.4)$$

where, η_{sp} is the specific viscosity, η_{sp}/c is the reduced viscosity (dl/g), k_H is the Huggins coefficient, and c is the polymer concentration (g/dl).

Figure 5.17 presents the reduced viscosity data for each polyaniline emeraldine base sample prepared at different temperatures.

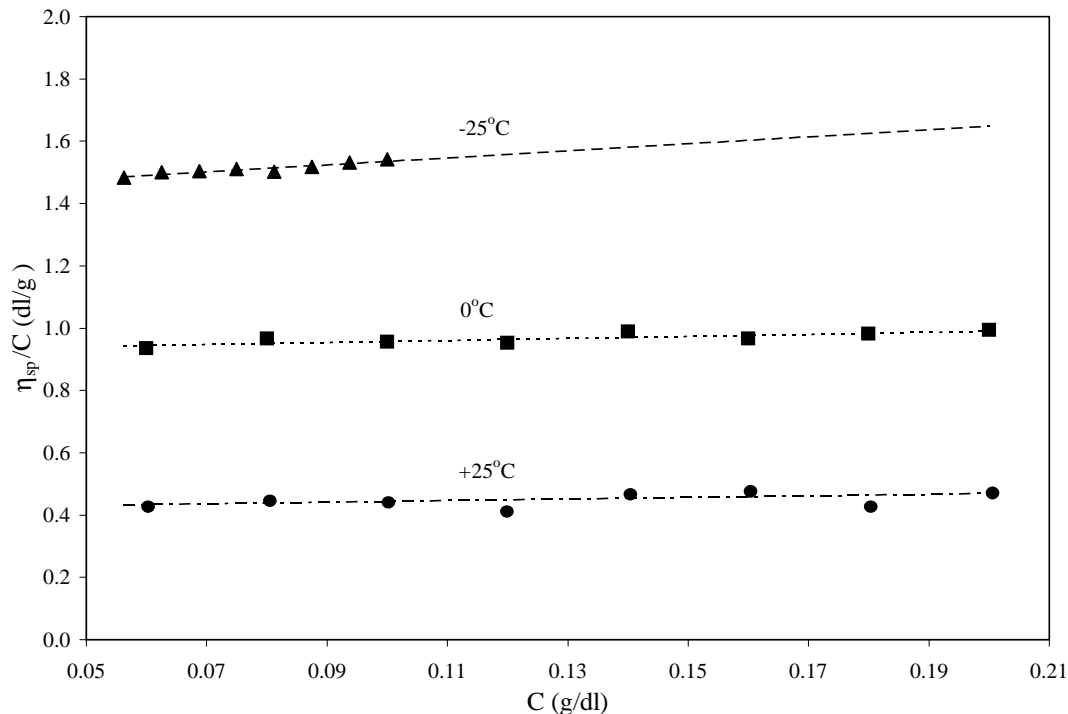


Figure 5.17: Reduced viscosity vs concentration for dilute EB/NMP/LiCl solutions at 28°C using three different EB molecular weights.

The addition of LiCl to the EB/NMP solutions yields linear data fits. Therefore, equation 5.4 is assumed to be valid for this system. Using equation 5.4 and Figure 5.17, the Huggins coefficient (k_H), and the intrinsic viscosity data for these polyaniline emeraldine base solutions were calculated and presented in Table 5.8.

The k_H values for polyaniline emeraldine base (EB) synthesized at 0°C and -25°C EB are in the typical range of 0.3~0.6 that most polymer systems exhibit. However, the k_H value for the same polymers prepared at +25°C EB is larger than expected. The Huggins coefficient, k_H , is a measure of polymer-polymer interactions in solution and experimentally, it is independent of molecular weight

Table 5.8: The intrinsic viscosity, $[\eta]$, Huggins coefficient, k_H and molecular weight (\bar{M}_w , found by static light scattering measurements, SLS) of EB/NMP/LiCl solutions.

Parameters	EB-1 (+25°C)	EB-2 (0°C)	EB-3 (-25°C)
$[\eta]$ (dl/g)	0.42	0.93	1.42
k_H	1.42	0.38	0.56
\bar{M}_w (g/mol) by SLS	29,200	78,700	157,000

for long chains. A higher k_H value implies that the interactions between different molecules become stronger. k_H assumes very high values when intermolecular association exists [161].

The correlation between the weight average molecular weight (\bar{M}_w) and the intrinsic viscosity of a polymer is described by the Mark-Houwink equation:

$$[\eta] = K \bar{M}_w^a \quad (5.5)$$

where, K and a are constants for a given polymer/solvent/temperature system. Generally, $0.5 \leq a \leq 0.8$ for flexible chain conformations, while $0.8 \leq a \leq 1.0$ for rigid molecules. Typically, the value of K decreases as the a increases, and its value for flexible chains is in the range of 10^{-4} to 10^{-2} dl/g.

Figure 5.18 is a power law fit of the experimental data using the values of \bar{M}_w given in Table 5.8 and equation 5.5 where $\log[\eta]$ was plotted against $\log \bar{M}_w$. The K value was calculated from the intercept as 2.34×10^{-4} dl/g and a , the slope of the line was 0.73 for this system. Both values of K and a indicate that the chains

conformation of polyaniline emeraldine base behave flexibly when dissolved in NMP with the presence of acceptable amount of lithium chloride.

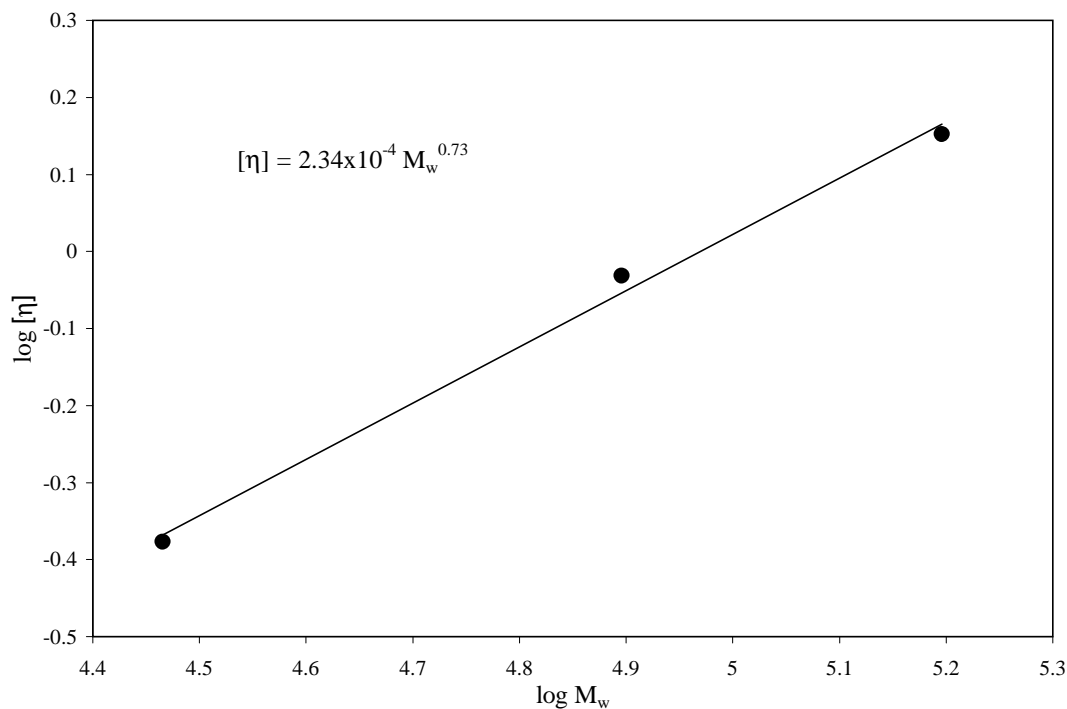


Figure 5.18: Intrinsic viscosity as a function of molecular weight for dilute solutions of EB/NMP/LiCl at 28°C.

5.2.3 Dynamic Light Scattering (DLS)

The DLS measurements were carried out on solutions of reduced polyaniline samples prepared at different temperatures of +25, 0, and -25°C. The chosen solvent was N-methyl-2-pyrrolidinone (NMP). Each polyaniline sample was diluted into four concentrations of 0.2, 0.15, 0.10, and 0.05 g/dl. The measurements were taken from polarized scattered light at the wavelength of 632.8 nm and 25°C with scattering angles of 30°, 45°, 90°, and 120° for each concentration separately. The results are shown through Figures 5.34 and 5.36 as D_{app} vs q^2 respectively.

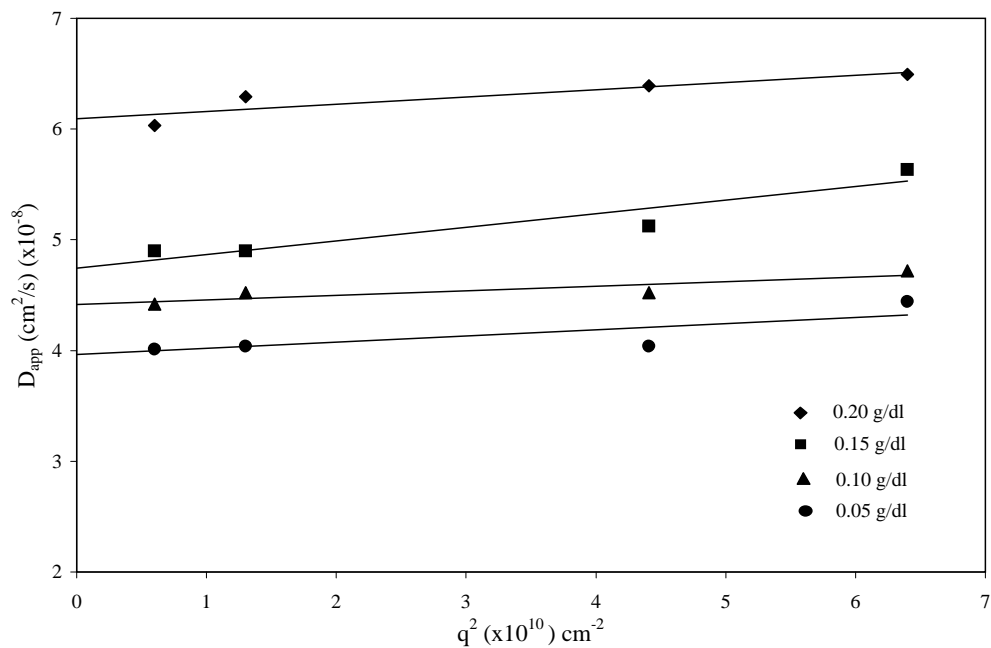


Figure 5.19: The apparent diffusion coefficient (D_{app}) vs the square of the wave vector (q^2) for polyaniline prepared at +25°C.

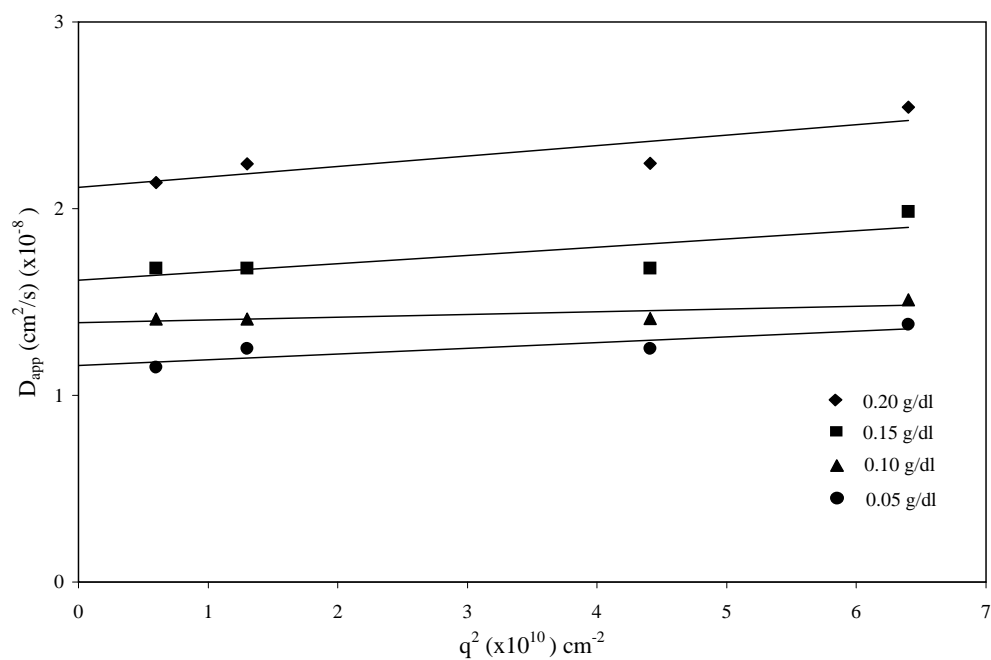


Figure 5.20: The apparent diffusion coefficient (D_{app}) vs the square of the wave vector (q^2) for polyaniline prepared at 0°C.

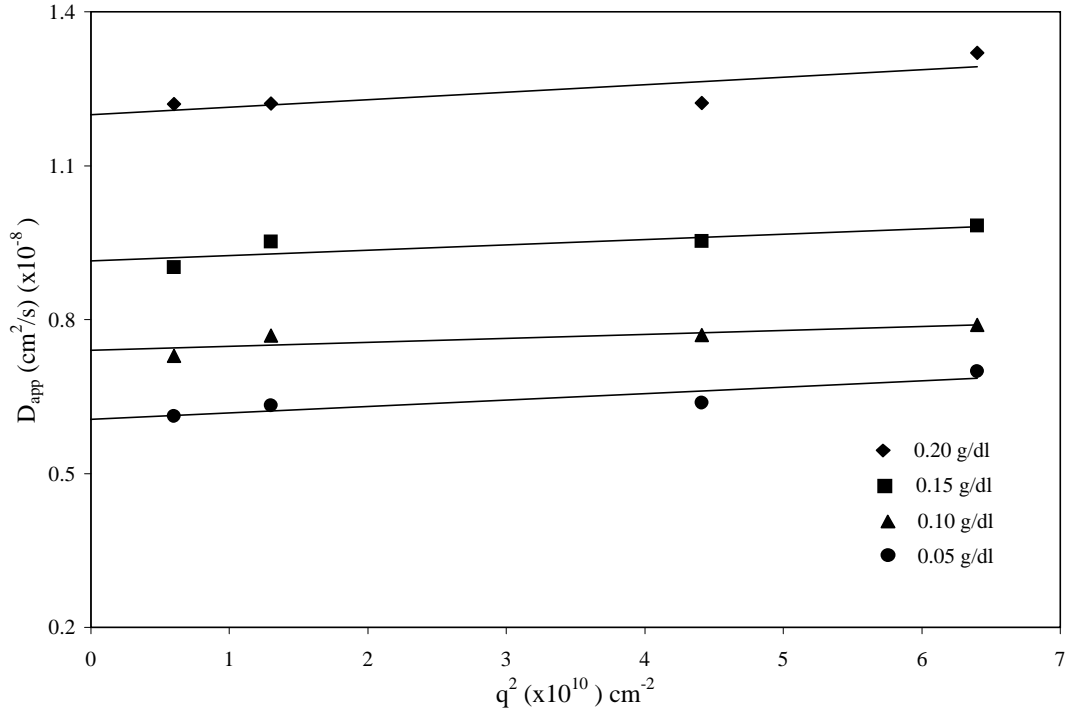


Figure 5.21: The apparent diffusion coefficient (D_{app}) vs the square of the wave vector (q^2) for polyaniline prepared at -25°C .

The double extrapolation of $D_{app}(q, c)$ in the limits of $c \rightarrow 0$ and $q \rightarrow 0$ can be alternatively carried out in a dynamic Zimm plot, giving the diffusion coefficient at infinite dilution (D_o) from which the hydrodynamic radius (R_H) can be obtained from the Stokes-Einstein relationship:

$$R_H = \frac{k_B T}{6\pi\eta D_o} \quad (5.6)$$

where η is the solvent viscosity and $k_B T$ is the Boltzmann constant multiplied by the absolute temperature. Values of D_o , k_D as well as the hydrodynamic radius, R_H from the Stokes-Einstein relationship are listed in Table 5.9.

Table 5.9: D_o , k_D , and R_H data obtained from dynamic light scattering measurement for reduced polyaniline solutions at 25°C.

Synthesis Temperature (°C)	$D_o \times 10^7$ (cm ² /sec)	R_H (nm)	k_D
+25	32	11.00	4.40
0	7.90	16.10	8.51
-25	4.10	18.90	9.10

The average hydrodynamic radius $\langle R_H \rangle$ of reduced polyaniline samples solutions prepared at different temperatures in NMP (solvent), shown in Table 5.9, had a similar trend as $\langle R_g \rangle$ value, i.e., $\langle R_H \rangle$ increased with increasing molecular weight. This results suggested that the hydrodynamic radius is not solely a function of the chain size or contour length, but it depends on the chain flexibility. The chain flexibility may vary with solvent or molecular weight, resulting in a more compact structure with a lower hydrodynamic radius.

k_D is the constant describing the concentration dependence of the diffusion coefficient. It is well known that in a sufficiently good solvent the diffusion coefficient increases with polymer concentration. As the solvent quality becomes poorer, k_D becomes eventually negative. From Table 5.9, for all our samples k_D values are positive, indicating that the solvent investigated is good solvent for the reduced polyaniline samples. k_D values also support the result of k_H as determined by viscometry.

Moreover, in Figure 5.22, plots of R_H versus PANI concentration obtained from dynamic light scattering measurements are shown for PANI samples with three different average molecular weights, one having an intrinsic viscosity of 0.42, the second of 0.93 and the third with 1.42 dl/g in NMP.

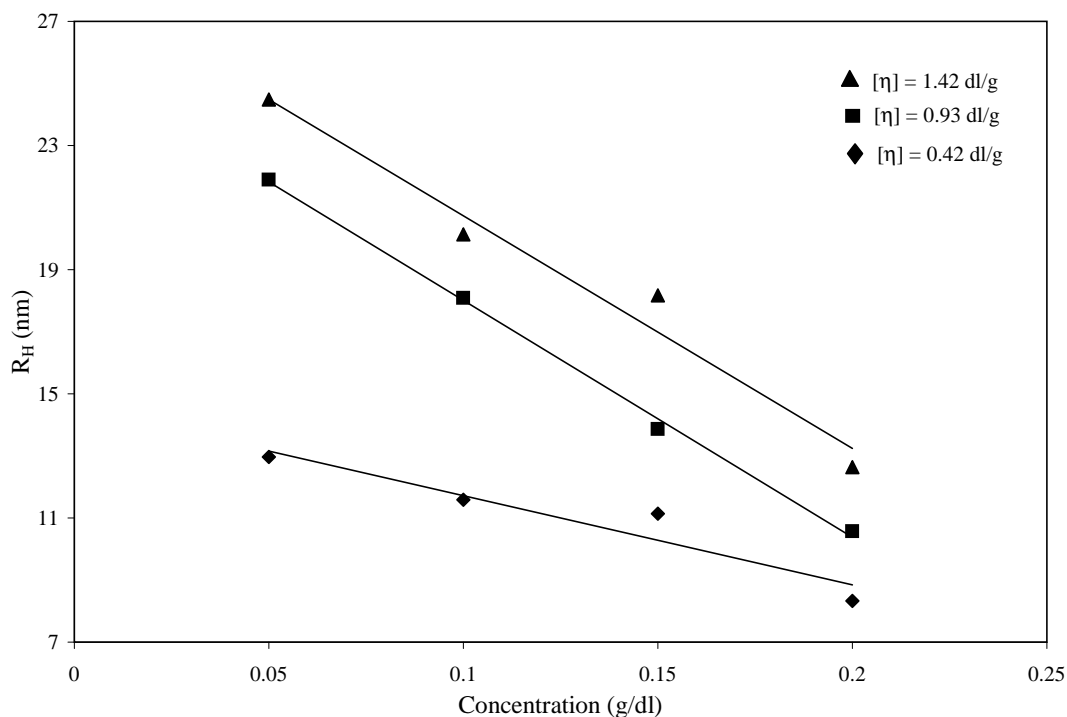


Figure 5.22: R_H vs reduced PANI concentration for PANI in NMP.

As expected, the sample with lower intrinsic viscosity exhibit smaller hydrodynamic radii at comparable concentrations, consistent with the lower molecular weight. In the concentration range of about 0.2 to 0.05 g/dl of polymer, the hydrodynamic radii of the samples increase with decreasing polymer concentration. This extension of the polymer chain with decreasing polymer concentration is a classic signature of polyelectrolyte in dilute solution and occurs because of the reduction in the concentration of ions in solution (ionic strength) as the overall

concentration of polymer is decreased. This reduction in ionic strength reduces screening of the charges along the backbone of the polymer. As the screening decreases, the charges along the backbone repel each other more strongly, and the polymer extends.

A combination of static and dynamic light scattering data is summarized in Table 5.10, as an average value of radius of gyration $\langle R_g \rangle$, and ratio of $\langle R_g \rangle / \langle R_H \rangle$ of reduced polyaniline samples.

Table 5.10: The ratio of DLS $\langle R_H \rangle$ and SLS $\langle R_g \rangle$ data of polyaniline solutions.

Synthesis Temperature ($^{\circ}\text{C}$)	$\langle R_H \rangle$ (nm)	$\langle R_g \rangle$ (nm)	$\langle R_g \rangle / \langle R_H \rangle$
+25	11.00	20.10	1.83
0	16.10	31.70	1.97
-25	18.86	39.80	2.11

During translational motion of the particles, the solvent can penetrate deeply into the fairly open molecular chains leading R_H to be smaller than R_g . However, if the particle is highly compact then only the outer shell is drained by solvent. Thus R_H is larger than R_g for compact molecules. The ratio $\langle R_g \rangle / \langle R_H \rangle$ is an indicator of the compactness of the polymers in solvents. The relation of polymer architecture with $\langle R_g \rangle / \langle R_H \rangle$ in solvents had been summarized by Burchard [162] and listed in Table 5.11, which shows that the ratio decreases with increasing compactness of the polymer chains.

Table 5.11: The ratio $\langle R_g \rangle / \langle R_H \rangle$ for selected structures.

Architecture	$\langle R_g \rangle / \langle R_H \rangle$
Homogeneous sphere	0.778
Random coil, monodisperse	
-theta condition	1.50
-good solvent	1.78
Random coil, polydisperse	
-theta condition	1.73
-good solvent	2.05
Rigid rod	
-monodisperse	>2.0
-polydisperse	>2.0

Comparing the $\langle R_g \rangle / \langle R_H \rangle$ ratios listed in Tables 5.10 and 5.11, we found that the polyaniline molecules behaved like random coils at low molecular weight and behaved like rigid rod at high molecular weight. These results are in consistent with $[\eta]$ and R_g data mentioned before.

5.3 Low Density Polyethylene-Based Polyaniline Conducting Polymer Composites

Polyethylene (PE) is a polymer with excellent mechanical properties, high resistance to chemical agents, and good processability. Polyaniline (PANI) emeraldine salt type was obtained chemically by oxidation at 25°C. Grains of low density polyethylene (LDPE) were mixed with Polyaniline emeraldine salt having a conductivity of about 0.2 S m⁻¹ as mentioned in Chapter 4 (Section 4.6). Thermal properties, mechanical properties, conductivity measurements, and morphological

properties of the resulting composites were studied and analyzed.

5.3.1 Thermal Analysis

Figure 5.23 shows the DSC melting curves for LDPE and its composites.

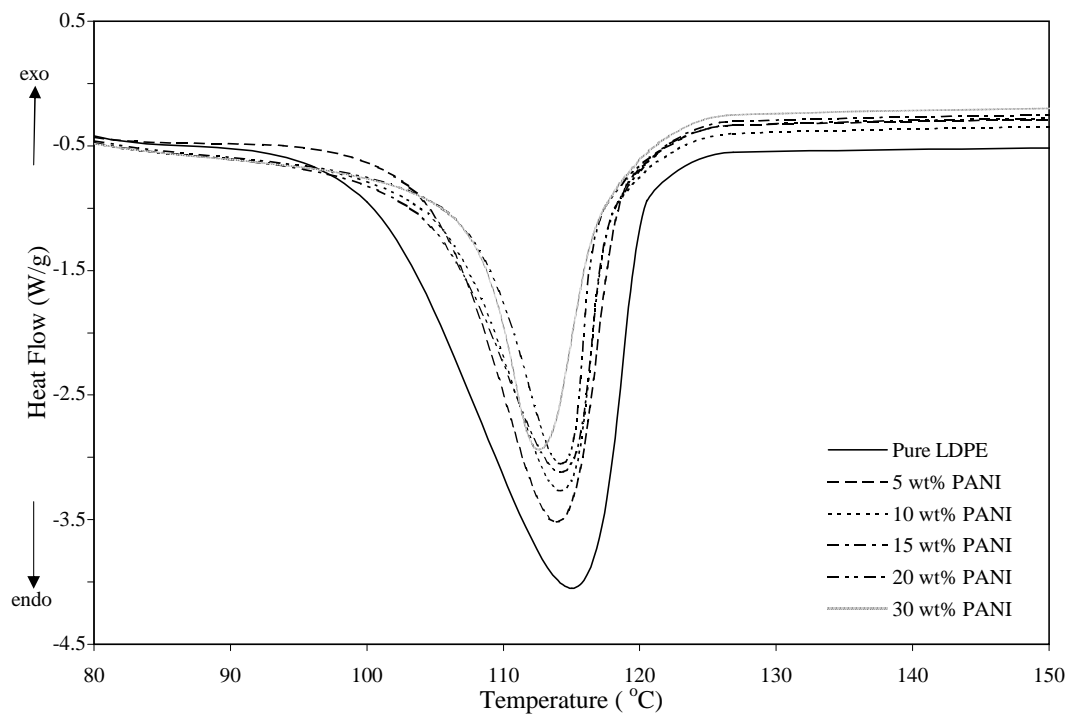


Figure 5.23: DSC melting curves of LDPE and its PANI powder composites.

Polyaniline (PANI) content does not seem to have much influence on the melting temperature of low density polyethylene (LDPE). The melting temperatures and heat of fusions, ΔH_f (area under the melt endotherm curve) for pure LDPE and its composites are given in Table 5.12.

The polyaniline powder used in this composite is completely amorphous. Therefore, the amorphous phase of the composite will increase at the expense of lower crystalline phase. So, there is a little change in the peak temperature of

melting with increasing polyaniline content which indicates that the percent crystallinity of the composites decrease slightly with increasing polyaniline content (Figure 5.23).

Table 5.12: Melting temperatures, T_m and heat of fusions, ΔH_f , for pure LDPE and its composites.

Material Type	Melting Temperature, T_m ($^{\circ}\text{C}$)	Heat of Fusion, ΔH_f (J/g)
LDPE	114.40	219.90
5 wt% PANI	113.39	186.60
10 wt% PANI	113.68	177.80
15 wt% PANI	112.72	162.10
20 wt% PANI	113.55	161.80
30 wt% PANI	113.44	139.40

Moreover, the TGA curves for LDPE and its polyaniline composites are shown in Figure 5.24. There is a clear increase in the thermal stability of LDPE with increasing polyaniline content. This may be explained through higher thermal stability of polyaniline. This will result in PE chains starting to degrade at higher temperatures.

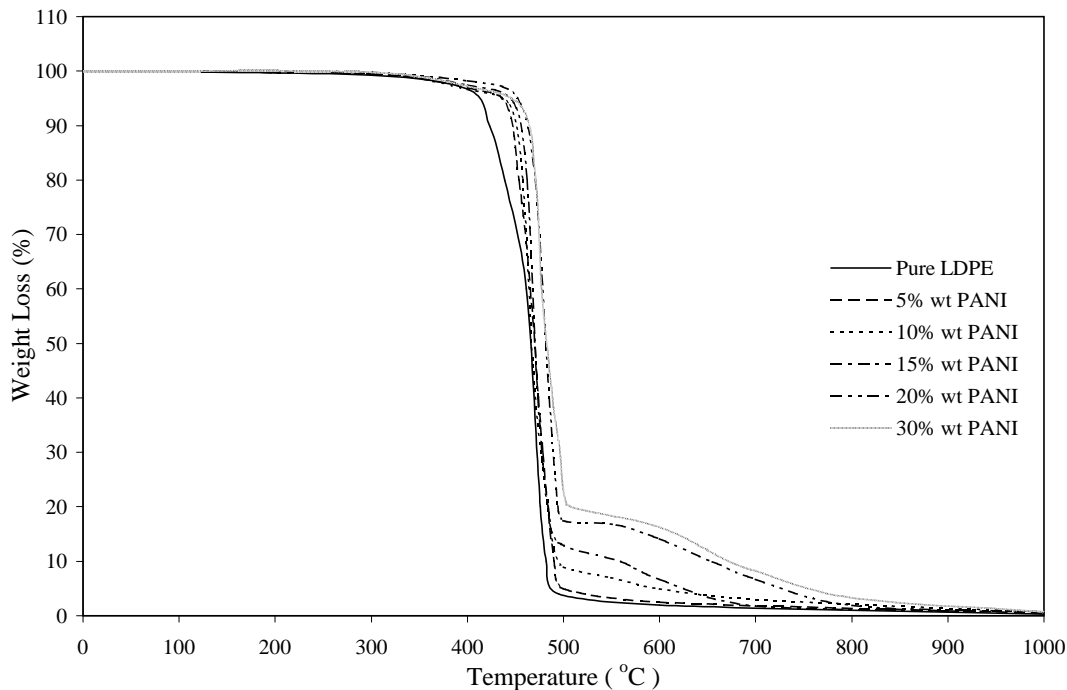


Figure 5.24: TGA curves of LDPE and its PANI powder composites.

5.3.2 Mechanical Properties

The incorporation of polyaniline particles synthesized at 25°C (as a filler), into thermoplastic low density polyethylene matrices produces significant changes in the mechanical properties of the resulting composites. These changes were investigated by using standard tensile test. The experimentally determined tensile strength, tensile strain at break, and tensile (elastic) modulus of Polyethylene-Polyaniline composites are given in Figure 5.26, Figure 5.27, and Figure 5.28 respectively. The results of all tensile properties obtained experimentally are shown in Table 5.13 below.

Table 5.13: Experimentally calculated data of tensile strength at maximum load (σ_{max}), tensile modulus (E), tensile strength at break (σ_b), and tensile strain at break (ε_b) with respect to polyaniline (PANI) contents in polyethylene matrix.

PANI (wt%)	σ_{max} (MPa)	E (MPa)	σ_b (MPa)	ε_b (%)
0	14.48 \pm 2.52	107.12 \pm 25.10	8.13 \pm 2.77	203.70 \pm 10.4
1.5	13.20 \pm 2.40	133.78 \pm 19.22	12.37 \pm 2.52	117.24 \pm 6.72
5	12.76 \pm 2.20	144.66 \pm 16.60	12.43 \pm 2.14	15.50 \pm 2.12
10	11.50 \pm 3.81	169.31 \pm 19.32	11.23 \pm 2.44	13.80 \pm 1.20
15	10.58 \pm 2.61	180.33 \pm 29.16	10.48 \pm 2.51	11.93 \pm 2.50
20	9.08 \pm 2.27	204.53 \pm 14.11	8.90 \pm 2.64	10.83 \pm 2.30
30	8.41 \pm 2.78	247.90 \pm 31.09	8.40 \pm 2.36	7.70 \pm 1.70

Figure 5.25 is the plot of the stress-strain curves of polyaniline (PANI) filled low density polyethylene (LDPE) composites. It can be seen from this figure that the tensile strain at break (ε_b) of the specimens decreases with increasing the weight percent of polyaniline (PANI) particles in low density polyethylene (LDPE) matrix. The tensile stress (σ_{max}) of the composites is lower than that of pure polyethylene, however, attention should be made here that the tensile stress of the composite decreases as the weight percent of polyaniline increases in LDPE matrices. This can be explained as follows: as the amount of polyaniline increases in the polyethylene matrix, polyaniline particles aggregate together in one side and hence good distribution of the filler in PE matrix becomes difficult

to be achieved. Therefore, the mechanical properties of this composite enhances at low polyaniline concentration and become poorer otherwise.

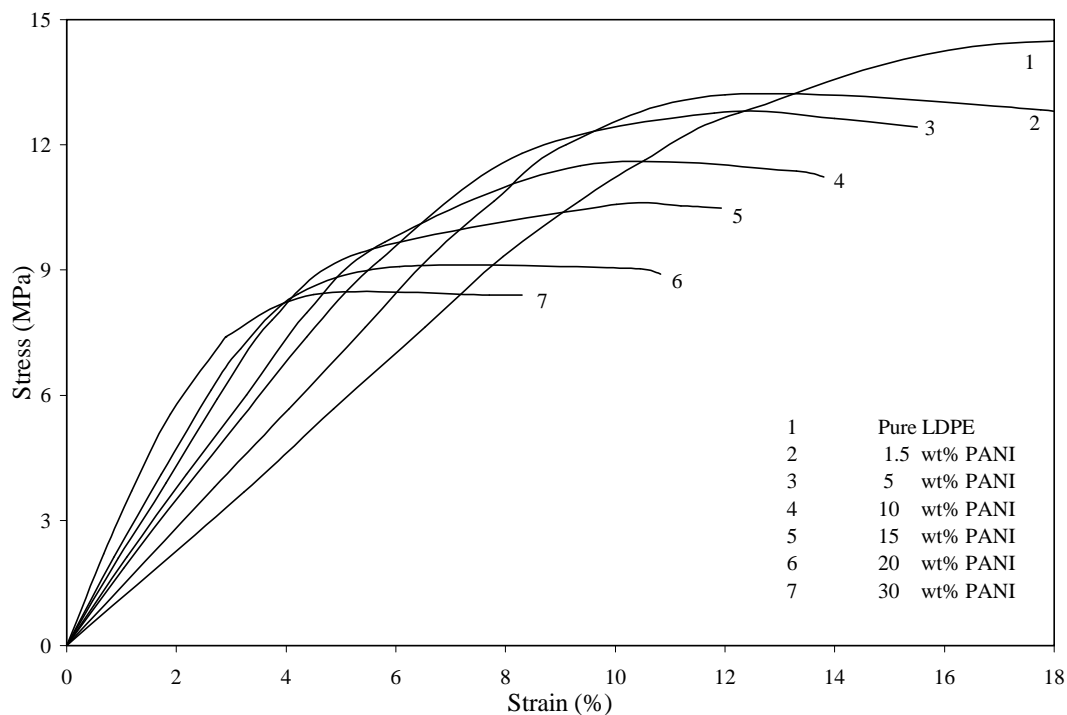


Figure 5.25: Tensile stress-strain curves of LDPE-PANI system.

As noticed from Figure 5.26, the tensile strength, σ_{max} , is reduced as the content of PANI (wt/wt) is increased. The elongation at break, ε_b , decreases drastically as PANI is introduced in PE (Figure 5.27). Also, the dependence of Young modulus of composites on the weight percentages of filler is shown in Figure 5.28. An increase in Young modulus with increasing PANI content is observed. The size and distribution of the filler particles play a significant role, since the filler is much stiffer than the polymer matrix, and the stiffness increases with increasing filler content. Hence, except Young modulus, the mechanical features of PE/PANI composites become poorer as the PANI content is increased.

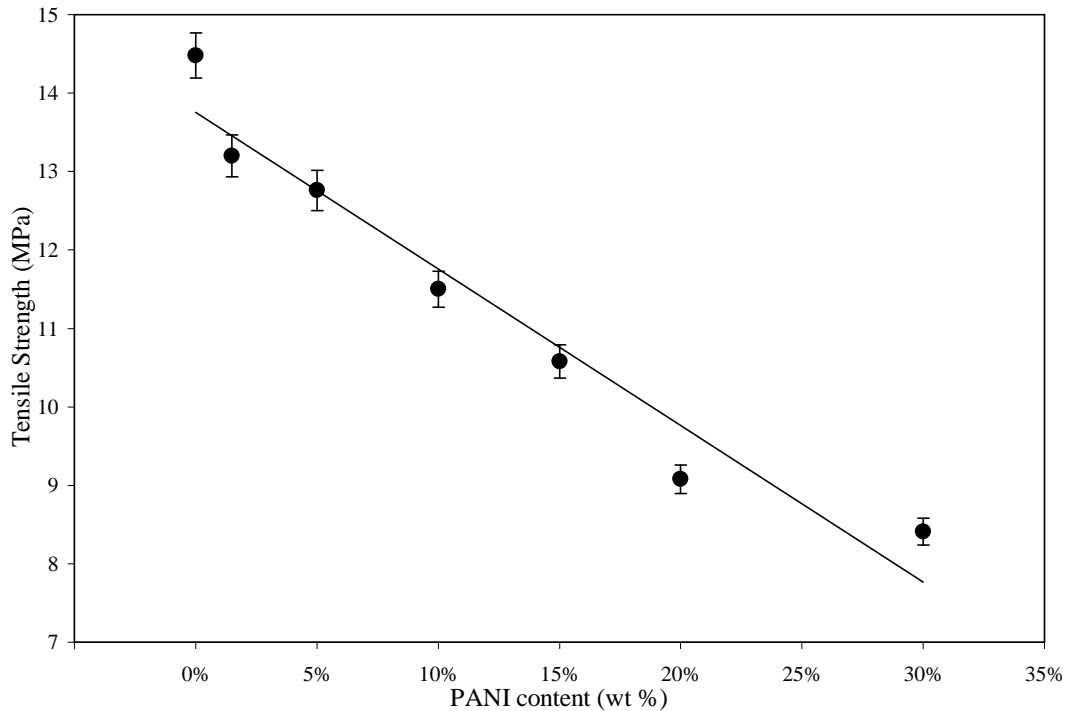


Figure 5.26: The dependence of tensile stress on polyaniline content.

In PE/PANI composites, the polymeric phase consists of linear chains with reduced branches. Due to the flexibility of PE macromolecular chain, the polymer is folded on closely packed crystalline domains. The macromolecular chain of PANI is shorter and has a reduced flexibility than PE chains. The low glass transition temperature of PE indicates that at room temperature, the segmental motions are activated and the amorphous domains will behave as a high viscosity fluid. This suggests a preferential location of PANI chains in PE crystalline domains [108].

By inspecting Figure 5.26 and Figure 5.27, it is noticed that the tensile strength is more sensitive to the adhesion between the filler and the polymeric matrix than the elongation at break.

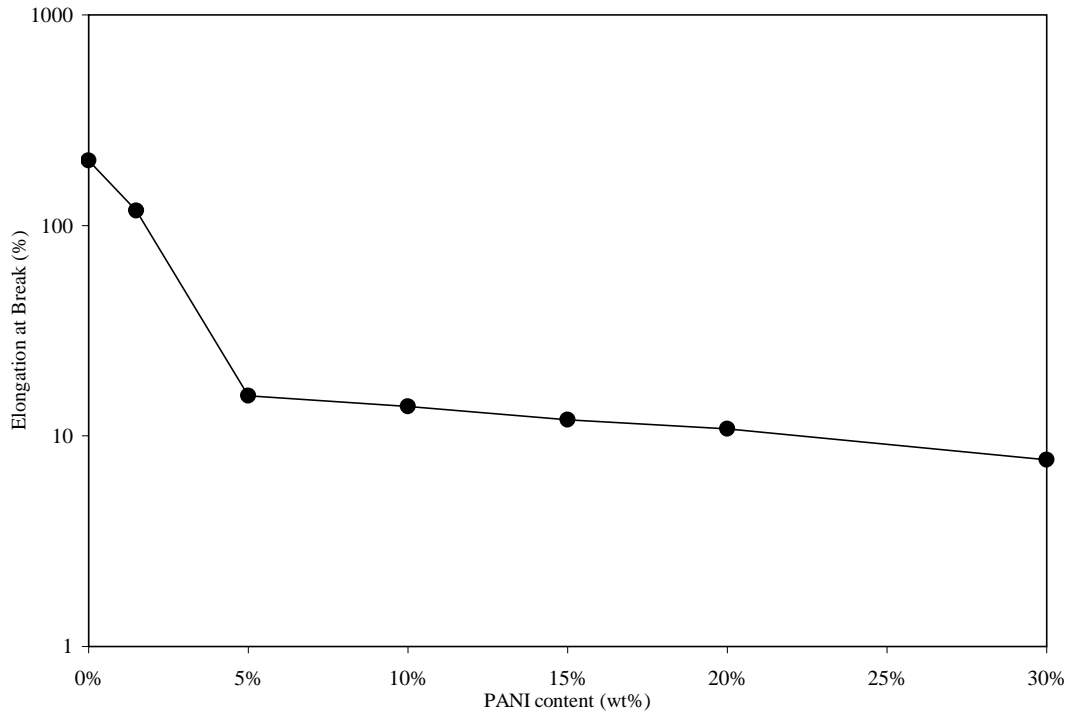


Figure 5.27: The dependence of elongation at break on polyaniline content.

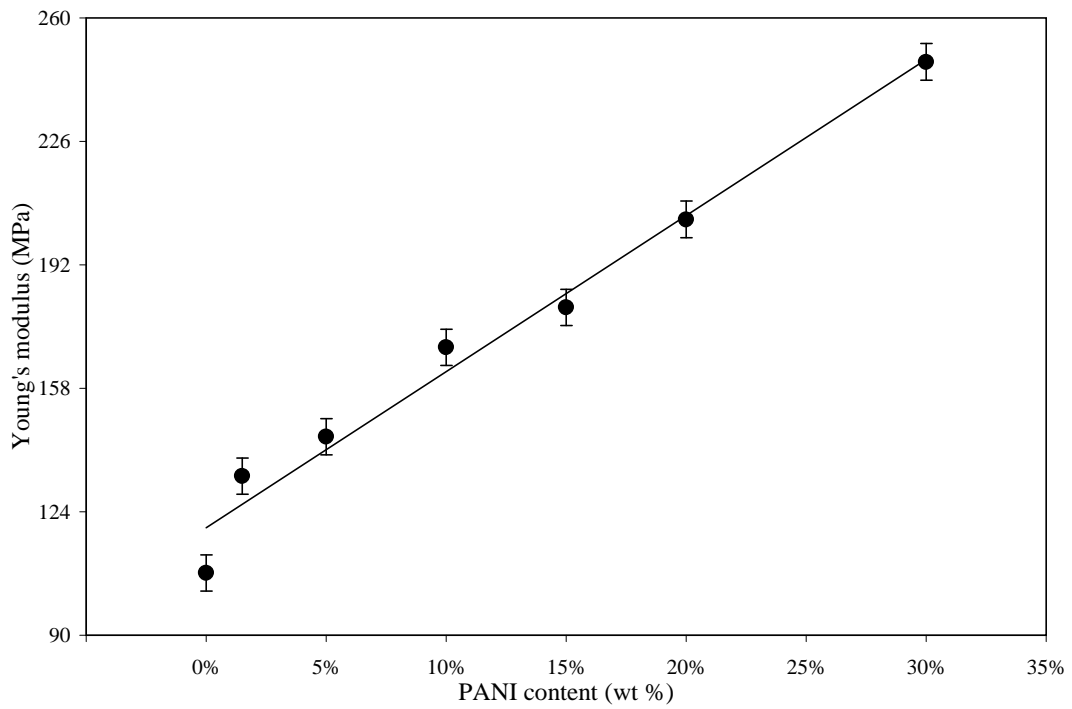


Figure 5.28: The dependence of Young modulus on polyaniline content.

The elongation at break is severely affected by the poor mechanical features of PANI. While the concentration of PANI increased, the distance between PANI particles is depressed. Due to the poor adhesion, the PE chains are able to slip along the PANI particles. This increases the stress exerted on PANI particles, which due to their extremely poor mechanical properties will generate microcracks and initiate the polymer fracture. A simple representation of the mechanical properties of the composite near the percolation threshold may be provided by the Voigt model [108], where the string is assigned to PE chains and a dashpot and a string with a very low elasticity represents PANI chains. The reduced elongation at break of PANI will trigger a rapid failure of the composite material. This suggests a formal analogy between the dependence of the DC conductivity on conducting particle concentration and the dependence of the elongation at break on PANI content, near the percolation concentration, as will be seen in the next section.

5.3.3 Relation Between Conductivity and Elongation at Break

An apparent coincidence of the dependencies of elongation at break and conductivity on the filler content is of particular interest. It was stated that steep drop in the elongation at break occurs within the concentration range around the conductivity percolation threshold [163]. Table 5.14 and Figure 5.29 demonstrate this effect in PE/PANI composite.

Table 5.14: The relationship between conductivity and elongation at break at different content of PANI in PE matrix.

PANI content (wt%)	Conductivity (S/cm)	Elongation at break (%)
0	1.00×10^{-17}	203.70
1.5	5.85×10^{-7}	117.24
5	1.95×10^{-5}	15.50
10	5.22×10^{-5}	13.80
15	9.68×10^{-5}	11.93
20	2.44×10^{-4}	10.83
30	8.30×10^{-4}	7.70

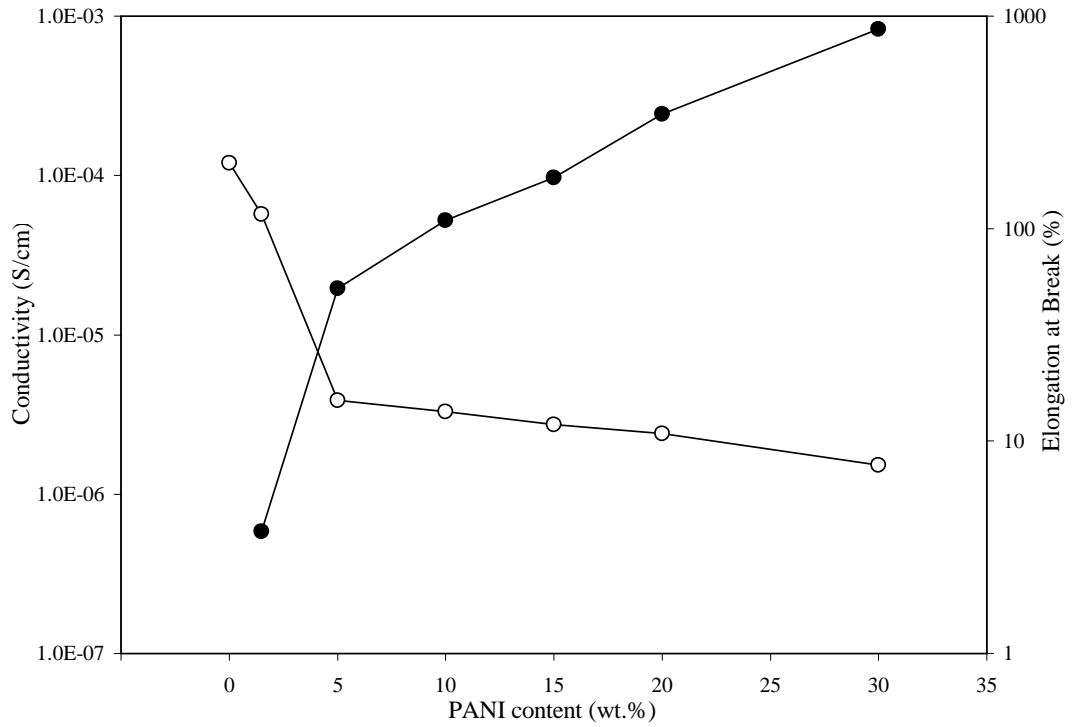


Figure 5.29: (●) Conductivity and (○) elongation at break of PEPANI composites as a function of the PANI content.

Although this observation is phenomenological, it is quite acceptable that the formation of the conductive network, leading to a substantial increase in conductivity, has a pronounced effect on the mechanical properties via a formation of a more or less continuous filler phase [164]. The critical crack formation and unstable crack growth in such a system is expected to be much easier and faster than in the virgin polymer matrix or in the material where the filler is present but the continuous network has not been formed yet. The less perfect distribution of PANI particles in PE matrix, leads to the formation conducting PANI “channels” already at lower concentrations, which leads to higher conductivity, on the one hand, but also to the formation of more frequent failure sites, on the other hands.

5.3.4 Morphological Analysis

Fracture surfaces of the tensile-tested composites were studied by SEM to observe the existence of adhesion between the filler (PANI), and the matrix (PE). In Figure 5.30, our discussion is aimed at showing the interfacial adhesion in this composite structure, and the effects that may arise from the incorporation of different filler content on the fracture behavior of this composite.

It is observed that the amount of polymer needed for complete coating of particle’s surface inside the composite structure decreases with increasing filler content. Therefore, cluster of solid particles within the structure impart brittle behavior to the composite and as a result, lower strain at break and lower fracture energy will arise.

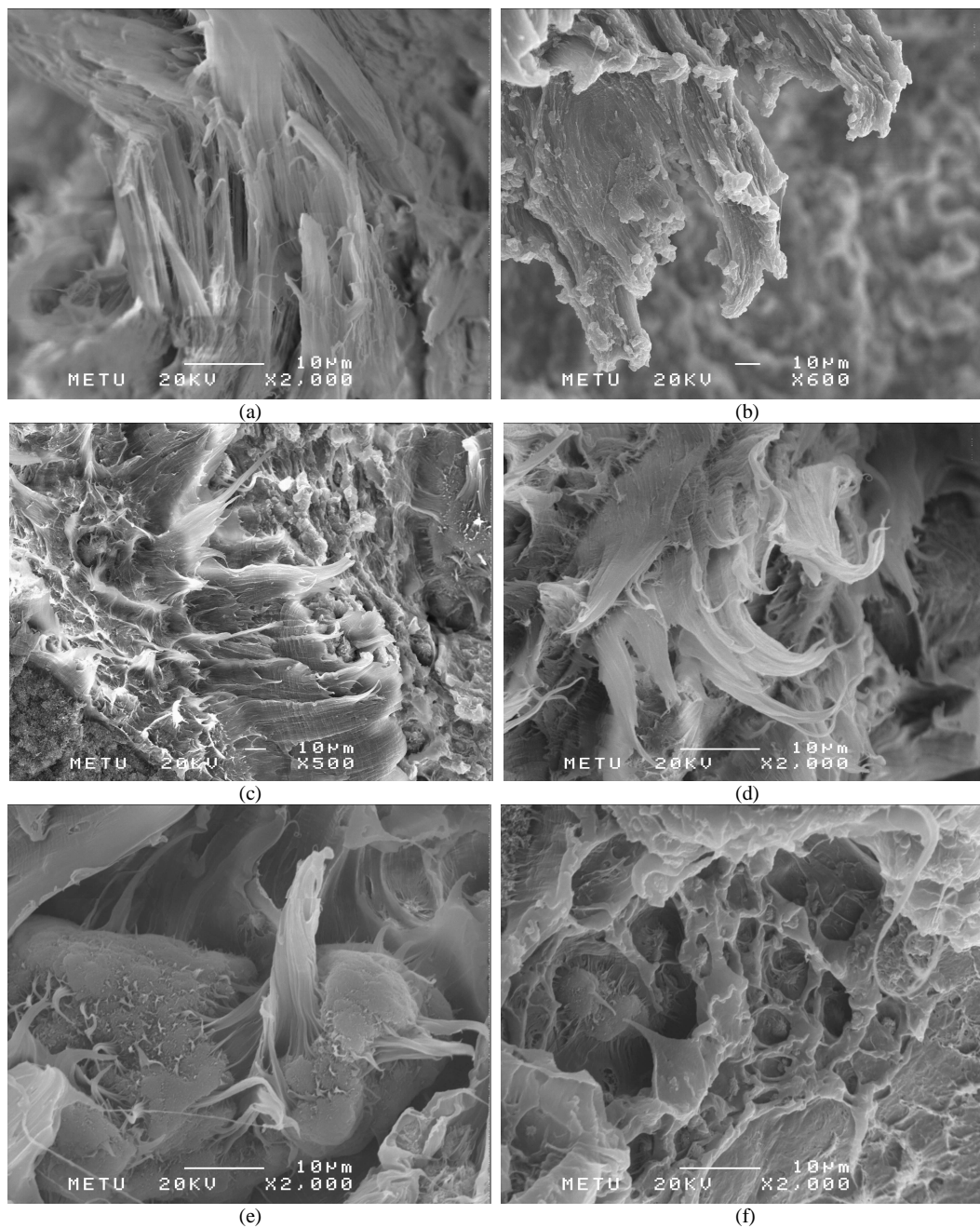


Figure 5.30: SEM micrographs of the surfaces of the stretched PEPANI composite: (a) pure LDPE, (b) 5 wt.%, (c) 10 wt.%, (d) 15 wt.%, (e) 20 wt.% and (f) 30 wt.% of PANI.

Orientation of PE matrix during tensile test is apparent in Figure 5.30 (a,b,c,d,e, and f). This fractograph shows that the PANI particles are driven out of the PE matrix, while PE shows orientation along the draw direction.

Furthermore, PANI particles weakly adhered to the matrix and resulted in splitting the polymer matrix along the draw direction.

There are obvious differences in the tensile morphologies of PE/PANI composites. A neck structure forms in the tensile process of the composites with low PANI contents and pure PE. With the increase in the PANI content, the length of the neck region decreases. When the PANI content exceeds 5% by weight, there is no neck structure.

Figure 5.30 shows the micromechanical deformation process of PE/PANI composite with different weight percentages of PANI. Before tensile deformation, the surface of the sample is smooth. When the sample yields, a cracklike structure can be observed that crosses to both sides of the sample perpendicularly to the loading direction. When the sample fractures, a zone with bounds of cracklike structures is seen near the fracture surface in low magnification. In a high-magnification micrograph, large plastic deformation of the matrix ligaments between the filler particles can be seen in cracklike regions, and numerous voids can be found.

The micromechanical deformation process of the PE/PANI composites is different from that of neat LDPE. In the tensile process of neat LDPE, an obvious neck structure can be observed, and plastic deformation mainly occurs at the edge of the neck before the neck structure develops to the ends of the sample. There is almost no plastic deformation in PE/PANI composites because of the

strain-hardening phenomenon. The strain rate of the LDPE sample is only considered the result of the plastic deformation at the edge of the neck, so the local strain rate of the edge is very high, which leads to an obvious neck structure. In the PE/PANI composites, the plastic deformation occurs in the whole neck region. The strain rate of the PE/PANI composites is considered the result of the deformation of the whole neck region.

5.4 Conducting Polymer Composite of Multi Wall Carbon Nanotubes Filled-Polyaniline

Tubular composite of protonic acid doped polyaniline (PANI) with multi wall carbon nanotubes (MWNT) was synthesized by *in situ* chemical oxidation polymerization as mentioned in Chapter 4 (Section 4.7). The properties of the resulting polymer was analyzed and discussed here.

5.4.1 Composite Formation Mechanism

The formation of tubular composites is believed to arise from the strong interaction between aniline monomer and MWNT. The interaction possibly comes from the $\pi - \pi$ electron interaction between MWNT and the aniline monomer. Such strong interaction ensures aniline monomer adsorbed on the surface of MWNT during the formation of tubular composite. MWNTs therefore serves as the template and the core during the formation of the tubular composites. Due to the random formation of MWNT bundles, there are some “special gaps” between individual MWNTs as shown in Figure 5.31.

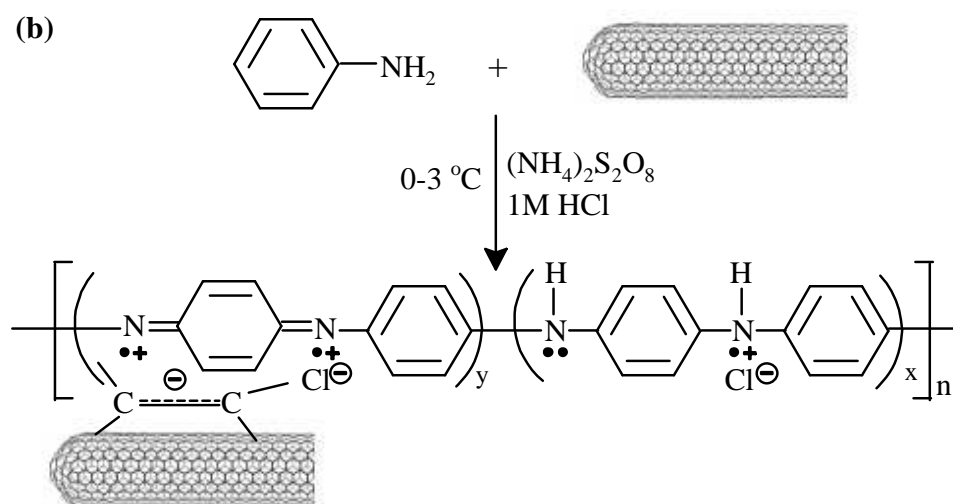
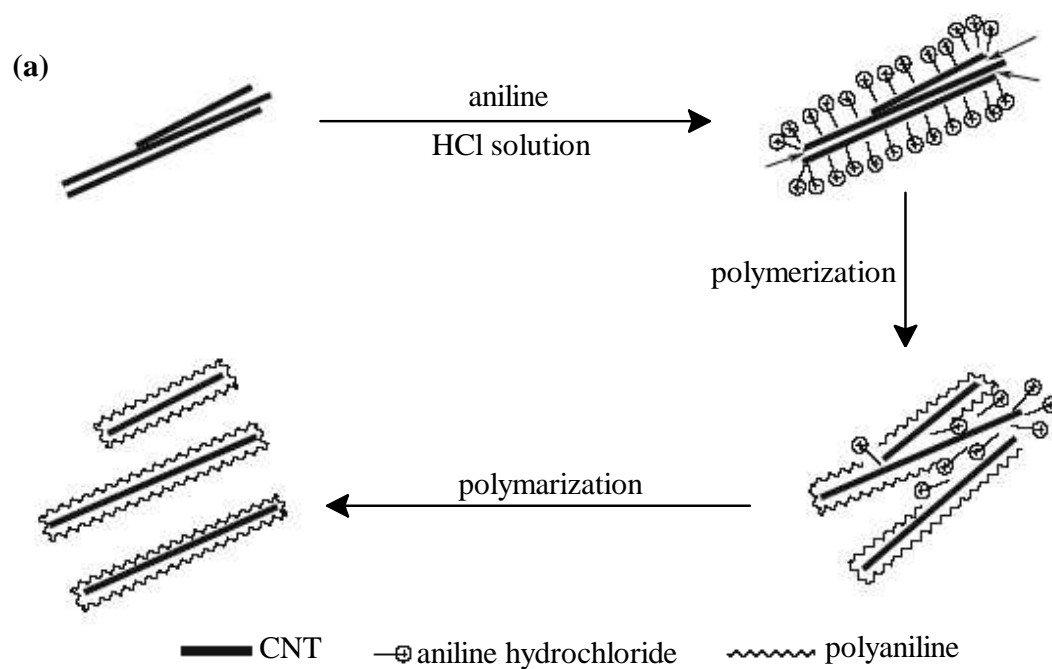


Figure 5.31: Schematic diagram of (a) the formation mechanism for tubular composites of MWNT and PANI, (b) in-situ polymerization and proposed composite interaction.

Aniline molecules were wedged into such “special gaps” because of the strong interaction between MWNTs and aniline monomers, and then in situ polymerization. As polymerization proceeds, the growing polyaniline macromolecules would break down the carbon nanotube bundles into individuals, and thus MWNTs can be dispersed into polyaniline matrices uniformly and individually. Owing to the site-selective interaction between the quinoid ring of the polymer and MWNT, polyaniline macromolecules were also adsorbed at the surface of the MWNT and formed the shell of tubular composites [165,166] as shown in Figure 5.31.

Another mechanism of the composite formations [167] can be explained as follows. When carbon nanotubes are dispersed in aniline/HCl solution, aniline hydrochloride ions get adsorbed on the nanotube surface. On addition of the oxidant (ammonium persulfate) the adsorbed species get oxidized and formed cation radicals which initiates polymerization on the surface. The reaction takes place faster on the surface of carbon nanotube than in the bulk due to low activation energy (based on the principles of heterogenous catalysis). This leads to the formation of the polyaniline shell over CNT. Thus the nanotubes act as template for the formation of tubular composites. In a well dispersed solution of carbon nanotube the adsorption of aniline hydrochloride will be high and uniform, which can lead to the formation of a thicker uniform coating of polyaniline.

5.4.2 Fourier Transform Infrared Spectroscopy Analysis

Figure 5.32 shows the FTIR spectra for the doped polyaniline and the doped *in-situ* prepared composite.

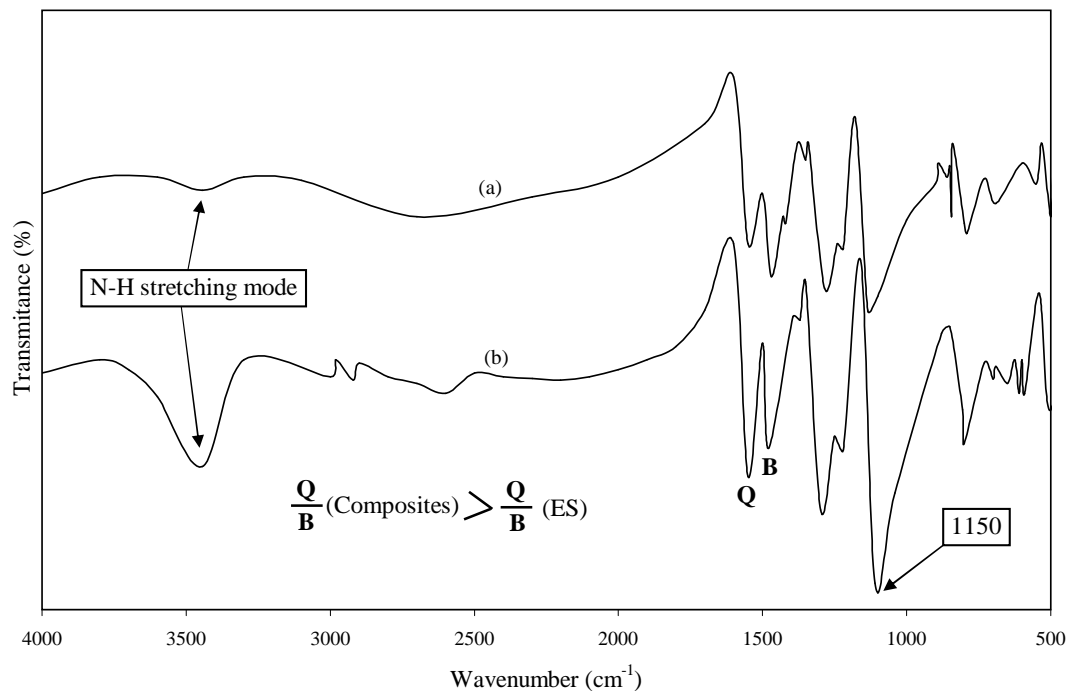


Figure 5.32: FTIR spectra of (a) PANI ES form and (b) 15%wt CNT-PANI ES composite.

Both spectra exhibit the clear presence of benzoid and quinoid ring vibrations at 1500 cm^{-1} and 1600 cm^{-1} , respectively, thereby indicating the oxidation state of emeraldine salt (ES) polyaniline. As commonly observed for ES polyaniline, the quinoid band at 1600 cm^{-1} is less intense than that of the benzoid band at 1500 cm^{-1} . The very weak and broad band near 3400 cm^{-1} is assigned to the N-H stretching mode. The strong band at 1150 cm^{-1} was described by MacDiarmid et al. [168] as the “electronic-like band” and is considered to be a measure of the degree of delocalization of electrons and thus it is a characteristic peak of PANI conductivity.

The FTIR spectrum of the PANI-ES/MWNT composite illustrates several

clear differences from the spectrum of the neat PANI-ES. The composite spectrum exhibits an inverse 1600/1500 cm^{-1} intensity ratio compared to that of the emeraldine salt without carbon nanotubes. These data reveal that the PANI in the composite is richer in quinoid units than the pure PANI-ES. This fact may suggest that nanotube/PANI interactions promote and/or stabilize the quinoid ring structure. The π -bonded surface of the carbon nanotubes might interact strongly with the conjugated structure of polyaniline, especially through the quinoid ring. Aromatic structures [169], in general, are known to interact strongly with the basal plane of graphitic surfaces via π -stacking.

A striking difference between the two spectra in Figure 5.32 is found in the N-H stretching region near 3400 cm^{-1} . This signal is broad and strong in the composite samples yet very weak in the pure ES polyaniline spectrum.

Although the origin of the N-H peak intensity difference is not clear, the interaction between polyaniline and MWNT may result in “charge transfer” as suggested previously [170] and proposed in Figure 5.31 part b. In this case, the carbon nanotube sp^2 carbons compete with the chloride ion (Figure 5.31 b) and thus perturb the H-bonding environment and increase the N-H stretch intensity.

The intensity of other peaks in the composite spectrum is also increased and shifted relative to the peaks observed for the pure emeraldine salt (ES) form. For example, the intensity of the signal at 1143 cm^{-1} increased and shifted to 1123 cm^{-1} . This dramatic increase of the designated “electronic-like absorption” peak defined as (-N=quinoid=N-) agrees well with our increased conductivity measurements. It appears that the interaction between PANI and MWNTs increases

the effective degree of electron delocalization, and thus enhances the conductivity of the polymer chains. The strong interaction may result in carbon nanotubes functioning as a chemical dopant for PANI conductivity.

5.4.3 X-Ray Analysis

The structural characteristics of the composites and its constituents have been analyzed by X-Ray powder diffraction measurements and is shown in Figure 5.33.

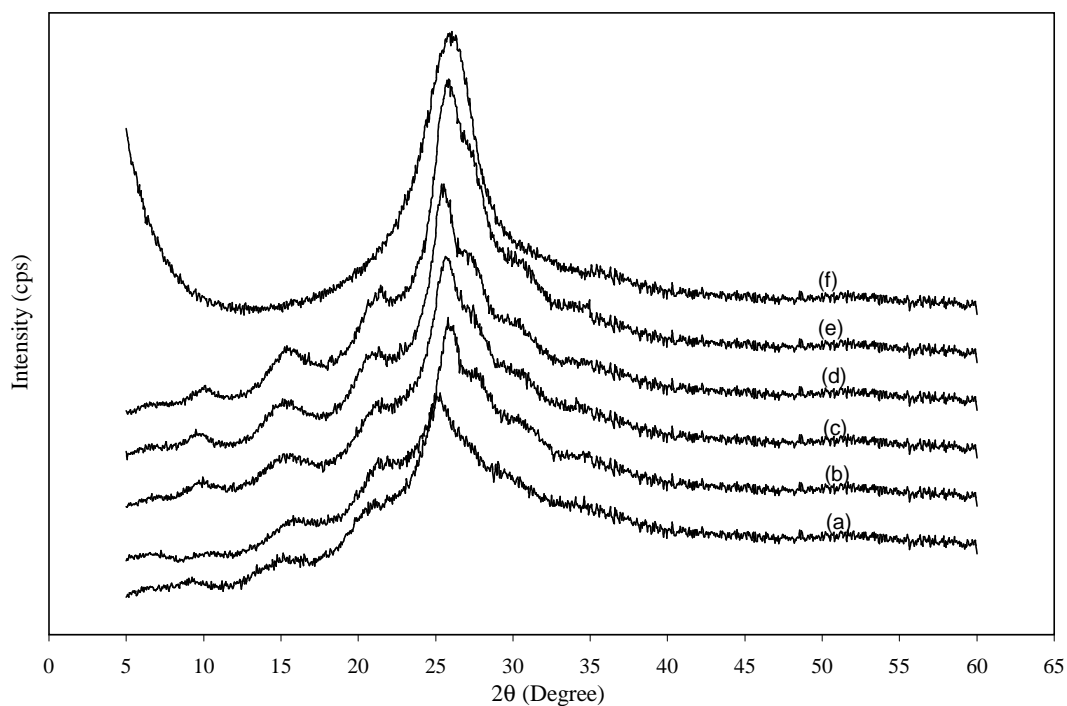


Figure 5.33: X-Ray diffractograms ($\text{Cu-K}\alpha$) of (a)doped PANI emeraldine salt type, (b)composites containing 5wt%, (c)composites containing 10wt%, (d)composites containing 15wt%, (e)composites containing 30wt% of MWNTs and (f)MWNTs.

At lower angles, the diffractograms of the PANI/MWNT materials show the highly pronounced oscillating structure of the primary doped PANI (emeraldine salt) with oxidation degree of 0.5 and at higher angles superimposed the typical

MWNT peaks whose heights increase proportionally to their weight percentages. Therefore, it is clear that from a structural point of view, no additional order has been introduced.

5.4.4 Thermal Gravimetric Analysis

Figure 5.34 shows the thermogravimetric analysis of MWNT/PANI composite powders.

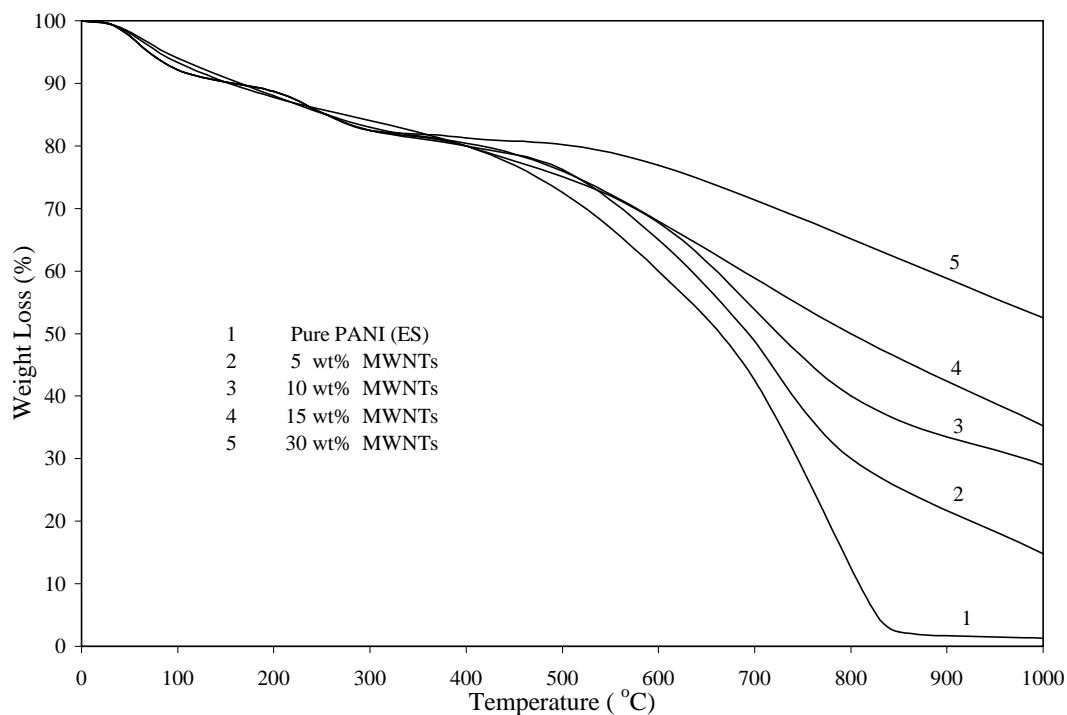


Figure 5.34: Thermogravimetric behavior (TGA) of pure Polyaniline (Emeraldine salt) and PANI/MWNTs composites.

This figure represents a typical three step weight loss behavior. In the first step, approximately 8% weight loss at temperatures up to 130°C is seen. This can be attributed to loss of water molecules from the composite structure. The second

weight loss of about 2-3% at temperatures in the range of 150-250°C may be due to possibly co-evolution of water or evolution of acid. The third step, starting at 350°C onwards, can be observed which represents the oxidative degradation of the composites and also indicates the chemical structure decomposition of the composites backbone. Moreover, by comparing the thermal behavior of composites containing different composition of MWNTs as shown in Figure 5.34, one can observe that MWNTs filler introduce higher thermal stability of the composite material.

5.4.5 Morphological Analysis

The detailed morphology and size of the composites were analyzed by scanning electron microscope (SEM). Figure 5.35 (a), shows the typical SEM image of pure MWNTs. It can be seen that the MWNTs are very long and highly entangled in the solid state to form a dense, robust, network structure. It is very difficult for the MWNTs to be well dispersed in the polymer matrix. The diameters of the MWNTs are in the range of 10-15 nm.

The SEM image of the composite with 30%wt MWNTs is given in Figure 5.35 (e,f). The microscopic studies showed tubular type morphology of the composite, which has a core-shell structure [171], the carbon nanotubes being the cores encapsulated by polyaniline shell. Also, the SEM image of the composite containing 5%wt, 10%wt, and 15%wt MWNTs is represented in Figure 5.35 b, c, and d respectively.

Compared to the carbon nanotube diameters, the diameters in the tubular

composite are high. The microscopic images show that in the composite the nanotubes are uniformly and thickly coated with polyaniline. The tubes are almost of uniform diameter, in the range of 90-105 nm. Moreover, it can also be observed that the tubes in the composite became crowded proportionally to MWNTs weight percent used in the composite.

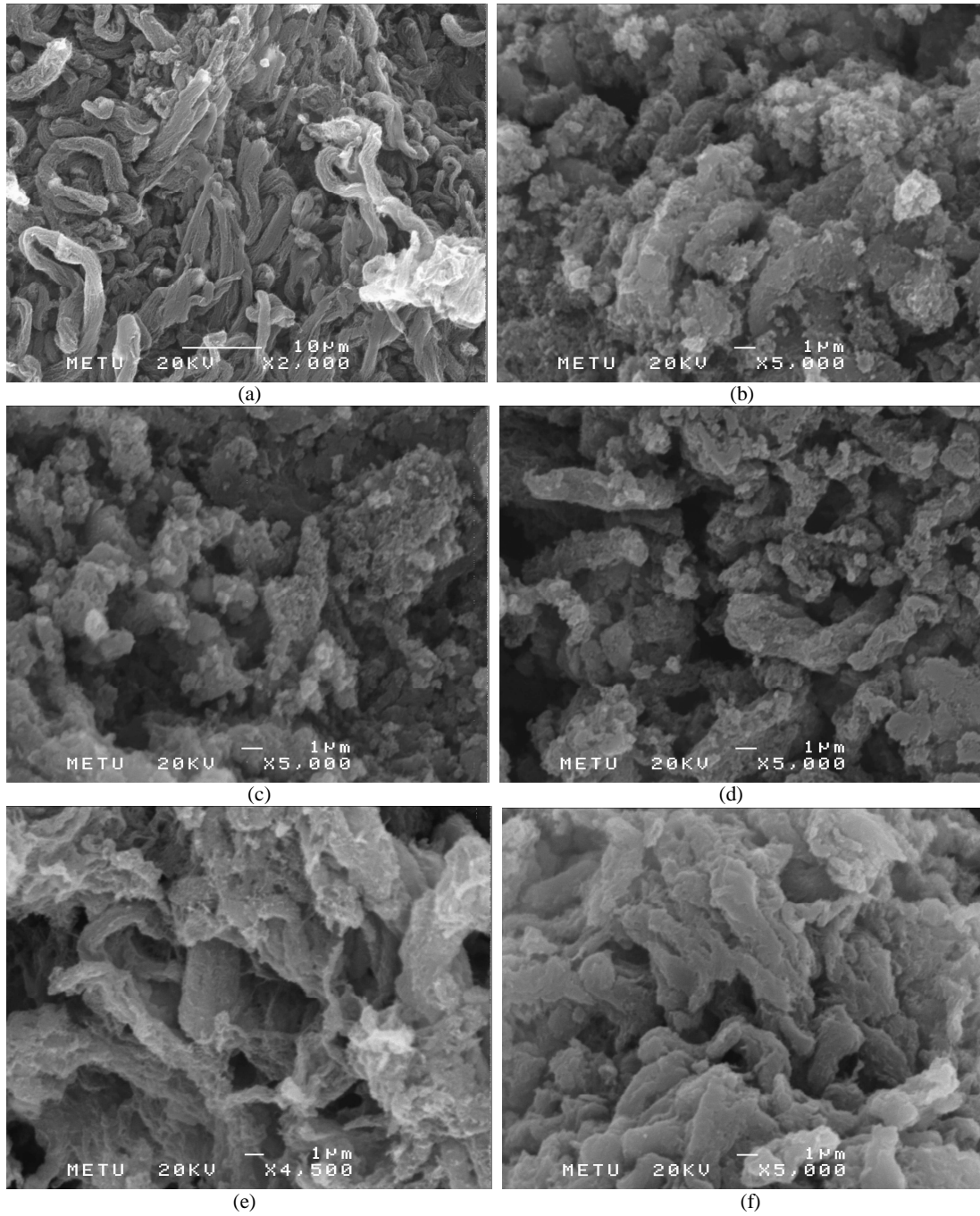


Figure 5.35: SEM image of (a) pure MWNTs, (b) 5%wt, (c) 10%wt, (d) 15%wt, and (e,f) 30%wt of MWNT/PANI composites.

5.4.6 Conductivity Measurement Analysis

The transport properties of the highly filled composites obtained by *in situ* polymerization exhibit the following remarkable facts: (i) The room temperature resistivity is decreased by one order of magnitude as compared to PANI. (ii) The low temperature resistivity is much smaller than both that of PANI as well as MWNTs. (iii) The temperature dependence of the resistivity is weaker than that of PANI.

Regarding point (iii), we can propose the following explanation. In this composite system, both the matrix (PANI) and the filler (MWNTs) are conducting. At high temperatures, the conductivity is obtained by the polymer. Decreasing the temperature, the matrix becomes more and more resistive. On the other hand, the filler network which shows a very weak temperature dependence becomes more conducting than the matrix at low temperature. This means that the low temperature conductivity is due to the MWNTs.

Figure 5.36 shows the room-temperature conductivity of MWNT/PANI composites as a function of the MWNT loading. The conductivity of the pure PANI and MWNT is 1.4×10^{-2} and 1.97 S/cm, respectively. Up to 15wt%, the conductivity of the composite increases rapidly with an increase of the MWNT loading. For 30wt% composite, the conductivity is 2.3×10^{-1} S/cm, which increases by one order of magnitude as compared with PANI. At higher concentrations, the increase of conductivity will plateau, i.e., the curve asymptotically will reach toward pure nanotubes (1.97 S/cm). Here, we note that in many published articles

[172], the loading of nanotubes is small (less than 5%) whereas the conductivity becomes saturated, which is possibly due to the highly conductive carbon nanotubes (5.1×10^4 S/cm) [172].

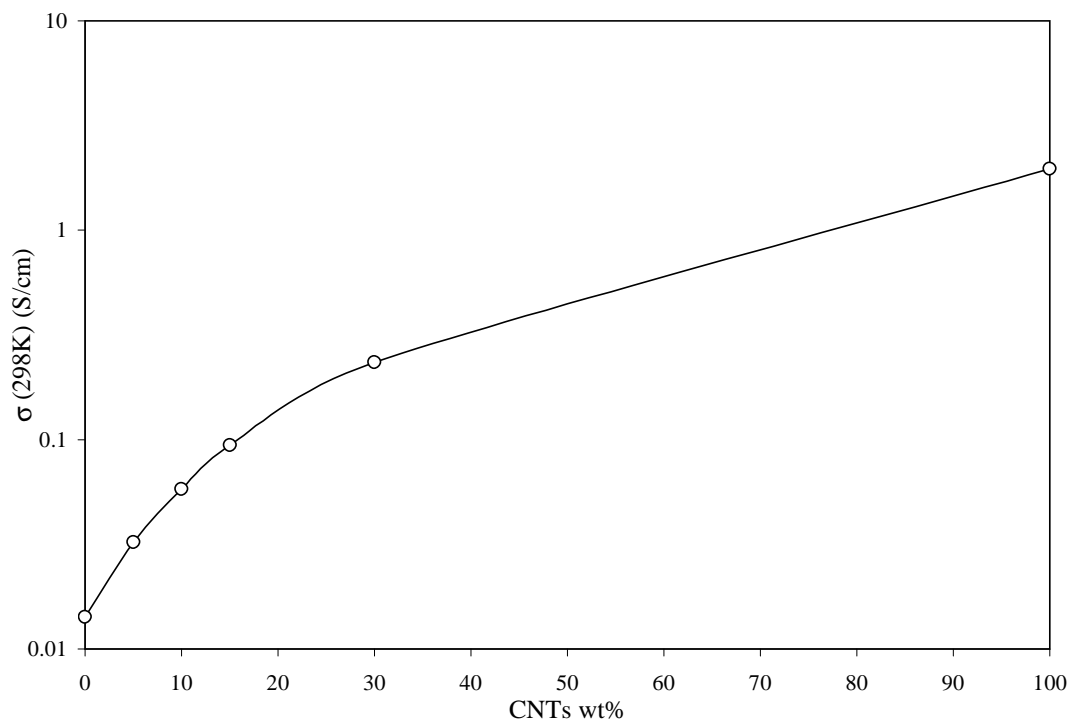


Figure 5.36: A semilogarithmic plot of the room-temperature conductivity of the composite vs the MWNT loading.

In order to explore how the MWNTs affect the composite's conductivity, we measured the temperature dependence of conductivity, as shown in Figure 5.37. The temperature dependence of conductivity becomes weaker and weaker with increasing MWNT loading. Furthermore, the pure polyaniline and composites show nearly the same behavior as plotted in Figure 5.37.

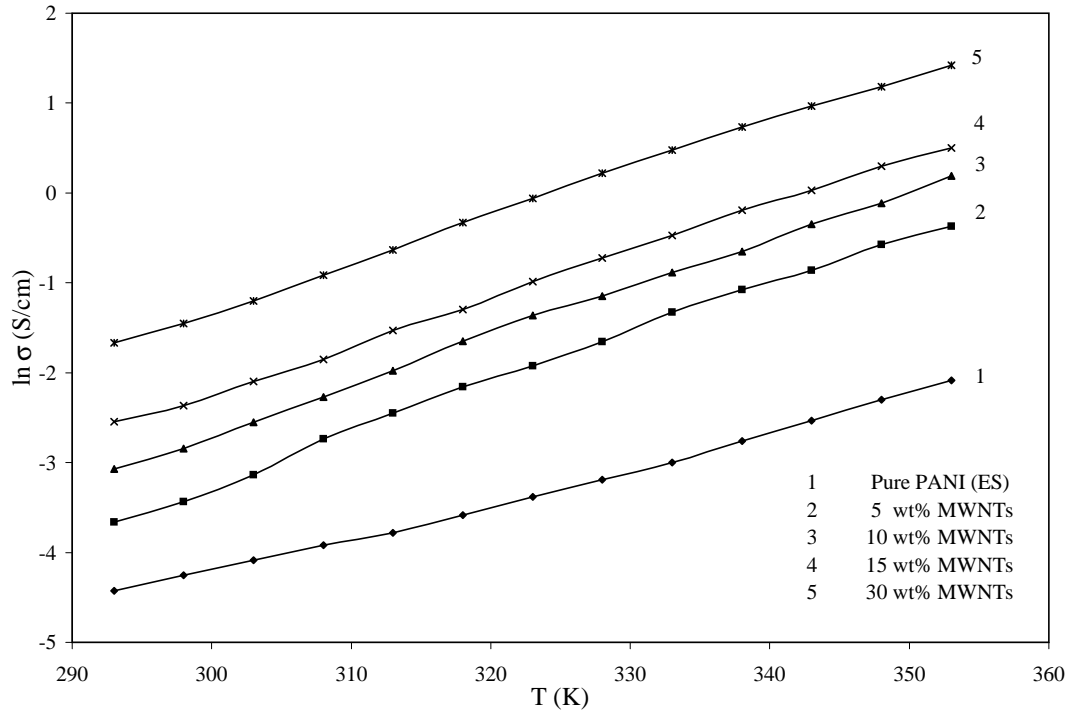


Figure 5.37: Temperature dependence on conductivity of the composites.

A polymer composite with MWNTs, can distinctly enhance the electronic properties of the polymer and even the MWNT. For example, it is reported that the conductivity of PANI/MWNT composites is higher than that of the pressed MWNT (or PANI) [173,174]. The possible reason is attributed to the fact that there is some interaction between the MWNT and the polymer chains. However, the nature of this interaction is not very clear yet. Maser et al. [174] pointed out that the synthesis by an in situ process leads to effective site-selective interactions between the quinoid ring of the PANI and the MWNT, which facilitate charge-transfer processes between the two components.

CHAPTER 6

SUMMARY AND CONCLUSIONS

6.1 Synthesis and Characterization of Polyaniline

Polyaniline (EB) powder was synthesized in aqueous hydrochloric acid solutions by oxidation with ammonium persulphate at three different temperatures of 25, 0, and -25°C . Lithium chloride was used at synthesis temperatures of 0 and -25°C as a mobile phase to prevent the reaction mixture from freezing. The structure and property of products were analyzed by DSC, TGA, FTIR, XRD, Solid-State ^{13}C -NMR, SEM, and Conductivity measurements.

The DSC thermal analysis indicated that the EB-form polyaniline powder had a discernible moisture content. This phenomenon was in agreement with the TGA results. Moreover, in the first run of DSC thermal analysis, an exothermic peak at $150\text{-}310^{\circ}\text{C}$ was found. This peak was due to the chain crosslinking, resulting from a coupling of two neighboring $-\text{N}=\text{Q}=\text{N}-$ groups to give two $-\text{NH}-\text{B}-\text{NH}-$ groups through a link of the N with its neighboring quinoid ring.

The TGA analysis of EB-form polyaniline undergo a three-step weight-loss process in the heating cycle. In the first step, water molecules escaped from the polymer chain. In the second step, a small amount of acid escaped as a volatile gas, and the polymer undergo oxidative degradation in the third step. The polymer was apparently stable up to 250°C, and after 275°C crosslinking took place. The results illustrated that the degradation temperature of the EB-form polyaniline powder was around 420-450°C.

FTIR spectrum suggested that the synthesized emeraldine base (EB) powder was significantly self-associated via interchain hydrogen bonds between the imine and amine nitrogen sites on the polymer backbone. Moreover, these spectrum indicated that, a significant amount of moisture was existed in the sample which supported the TGA results.

The XRD results, showed a well-developed crystallinity in the samples prepared at 0 and -25°C, while the sample prepared at +25°C was nearly amorphous.

The chemical shifts of EB-form polyaniline powder found by Solid-State ¹³C-NMR indicated that EB is primarily an alternating head-to-tail copolymer to reduced and oxidized repeat units. Moreover, the spectral line widths measured for EB-form polyaniline powder were attributed to local fluctuations in conformational and configurational geometries, a distribution chain packing, and compositional defects.

The SEM studies of EB, synthesized in aqueous hydrochloric acid solution, illustrated that the polymer had an irregular structure, with both large and small grains. Also, it was shown that the reduction in synthesis temperature leads to

longer chains of the polymer under study. The polyaniline synthesized at lower temperatures showed hollow tubular like morphology with relatively different sizes. In addition, the large particles observed might due to an excess of dopant that did not react with polyaniline-EB form.

It was proved that polymerization at low temperatures results in polyaniline of higher molecular weight. However, the effects of molecular weight on the polymer conductivity was marginal.

6.2 Solution Properties of Polyaniline

The solution properties of polyaniline leucoemeraldine base was depicted by static light scattering, viscometry, and dynamic light scattering.

Numerical values of weight average molecular weight, \bar{M}_w , radius of gyration, R_g , and second virial coefficient, A_2 , were calculated by static light scattering. The results indicated that the weight average molecular weight, \bar{M}_w , and radius of gyration, R_g , increased with decreasing synthesis temperature. This is expected, since the polymerization of polyaniline is an exothermic reaction in which the side reactions are depressed as the temperature of synthesis is lowered. Moreover, the dependence of $\log R_g$ on $\log \bar{M}_w$ showed that the polyaniline samples investigated had random coil conformation in NMP. The second virial coefficient, A_2 , was also decreased with increasing \bar{M}_w . From this result, it can be concluded that the polyaniline coils synthesized at lower temperature are more compact than that synthesized at higher temperatures. In addition, the positive values of A_2 , indicate that the polymer molecules prefer contacts with solvent molecules to

contact with other polymer molecules.

Intrinsic viscosity measurements for polyaniline samples showed a descending trend with increasing synthesis temperatures. The Huggins equation was assumed to be valid for EB/NMP/LiCl system and the Huggins coefficient, k_H , values for polyaniline synthesized at 0 and -25°C were found to be in a typical range that most polymer systems exhibit. However, the k_H value for -25°C EB was larger than expected. The Mark-Houwink coefficients ($a = 0.73$, and $K = 2.34 \times 10^{-4}$) for EB/NMP/LiCl system were determined by correlating their weight average molecular weight values determined by static light scattering (SLS), with their measured intrinsic viscosity values.

Dynamic light scattering (DLS) showed that hydrodynamic radius (R_H) and k_D increased with increasing molecular weight of polyaniline. However, diffusion coefficient at infinite dilution (D_o), decreased with increasing molecular weight. The increase in hydrodynamic radius (R_H) suggested that R_H is not a function of the chain length size or contour length, but it depends on the chain flexibility.

The positive values of k_D , which is a constant describing the concentration dependence of the diffusion coefficient, indicated that the solvent N-methyl-2-pyrrolidinone (NMP) used for dissolving polyaniline was a good solvent. Moreover, the k_D was in agreement with Huggins coefficient, k_H .

It was also observed that R_H increased with decreasing polymer concentration, which is a classical signature of polyelectrolyte in dilute solution and occurs because of the reduction in ions concentration in solution (ionic strength) as the overall concentration of polymer is decreased.

A combination of static and dynamic light scattering indicated that polyaniline molecules behaved like random coils at low molecular weight and rigid rod at high molecular weight.

To sum up, by investigating the intrinsic viscosity, $[\eta]$, hydrodynamic radius, R_H , and radius of gyration, R_g , for polyaniline synthesized at different temperatures in NMP solutions, we showed that the particle sizes of polyaniline molecules increased with decreasing polymerization temperatures (increasing molecular weight).

6.3 Low Density Polyethylene-Based Polyaniline Conducting Polymer Composites

Polyaniline (PANI) obtained chemically by oxidation at 25°C, with a conductivity of about 0.2 S m⁻¹, and doped with about 15% HCl, was incorporated into a thermoplastic low density polyethylene (LDPE) matrix. The melting curves of LDPE and its composites studied by DSC indicated that PANI content did not seem to have much influence on the melting temperature of LDPE. PANI particles used was completely amorphous and due to the low crystallinity of LDPE, the crystallinity of the composites were shown to decrease as the amount of PANI increased as indicated by the area under the melting curves. Moreover, there was a clear increase in the thermal stability of LDPE with increasing PANI content as proved by TGA.

Factors affecting the tensile mechanical properties of PANI filled-LDPE composites were investigated by using an Lloyd Universal Testing Machine. It was

found that with increasing PANI content, the tensile strength at maximum load, σ_{max} , and elongation at break, ε_b , decreased. However, the tensile modulus, E , was found to increase with PANI content.

A coincidence of a sudden increase in the electrical conductivity (percolation threshold) and a dramatic decrease in the deformation at break was observed for the dependencies on the filler content. The effect was explained in terms of the formation of a continuous network consisting of filler particles, which had a positive effect on the electrical but a negative effect on the deformational behavior of the material.

The morphology of the PANI filled-LDPE composites was also studied. The orientation of PE matrix was apparent and PANI particles were driven out of the PE matrix, while PE showed orientation along the draw direction.

In general, it can be said that the dependence of the tensile strength on PANI concentration was governed by the poor adhesion between the PANI particles and the polymeric matrix.

6.4 Conducting Polymer Composites of Multi Wall Nanotubes Filled-Polyaniline

We demonstrated the synthesis of PANI/MWNTs composites with enhanced electronic properties by the *in situ* chemical oxidative polymerization. The composites exhibited an order of magnitude increase in electrical conductivity with increase of the CNT content over neat PANI, and became weakly temperature dependent. The measured increase in conductivity of the composites may be

due to a doping effect of carbon nanotubes where the nanotubes compete with chloride ion.

Infrared spectroscopy showed that the synthesis by *in situ* process leads to effective site-selective interactions between the quinoid ring of the polyaniline and the MWNTs facilitating charge-transfer processes between the two components. Moreover, it was also showed that MWNTs affect both the free N-H environment and quinoid units along the polymer backbone and perhaps described the strong interactions between the nanotubes and polyaniline.

Wide angle X-Ray diffraction (WAXD), showed highly pronounced oscillating structure of the primary doped polyaniline emeraldine salt at lower angles, and superimposed the typical MWNT peaks at higher angles and therefore, no additional order was introduced.

Thermal gravimetric analysis (TGA) indicated three-step weight loss behavior at 130°C, between 150-250°C, and 350°C demonstrating the loss of water, co-evolution of water or evolution of acid and decomposition of the composites backbone, respectively. Also, it was observed that MWNTs filler introduced higher thermal stability to the composites.

Finally, SEM measurements indicated that the MWNTs were well dispersed and isolated, and the tubes became crowded proportionally to MWNTs weight percent used in the composites.

REFERENCES

- [1] Raymond B. Seymour, *Conductive Polymers*, Plenum Press, New York, (1981).
- [2] Soli-State Century, Scientific American, Special Issue, 8, (1997).
- [3] C.K. Chiang, C.R. Ficher, Y.W. Park, A.J. Heeger, H. Shirakawa, E.J. Louis, S.C. Gau, A.G. MacDiarmid, Journal of the American Society, **100**, 1013 (1977).
- [4] T.A. Skotheim, *Handbook of Conducting Polymer*, Marcel Dekker, New York, NY (1986).
- [5] A.R. West, *Solid State Chemistry and Its Applications*, John Wiley & Sons Ltd, East Kilbride, Scotland, p.453 (1987).
- [6] D. Jiles, *Introduction to the Electronic Properties of Materials*, Chapman & Hall, London, UK (1994).
- [7] B.G. Streetman, *Solid State Electronic Devices*, 2nd. Prentice-Hall Inc., Englewood Cliffs, NJ, p.295 (1980).
- [8] M.G. Kanatzidis, Chemical & Engineering News, December, p.36 (1990).
- [9] C.K. Chiang, E.J. Gau, A.G. MacDiarmid, Journal of the American Chemical Society, **100**, p.1013 (1977).
- [10] T.A. Skotheim, *Handbook of Conducting Polymers*, Marcel Dekker, New York, NY, vol.1-2, (1986).
- [11] R.L. Elsenbaumer, L.W. Shacklette, in, *Handbook of Conducting Polymers*, T.A. Skotheim, Marcel Dekker, New York, NY, vol.1, p.224 (1986).
- [12] G.B. Street, in, *Handbook of Conducting Polymers*, T.A. Skotheim, Marcel Dekker, New York, NY, vol.1, p.265 (1986).
- [13] G. Tourillon, in, *Handbook of Conducting Polymers*, T.A. Skotheim, Marcel Dekker, New York, NY, vol.1, p.293 (1986).
- [14] G.A. Kossmehl, in, *Handbook of Conducting Polymers*, T.A. Skotheim, Marcel Dekker, New York, NY, vol.1, p.351 (1986).
- [15] T.A. Skotheim, *Handbook of Conducting Polymers*, Marcel Dekker, New York, NY, vol.1-2, (1986).

- [16] A.G. MacDiarmid, A.J. Epstein, Chemical Society, Faraday Discussion, **88**, p.317 (1989).
- [17] H. Naarmann, N. Theophilou, Synthetic Metals, **22**, p.1 (1987).
- [18] S.C. Gao, Ph.D. Thesis, University of Pennsylvania, p.203 (1984).
- [19] J.C. Chiang, A.G. MacDiarmid, Synthetic Metals, **13**, p.193 (1986).
- [20] C.C. R.L. Esenbaumer, Synthetic Metals, **30**, p.123 (1989).
- [21] A.G. MacDiarmid, A.J. Epstein, Makromolekular Chemie, Macromolecular Symposium, **51**, p.11 (1991).
- [22] J.C.W. Chein, *Polyacetylene Chemistry, Physics and Material Science*, Academic Press Inc., Orlando, FL, p.87 (1984).
- [23] S. Roth, *One-Dimensional Metals: Physics and Material Science*, VCH, Germany, (1995).
- [24] A. Syed Akheel, K. Dinesan Maravattickal, Talanta, **38**, No.8, p.815 (1991).
- [25] E.M. Genirs, A. Boyle, M. Lapkowski, C. Tsintavis, Synthetic Metals, **36**, p.139 (1990).
- [26] A.G. MacDiarmid and A.J. Epstein, Faraday Discuss. Chem. Soc., **88**, p.317 (1989).
- [27] S.P. Armes and J.F. Miller, Synthetic Metals, **22**, p.385 (1988).
- [28] A. Pron, F. Genoud, C. Menarod and M. Nechtstein, Synthetic Metals, **24**, p.193 (1988).
- [29] Y. Cao, A. Andreatta, A.J. Heeger and P. Smith, Polymer, **30**, p.2305 (1989).
- [30] S.K. Manohar, A. Fagot, A.G. MacDiarmid, R.C.Y. King, and A.J. Epstein, Bull. Am. Chem. Soc., **37**, p.506 (1992).
- [31] E.J. Oh, Y. Min, J.M. Wiesinger, S.K. Manohar, E.M. Scherr, P.J. Prest, A.G. MacDiarmid and A.J. Epstein, Synthetic Metals, **55-57**, p.977 (1993).
- [32] L.H.C. Mattoso, A.G. MacDiarmid and A.J. Epstein, Synthetic Metals, **68**, p.1 (1994).
- [33] L.H.C. Mattoso, R.M. Farria, L.O.S. Bolhves and A.G. MacDiarmid, Polymer, **35**, p.5104 (1994).
- [34] P.N. Adams, A.P. Monkman, Synthetic Metals, **87**, p.165 (1997).

- [35] P.N. Adams, P.J. Laughlin, A.P. Monkman, *Synthetic Metals*, **76**, p.157 (1996).
- [36] H. Letheby, *Journal of the Chemical Society*, **15**, p.161 (1862).
- [37] A.G. Green, A.E. Woodhead, *Journal of the Chemical Society*, **97**, p.2388 (1910).
- [38] A.G. Green, A.E. Woodhead, *Journal of the Chemical Society*, **101**, p.1117 (1912).
- [39] J.G. Masters, Y. Sun, A.G. MacDiarmid, A.J. Epstein, *Synthetic Metals*, **41**, p.715 (1991).
- [40] G.E. Asturias, Ph.D. Thesis, University of Pennsylvania, (1993).
- [41] G.E. Asturias, A.G. MacDiarmid, R.P. McCall, A.J. Epstein, *Synthetic Metals*, **9**, E.157 (1989).
- [42] A.G. MacDiarmid, J.C. Chiang, A.F. Richter, N.L.D. Somasiri, A.J. Epstein, in, *Conducting Polymers*, L. Alcacer, ed., Reidel Publication, Dordrecht, p.105 (1987).
- [43] R. Willstatter, S. Dorogi, *Ber.*, **42**, p.4118 (1909).
- [44] G.V. Austerweil, Patent No. 973, 528 as cited in *Chemical Abstract*, **46**, p.10492 (1952).
- [45] A. Yasuda, T. Shimidzu, *Synthetic Metals*, **61**, p.239 (1993).
- [46] R.H. Land, R.F. Nelson, *Journal of Electrochemical Society*, **125**, p.1059 (1978).
- [47] R.H. Land, R.F. Nelson, *Journal of Chemical Society*, **96**, p.850 (1974).
- [48] Y. Cao, A. Andreatta, A.J. Heeger, *Polymer*, **30**, p.2305 (1989).
- [49] W.W. Focke, G.E. Wnek, Y. Wei, *Journal of Physical Chemistry*, **91**, p.5813 (1987).
- [50] S.K. Manohar, Ph.D. Thesis, University of Pennsylvania, (1992).
- [51] L.H.C. Mattoso, A.G. MacDiarmid, A.J. Epstein, *Synthetic Metals*, **68**, p.1 (1994).
- [52] A.M. Kenwright, W.J. Feast, P. Adams, A.J. Milton, A.P. Monkman, B.J. Say, *Polymer*, **33**, p.4292 (1992).
- [53] A.F. Richter, A. Ray, K.V. Ramanathan, S.K. Manohar, G.T. Furst, S.J. Oppela, A.G. MacDiarmid, A.J. Epstein, *Synthetic Metals*, **29**, E.243 (1989).

- [54] D.M. Mohilner, R.N. Adamsand, J.W. Argersinger, Journal of the American Chemical Society, **84**, p.3618 (1962).
- [55] E.M. Genies, C. Tsintavis, Journal of Electrochemical Chemistry, **195**, p.109 (1985).
- [56] W.S. Huang, B.D. Humphery, A.G. MacDiarmid, Journal of Chemical Society, Faraday Transaction, **82**, p.2385 (1986).
- [57] E.M. Genies, M. Lapkowski, Journal of Electrochemical Chemistry, **220**, p.67 (1987).
- [58] M. Angelopoulos, G.E. Asturias, S.P. Ermer, A. Ray, E.M. Sherr, A.G. MacDiarmid, M. Akhtar, Z. Kiss, A.J. Epstein, Molecular Crystal & Liquid Crystal, **160**, p.151 (1988).
- [59] J.M. Ginder, A.F. Richter, A.G. MacDirmid, A.J. Epstein, Solid State Communication, **63**, p.97 (1987).
- [60] A.G. MacDiarmid, J.C. Chiang, A.F. Richter, A.J. Epstein, Synthetic Metals, **18**, p.285 (1987).
- [61] B.J. Berne, R. Pecora, *Dynamic Light Scattering with Applications to Chemistry, Biology and Physics*, R.E. Krieger Pub. Co. Malabar, p.143-144 (1990).
- [62] E.F. Casassa, *Particle Factors in Rayleigh Scattering*, in Polymer Handbook, J. Brandup and E.H. Immngut, editors. Tohn Wiley & Sons, New York, vol.2, p.485-491 (1989).
- [63] B. Chu, *Laser Light Scattering, Basic Principles and Practice*, Academic Press, New York, p.13-20 (1991).
- [64] M. Doi, and S.F. Edwards, *The Theory of Polymer Dynamics*, Oxford University Press, Oxford, p.289-323 (1986).
- [65] K.S. Schmitz, *An Introduction to Dynamic Light Scattering by Macromolecules*, Academic Press, San Diego, p.22 (1990).
- [66] B.H. Zimm, Journal of Chemical Physics, **16**, p.1099 (1948).
- [67] N.C. Santos and M.A.R.B. Castanho, Biophysical Journal, **71**, p.1641 (1996).
- [68] Berne and Pecora, *Daynamic Light Scattering*, John Wiley & Sons, (1975).
- [69] W. Fred Billmeyer, JR., *Textbook of Polymer Science*, 3rd Edition, John Wiley & Sons, (1984).
- [70] L. Rosen Stephen, *Fundamental Principles of Polymeric Materials*, 2nd Edition, John Wiley & Sons Inc., (1993).

- [71] R. Fried Joel, *Polymer Science and Technology*, 2nd Edition, Pearson Education Inc., (2003).
- [72] P.J. Flory, *Principles of Polymeric Chemistry*, Ithaca, Cornell University Press, (1953).
- [73] S. Iijima, *Nature*, **354**, p.46-58 (1991).
- [74] F. Li Cheng, H.M. Bai, S. Sun, G.M. Dresselhouse, *Appl. Phys. Lett.*, **77**, p.3161 (2002).
- [75] A. Thess, R. Lee, P. Nikolaev, H. Dai, P. Petit, J. Robert, C. Xu, Y.H. Lee, S.G. Kim, A.G. Rinzler, D.J. Colbert, G.E. Scuseria, D. Tomanek, J.E. Fischer, R.E. Smalley, *Science*, **284**, p.1340 (1999).
- [76] I. Sayago, E. Terrado, E. Lafuente, M.C. Horrillo, W.K. Maser, A.M. Benito, R. Navarro, E.P. Urriolabeitia, M.T. Martinez and J. Gutierrez, *Synthetic Metals*, **148**, p.15 (2005).
- [77] Q. Jiang, M.Z. Qu, G.M. Zhou, B.L. Zhang, *Matter. Lett.*, **57**, p.988 (2002).
- [78] R.H. Banghman, C. Cui, A.A. Zakhidov, Z. Iqbal, J.N. Barisci, G.M. Spinks, G.G. Wallace, A. Mozzoldi, De Rossi, D. Rinzler, A.G. Jasschinski, O. Roth and M. Kertesz, *Science*, **284**, p.1340 (1999).
- [79] P. Poulin, B. Vigolo and P. Launois, *Carbon*, **40**, p.1741 (2002).
- [80] M.S.P. Shaffer, A.H. Windle, *Adv. mater.*, **11**, p.937 (1999).
- [81] B.Z. Tang, H.Y. Xu, *Macromolecules*, **32**, p.2569 (1999).
- [82] D.B. Remero, M. Carrard, W.A. de Heer, L. Zuppiroli, *Advanced Materials*, **8**, p.899 (1996).
- [83] S.A. Curran, P.M. Ajayan, A. Strevens, et al., *Advanced Materials*, **10**, p.1091 (1998).
- [84] H. Ago, P.M. Ajayan, A. Strevense, et al., *Advanced Materials*, **11**, p.1281 (1999).
- [85] P.M. Ajayan, O. Stephan, C. Colliex, D. Cooiex, D. Trauth, *Science*, **265**, p.1212 (1994).
- [86] L.S. Schadler, S.C. Giannaris, P.M. Ajayan, *Applied Phys. Lett.*, **73**, p.3842 (1998).
- [87] H.D. Wagner, O. Lourie, Y. Feldman, R. Tenne, *Applied Physical Letters*, **72**, p.188 (1998).
- [88] D.Qian, E.C. Dickey, R. Andrews, T. Rantell, *Applied Physical Letters*, **76**, p.2868 (2000).

- [89] G.Z. Chen, M.S.P. Shaffer, D. Coleby, G. Dison, W. Zhou, D.J. Fray, A.H. Windle, *Advanced Materials*, **12**, p.522 (2000).
- [90] I. Musa, M. Baxendale, G.A.J. Amaratunga, W. Eccleston, *Synthetic Metals*, **102**, p.1250 (1999).
- [91] A. Hassanien, M. Gao, M. Tokumoto, L. Dai, *Chem. Phys. Lett.*, **342**, p.484 (2002).
- [92] J. Deng, X. Ding, W. Zhang, Y. Peng, J. Wang, X. Long, P. Li, and A.S.C. Chan, *European Polymer Journal*, **38**, p.2497 (2002).
- [93] W.K. Maser et al., *Material Science and Engineering: C* **23**, p.87 (2003).
- [94] X.H. Li, B. Wu, J.E. Huang, J. Zhang, Z.F. Liu, H.L. Li, *Carbon*, **411**, p.1670 (2002).
- [95] T.M. Wu, Y.W. Lin, and C.S. Liao, *Carbon*, **43**, p.734 (2005).
- [96] W.K. Maser, A.M. Benito et al., *Materials Science and Engineering: C* **23**, p.87 (2003).
- [97] J.E. Huang, X.H. Li, J.C. Xu, and H.L. Li, *Carbon*, **41**, p.2731 (2003).
- [98] M. Guo, J.H. Chem, J. Li, B. Tao and S. Yao, *Analytical Chimica Acta*, **532**, p.71 (2005).
- [99] M. Tahhan, V.T. Truong, G.M. Spinks, and G.G. Wallance, *Smart Mater. Struct.*, **12**, p.626 (2003).
- [100] M. Baibarac, I. Baltog, S. Lefrant, J.Y. Mevellec, O. ChaUVET, *Chem. Mater.*, **15**, p.4149 (2003).
- [101] P.C. Ramamurthy, W.R. Harrell, R.V. Gregory, B. Sadanadan, A.M. Rao, *J. Electrochem. Soc.*, **151**, p.502 (2004).
- [102] P.C. Ramamurthy, A.M. Malshe, W.R. Harrel, R.V. Gregoy, K. McGuire, and A.M. Rao, *Solid State Electronics*, **48**, p.2019 (2004).
- [103] P.C. Ramamurthy, W.R. Harrell, R.V. Gregory, B. Sadanadan, nad A.M. Rao, *Synthetic Metals*, **137**, p.1497 (2003).
- [104] D.M. Bigg, *Metal-Filled Polymers: Properties and Application*, S.K. Bhattacharya, Ed., Marcel Dekker, New York, (1986).
- [105] B.A. Crossman, *Polymer Engineering Science*, **25**, p.507 (1985).
- [106] K. Yoshino, X.H. Yin, S. Morita, Y. Nakanishi, S. Nakagawa, H. Yamamoto, *Japan Journal of Applied Physics*, **32**, p. 979 (1993).

- [107] M. Omastova, S. Kosina, J. Pionteck, A. Janke, J. Pavlinec, *Synthetic Metals*, **81**, p.49 (1996).
- [108] M. Chipara, D. Hui, P.V. Notingher, M.D. Chipara, K.T. Lau, J. Sankar, D. Panaitescu, *Composites: Part B*, **34**, p.637 (2003).
- [109] J. Planens, A. Wolter, Y. Cheguettine, A. Pron, F. Genoud, M. Nechtschein, *Physical Rev. B*: **58**(12), p.7774 (1998).
- [110] A. Ragunathan, P.K. Kahol, J.C. Ho, Y.Y. Chen, Y.D. Dao, Y.S. Lin, *Physical Rev. B*: **58**(18), p.15955 (1998).
- [111] B. Sanjai, A. Ragunathan, T.S. Natarajan, G. Rangarajan, *Physical Rev. B*: **55**(16), p.10734 (1997).
- [112] B. Sixou, J.P. Travers, C. Barthet, M. Guglielmi, *Physical Rev. B*: **56**(8), p.4604 (1997).
- [113] J.P. Yang, P. Rannou, J. Planes, A. Pron, M. Nechtschein, *Synthetic Metals*, **93**, p.169 (1998).
- [114] A.I. Medalia, *Rubb. Chem. Technol.*, **59**, p.432 (1986).
- [115] F. Carmona, *Physica A*: **157**, p.461 (1989).
- [116] F. Lux, *Journal of Material Science*, **28**, p.285 (1993).
- [117] I. Chodak, M. Omastova, J. Pionteck, *Journal of Applied Polymer Science*, **82**, p.1903 (2001).
- [118] D. William, Jr. Callister, *Material Science and Engineering: An Introduction*, 2nd Edition, John Wiley & Sons Inc., (1991).
- [119] F.L. Mathews and R.D. Rawlings, *Composite Materials: Engineering and Science*, Britain, Alden Press, Oxford, (1994).
- [120] S. Roth, *One-Dimensional Metals*, VCH Publisher Inc., New York, NY, USA, p.116 (1995).
- [121] Y.P. Khanna, in *Material Characterization and Chemical Analysis*, J.P. Sibilica ed., 2nd Edition, VCH Publishers Inc., New York, NY, p.261 (1996).
- [122] N.S. Murthy, F. Reidinger, in *Material Characterization and Chemical Analysis*, J.P. Sibilica ed., 2nd Edition, VCH Publishers Inc., New York, NY, p.143 (1996).
- [123] B. Berne, R. Pecora, *Dynamic Light Scattering with Applications to Chemistry, Biology and Physics*, John Wiley & Sons, New York, (1976).
- [124] E.Frato Katherine, Physics Department, the College of Wooster, Ohio 44691, May 7, (2003).

- [125] A. Akheel Sayed and K. Maravattickal Dinesam, *Talanta*, **38**, p.815 (1991).
- [126] N. Mermilliod, J. Tanguy, M. Hoclet and A.A. Syed, *Synthetic Metals*, **18**, p.359 (1987).
- [127] A. Kitan, J. Izumi, J. Yano, Y. Hiromoto and K. Sakaki, *Bull. Chem. Soc. Jpn.*, **57**, p.2254 (1984).
- [128] S.P. Armes and J.F. Miller, *Synthetic Metals*, **22**, p.385 (1985).
- [129] A.N. Adams, P.J. Laughlin, A.P. Monkman and A.M. Kemwright, *Polymer*, Accepted for Publication.
- [130] P.N. Adams, P.J. Laughlin, A.P. Monkman, *Synthetic Metals*, **76**, p.157 (1996).
- [131] J. Stejskal, A. Riedo, D. Hlavata, J. Prokes, M. Helmstadt, and P. Holler, *Synthetic Metals*, **96**, p.55 (1998).
- [132] Cheng-Ho Chem, *Journal of Applied Polymer Science*, **89**, p.2142 (2003).
- [133] Y. Cao, A. Andreatta, A.J. Heeger, *Polymer*, **30**, p.2305 (1989).
- [134] Y. Wei, G.W. Jang, K.F. Hsueh, E.M. Scherr, A.G. MacDiarmid, A.J. Epstein, *Polymer*, **33**, p.314 (1992).
- [135] Sherr et al., *Synthetic Metals*, **41**, p.735 (1991).
- [136] W. Zheng, M. Angelopoulos, A.J. Epstein, and A.G. MacDiarmid, *Macromolecules*, **30**, p.2953 (1997).
- [137] I. Harada, Y. Furukawa, F. Ueda, *Synthetic Metals*, **29**, E.303 (1989).
- [138] 142.S. Quillard, G.Louarn, S. Lafrant, A.G. MacDiarmid, *Phys. Rev. B*: **50**, p.12496 (1994).
- [139] M. Angelepoulos, R. Dipietro, W.G. Zheng, A.G. Diarmid, *Synthetic Metals*, **84**, p.35 (1997).
- [140] V. Milind Kulkarni and Annamraju Kasi Viswanath, *Journal of Macromolecular Science, Part A-Pure and Applied Chemistry*, **A41**, p.1173 (2004).
- [141] T.L.A. Campos, D.F. Kersting, C.A. Ferreira, *Surface and Coatings Technology*, **122**, p.3 (1999).
- [142] A.A. Syed, and M.K. Dinesan, *Talanta*, **38**, p.815 (1991).
- [143] S. Jaroslav, H. Drahomira, T. Miroslava, P. Jan and S. Irima, *Polymer International*, **53**, p.294 (2004).

- [144] H.K. Chaudhari and D.S. Kelkar, *Journal of Applied Polymer Science*, **62**, p.15 (1996).
- [145] B. Wang, J. Tang and F. Wang, *Synthetic Metals*, **13**, p.329 (1986).
- [146] S.A. Chen, and T.S. Lee, *Journal of Polymer Science, Polymer Letter Edition*, **25**, p.455 (1987).
- [147] A. Kitani, M. Kang, S.I. Tsujioka and K. Sakaki, *Journal of Polymer Science, Part A: Polymer Chemistry*, **26**, p.1531 (1988).
- [148] Y. Lu, J. Li, and W. Wu, *Synthetic Metals*, **30**, p.87 (1989).
- [149] Y. Hsin Liao, T. Kang Kwei, K. Levon, *Macromol. Chem. Phys.*, **196**, p.3107 (1995).
- [150] J. Stejskal, P. Kratochvil, N. Gospodinova, L. Terlemezyan, P. Mokreva, *Polymer*, **33**, p.4857 (1992).
- [151] A.G. MacDiarmid, A.J. Epstein, *Mater. Res. Soc. Symp. Proc.*, **247**, p.565 (1992).
- [152] A. Ohtani, M. Abe, M. Ezoe, T. Doi, T. Miyata, A. Miyake, *Synthetic Metals*, **55-57**, p.3696 (1993).
- [153] E.J. Oh, Y. Min, J.M. Wiesinger, S.K. Mahonar, E.M. Sherr, P.J. Prest, A.G. MacDiarmid, A.J. Epstein, *Synthetic Metals*, **55-57**, p.977 (1993).
- [154] L.H.C. Mottaso, A.G. MacDiarmid, A.J. Epstein, *Synthetic Metals*, **68**, p.1 (1994).
- [155] P.N. Adams, P.J. Laughlin, A.P. Monkman, A.M. Kenwright, *Polymer*, **37**, p.3411 (1996).
- [156] P.N. Adams, P.J. Laughlin, A.P. Monkman, *Synthetic Metals*, **76**, p.157 (1996).
- [157] P.N. Adams, L. Abell, A. Middleton, A.P. Monkman, *Synthetic Metals*, **84-86**, p.61 (1997).
- [158] J. Barvo, M.P. Tarazona, E. Saiz, *Macromolecules*, **24**, No.14 (1991).
- [159] P. Kratochvil, *Classical Light Scattering from Polymer Solutions*, Elsevier, Amsterdam, Chapter-6, p.266-268 (1987).
- [160] L. Utraki, R. Simha, *Journal of Polymer Science: Part A*, **1**, p.1089 (1963).
- [161] M. Bohdanecky, J. Kovar, *Viscosity of Polymer Solutions*, Amsterdam, Elsevier, (1982).

- [162] W. Burchard, *In Light Scattering-Principles and Development*, W. Brown, Ed.; Chap.13, Clarendon Press: Oxford, (1996).
- [163] I. Chodak, I. Krupa, *Journal of Material Science Letter*, **18**, p.1457 (1999).
- [164] I. Chodak, M. Omastova, J. Pionteck, *Journal of Applied Polymer Science*, **82**, p.1903 (2001).
- [165] X. Zhang, J. Zhang, and Z. Liu, *Applied Physics*, **A80**, p.1813 (2005).
- [166] M. Cochet, W.K. Maser, A.M. Benito, M.A. Callejas, M.T. Martinez, J.M. Benoit, J. Schreiber, O. Chauvet, *Chem. Commun.*, p.1450 (2001).
- [167] B. Philip, J. Xie, J.K. Abraham, and V.K. Varadam, *Polymer Bulletin*, **53**, p.127 (2005).
- [168] S. Quillard, G. Louarn, S. Lefrant, A.G. MacDiarmid, *Phys. Rev. B*, **50**, p.12496 (1994).
- [169] R.J. Chen, Y. Zhang, D. Wang, H. Dai, *Journal of American Chemical Society*, **123**, p.3838 (2001).
- [170] M. Cochet, W.K. Maser, A.M. Benito, M.A. Callejas, M.T. Martinez, J.M. Benoit, J. Schreiber, O. Chauvet, *Chem. Commun.*, p.1450 (2001).
- [171] B. Philip, J. Xie, J.K. Abraham, and V.K. Varadan, *Smart Mater. Struct.*, **13**, p.105 (2004).
- [172] R. Ramasubramaniam, J. Chen, and H.Y. Liu, *Applied Physical Letter*, **83**, p.2928 (2003).
- [173] B.I. Shlovskii and A.L. Efros, *Electronic Properties of Doped Semiconductors*, Springer, Berlin, (1984).
- [174] M. Cochet, W.K. Maser, A.M. Benito, M.A. Callejas, M.T. Martinez, J. Scheiber and O. Chauvet, *Chem. Commun., Cambridge*, p.1450-1451 (2001).

CURRICULUM VITAE

Faris Yılmaz was born in Palestine on October 7, 1969. After pre-college education in Jineen, he was accepted to the Chemical Engineering Department of Middle East Technical University (METU) in Ankara. He got his Bachelor of Science degree in Chemical Engineering and Master of Science degree in Polymer Science & Technology in 1998 and 2001, respectively.

His research has mainly concentrated on the conducting polymers, their solution properties, and nanocomposites under the guidance of Professor Zuhâl Küçükyavuz from the Chemistry Department of METU, and Professor Ülkü Yılmaz from the Chemical Engineering Department of METU.

He is married and has two children.